Lappeenranta
University of Technology

Henry Hämäläinen

# IDENTIFICATION OF SOME ADDITIONAL LOSS COMPONENTS IN HIGH-POWER LOW-VOLTAGE PERMANENT MAGNET GENERATORS

Thesis for the degree of Doctor of Science (Technology) to be presented with due permission for public examination and criticism in the Auditorium 1382 at Lappeenranta University of Technology, Lappeenranta, Finland on the 13th of August, 2013, at noon.

Acta Universitatis
Lappeenrantaensis 523

Supervisors

Professor Juha Pyrhönen
Department of Electrical Engineering
LUT Institute of Energy Technology (LUT Energy)
LUT School of Technology
Lappeenranta University of Technology
Finland

Dr. Janne Nerg
Department of Electrical Engineering
LUT Institute of Energy Technology (LUT Energy)
LUT School of Technology
Lappeenranta University of Technology
Finland

Reviewers and opponents

Professor Peter Sergeant
Electrical Energy Laboratory
Ghent University
Ghent, Belgium

Dr. Sami Ruoho
Teollisuuden Voima Oyj
Finland

ISBN 978-952-265-428-1
ISBN 978-952-265-429-8 (PDF)
ISSN-L 1456-4491
ISSN 1456-4491

Lappeenrannan teknillinen yliopisto
Yliopistopaino 2013

# Abstract

Lappeenranta University of Technology
Acta Universitatis Lappeenrantaensis 523

Henry Hämäläinen

## Identification of Some Additional Loss Components in High-Power Low-Voltage Permanent Magnet Generators

Lappeenranta 2013
42 p.

ISBN 978-952-265-428-1
ISBN 978-952-265-429-8 (PDF)
ISSN-L 1456-4491, ISSN 1456-4491

Permanent magnet generators (PMG) represent the cutting edge technology in modern wind mills. The efficiency remains high (over 90%) at partial loads. To improve the machine efficiency even further, every aspect of machine losses has to be analyzed. Additional losses are often given as a certain percentage without providing any detailed information about the actual calculation process; meanwhile, there are many design-dependent losses that have an effect on the total amount of additional losses and that have to be taken into consideration.

Additional losses are most often eddy current losses in different parts of the machine. These losses are usually difficult to calculate in the design process. In this doctoral thesis, some additional losses are identified and modeled. Further, suggestions on how to minimize the losses are given.

Iron losses can differ significantly between the measured no-load values and the loss values under load. In addition, with embedded magnet rotors, the quadrature-axis armature reaction adds losses to the stator iron by manipulating the harmonic content of the flux. It was, therefore, re-evaluated that in salient pole machines, to minimize the losses and the loss difference between the no-load and load operation, the flux density has to be kept below 1.5 T in the stator yoke, which is the traditional guideline for machine designers.

Eddy current losses may occur in the end-winding area and in the support structure of the machine, that is, in the finger plate and the clamping ring. With construction steel, these losses account for 0.08% of the input power of the machine. These losses can be reduced almost to zero by using nonmagnetic stainless steel. In addition, the machine housing may be subjected to eddy current losses if the flux density exceeds 1.5 T in the stator yoke.

Winding losses can rise rapidly when high frequencies and 10–15 mm high conductors are used. In general, minimizing the winding losses is simple. For example, it can be done by

dividing the conductor into transposed subconductors. However, this comes with the expense of an increase in the DC resistance. In the doctoral thesis, a new method is presented to minimize the winding losses by applying a litz wire with noninsulated strands. The construction is the same as in a normal litz wire but the insulation between the subconductors has been left out. The idea is that the connection is kept weak to prevent harmful eddy currents from flowing. Moreover, the analytical solution for calculating the AC resistance factor of the litz-wire is supplemented by including an end-winding resistance in the analytical solution. A simple measurement device is developed to measure the AC resistance in the windings. In the case of a litz-wire with originally noninsulated strands, vacuum pressure impregnation (VPI) is used to insulate the subconductors. In one of the two cases studied, the VPI affected the AC resistance factor, but in the other case, it did not have any effect. However, more research is needed to determine the effect of the VPI on litz-wire with noninsulated strands.

An empirical model is developed to calculate the AC resistance factor of a single-layer form-wound winding. The model includes the end-winding length and the number of strands and turns. The end winding includes the circulating current (eddy currents that are traveling through the whole winding between parallel strands) and the main current. The end-winding length also affects the total AC resistance factor.

Keywords: Permanent magnet generator, eddy currents, proximity effect, skin effect, form-wound winding, litz wire
UDC 621.311.245:621.313.8:621.548:537.612

# Acknowledgments

The research documented in this doctoral thesis was carried out at the Department of Electrical Engineering at the Institute of Energy Technology (LUT Energy) at Lappeenranta University of Technology (LUT) during the years 2009–2012. The research was funded by The Switch Drive Systems Oy.

I would like to thank Professor Juha Pyrhönen for his guidance and patience to explain things thoroughly when I did not understand something. Professor Pyrhönen was also of great help when I was writing the journal papers. I would like to express my gratitude to Dr. Janne Nerg for his guidance and expertise in the doctoral thesis project. I would also like to thank Dr. Vesa Ruuskanen for many technical discussions. Vesa was always lending a helping hand when I was stuck with the Flux 2D/3D program. I would like to thank Dr. Paula Immonen for her help in the process. My gratitude also goes to Joonas Talvitie, M.Sc., who designed and built the measurement device to measure the AC resistance of the litz wires. Without his help it would have been difficult to acquire accurate measurement results. I would like to thank The Switch and especially Dr. Jussi Puranen for their assistance during the research and giving me challenging tasks to study. I would also like to thank Martti Lindh, who has helped with his expertise in the measurement setups.

The comments by the preliminary examiners, Professor Peter Sergeant and Dr. Sami Ruoho, are highly appreciated.

I would like to express my gratitude to Peter Jones for his work on improving the language in two journal papers and a part of this doctoral thesis. I would also like to thank Dr. Hanna Niemelä for her contribution towards editing the language of this doctoral thesis and the two other journal articles.

I would like to thank Walter Ahlström Foundation and Lappeenranta University of Technology Foundation for the financial support.

Finally, I express my gratitude to my family, especially to my wife Inka Hämäläinen for her support and encouragement during the research. I would like to thank my father Aarre Hämäläinen and my mother Merja Kaivola for giving me the support to continue studying and eventually pursue a doctor's degree. I would also like to thank Pekka Kaivola, Rauno Kaivola, Hannu Hyvönen, and Inkeri Hyvönen for their support.

Lappeenranta, June 12th, 2013

Henry Hämäläinen

# Contents

# Symbols and Abbreviations

## Roman letters

| | |
|---|---|
| $L_q$ | quadrature-axis inductance [H] |
| $L_d$ | direct-axis inductance [H] |
| $I$ | current [A] |
| $R$ | resistance [Ω] |
| $n$ | number of strands |
| $d_s$ | diameter of each strand [m] |
| $b_b$ | slot width [m] |
| $l_{stack}$ | length of the winding inside a stack [m] |
| $l_{end\text{-}winding}$ | length of the end winding [m] |
| $l_{turn}$ | length of the turn [m] |
| $k_r$ | AC resistance factor ($R_{AC}$/ $R_{DC}$) |
| $h_c$ | solid conductor height [m] |
| $b_c$ | conductor width [m] |
| $b$ | slot width [m] |
| $z_Q$ | number of turns in a slot |

## Greek Letters

| | |
|---|---|
| $\omega$ | angular frequency of a sinusoidal current [rad/s] |
| $\mu_0$ | vacuum permeability [Vs/Am] |
| $\rho$ | resistivity of the conducting material [Ωm] |

## Acronyms

| | |
|---|---|
| PMG | permanent magnet generator |
| FEA | finite element analysis |
| FEM | finite element method |
| IEC | International Electrotechnical Commission |
| LS | loss surface |
| 2D | two-dimensional |
| 3D | three-dimensional |
| NdFeB | neodymium iron boron |
| VPI | vacuum pressure impregnation |

# List of publications

**Publication I**

H. Hämäläinen J. Pyrhönen, J. Nerg, "Effects of Quadrature Axis Armature Reaction on Magnetic Circuit Time Harmonics and Stator Iron Losses in a Permanent Magnet Synchronous Generator with Embedded Magnets," *International Review of Electrical Engineering*, vol. 5, no. 5, Part A, pp. 2057–2062, 2010.

**Publication II**

H. Hämäläinen J. Pyrhönen, J. Nerg, J, Puranen "3D Finite Element Method Analysis of Additional Load Losses in the End Region of Permanent Magnet Generators," *IEEE Transactions on Magnetics*, vol. 48, no. 8, pp. 2352–2357, August 2012.

**Publication III**

H. Hämäläinen J. Pyrhönen, J. Nerg, J. Talvitie, "AC resistance Factor of Litz wire Windings Used in Low-Voltage Generators," *IEEE Transactions on Industrial Electronics*, forthcoming.

**Publication IV**

H. Hämäläinen J. Pyrhönen, J. Nerg, "AC Resistance Factor in One-Layer Form-Wound Winding Used in Rotating Electrical Machines," *IEEE Transactions on Magnetics*, vol. 49, no. 6, Jun. 2013.

The author of this doctoral thesis is the principal author and investigator in Publications I–IV, and is solely responsible for the scientific contribution in the papers and the introductory section of the thesis.

# Chapter 1

# Introduction

Today's global trend is to promote energy efficiency and the deployment of renewable energy sources. Although energy efficiency is not a new idea [1], it has taken and will take dozens of years to reach acceptable energy efficiency levels. In today's energy chains containing thermal power plants, the energy used efficiently in a process can be less than 10% of the primary energy fed into the chain. The 1970s oil crisis was one of the wake-up calls, after which energy efficiency actions have been considered more seriously because of the ever-growing energy price. Today, we are also increasingly concerned about the environment. The main idea is to turn electricity production from fossil-fuel-based systems into systems based on renewable energy sources [2] to make use of natural resources in a more sustainable manner. This can be done with solar, wind, or hydro energy, of which wind and solar energy have a very high potential.

The European Union is planning to cover 20% of its energy demand with renewable energy sources by 2020. The decision made in Germany to give up nuclear power by 2020 will also increase the need for renewable energy sources even further. Over the recent years, the global average annual growth in wind energy has been about 30% [3]. The key here is to increase the annual power production efficiency.

Electric motors in the industry consume 30–40% of the energy generated in the world [4], [5]. This is why the energy efficiency of the motors is a topical and relevant issue. Furthermore, by increasing the energy efficiency, the energy output can be maximized. More efficient motors will help to reduce energy consumption and carbon foot print. Therefore, minimizing the losses in the generators and motors is highly important. The International Electrotechnical Commission (IEC) has established new energy efficiency classes to globally harmonize the energy classes for general purposes in the standard IEC 600034-30 [5]. The classes are designated as IE1, IE2, IE3, and IE4. The easiest way to reach the IE4 super premium class is to use PM motors [5]. Environmental concerns and increasing energy prices are also pushing towards nonstandard technologies, where PM motors have proven to be more efficient than induction motors [4], [6].

Obviously, appropriate estimation of losses is one of the most important tasks when designing an electrical machine, because the losses define the need for the cooling system. Most electromagnetic loss mechanisms in an electrical machine are well-known design factors and can be calculated with an acceptable accuracy.

When trying to reach the highest possible efficiencies of the rotating machinery, also the additional losses of the machines become important. Normally, additional losses are assumed to represent only a few percents of the total losses, at least according to the standard IEC 60034-2 [7]. Additional losses occur, for instance, in the supporting structures of the machine [8], in the windings [9], in the laminated iron core of the stator, and in the rotor [10]. Stator finger plates and clamping rings are subjected to additional load losses as they are located close to the armature end windings. Losses in the finger plate and in the clamping ring are maybe the most difficult losses to calculate or measure. Modern simulation tools allow more accurate identification of these losses, enabling their minimization by correct design and material selection.

Over a couple of decades, permanent magnet generators have gained popularity [11]–[21]. Figure 1 illustrates a 3 MW, 1600 $\text{min}^{-1}$ PM generator manufactured by The Switch Oy. The specification of the machine is given in Table I.

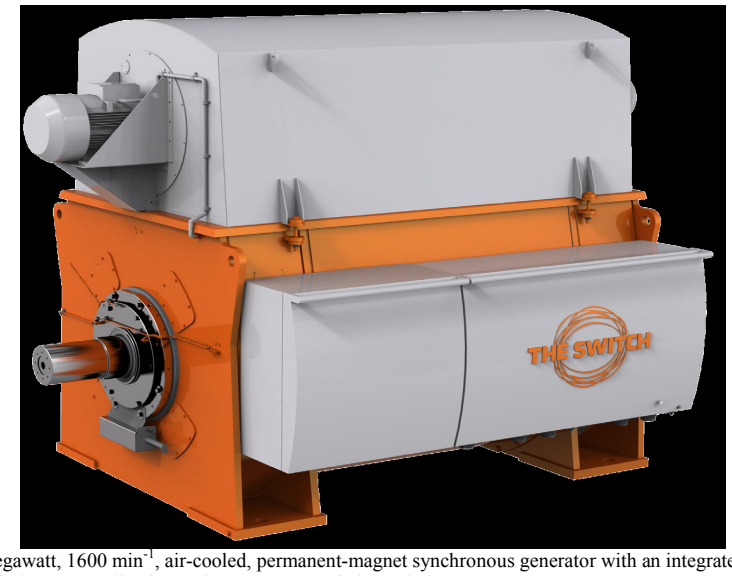


Fig. 1. Three-megawatt, 1600 $\text{min}^{-1}$, air-cooled, permanent-magnet synchronous generator with an integrated air-to-air heat exchanger for wind power applications. Figure courtesy of The Switch Oy.

TABLE I
SPECIFICATIONS OF THE HIGH-SPEED PERMANENT MAGNET MACHINE PRESENTED IN FIG. 1. COURTESY OF THE SWITCH OY.

| High-speed permanent magnet generator | |
|---|---|
| Power (kW) | 3000 |
| Speed (rpm) | 1600 |
| Shaft height (mm) | 560 |
| Length including housing (mm) | 2430 |
| Height including housing (mm) | 1821 |
| Generator mass (kg) | 7900 |
| Nominal current (A) | 2550 |
| Nominal voltage (V) | 690 |
| AC resistance factor at nominal frequency ($R_{AC}/R_{DC}$) | 1.27 |
| Efficiency at 100% load | 97.7 |
| Efficiency at 75% load | 97.4 |
| Efficiency at 50% load | 96.7 |
| Efficiency at 25% load | 94.2 |

In Fig. 2, the efficiency map of the machine in Fig. 1 is presented. The efficiency map depends on the machine control. In this case, the voltage is optimized when calculating the efficiency map, and therefore, it may not completely reflect the actual machine efficiency map when the machine is controlled by an actual converter, which is not necessarily operating with the optimum voltage in each point. Cooling losses are included in the calculation to make the result more realistic. Further, saturation effects are not fully included in the calculation. According to the map, the machine is very efficient in a wide operating area. The efficiency at a 25% load is taken at the nominal speed because there is no exact information of the turbine with which the machine is driven. Usually, the turbines are operated at lower speeds only at the lowest wind speeds, and therefore, the 25% load optimal point is probably quite close to the rated speed as the optimal turbine tip speed ratio is followed. 25% power is, in principle, reached at 63% of the rated wind speed.

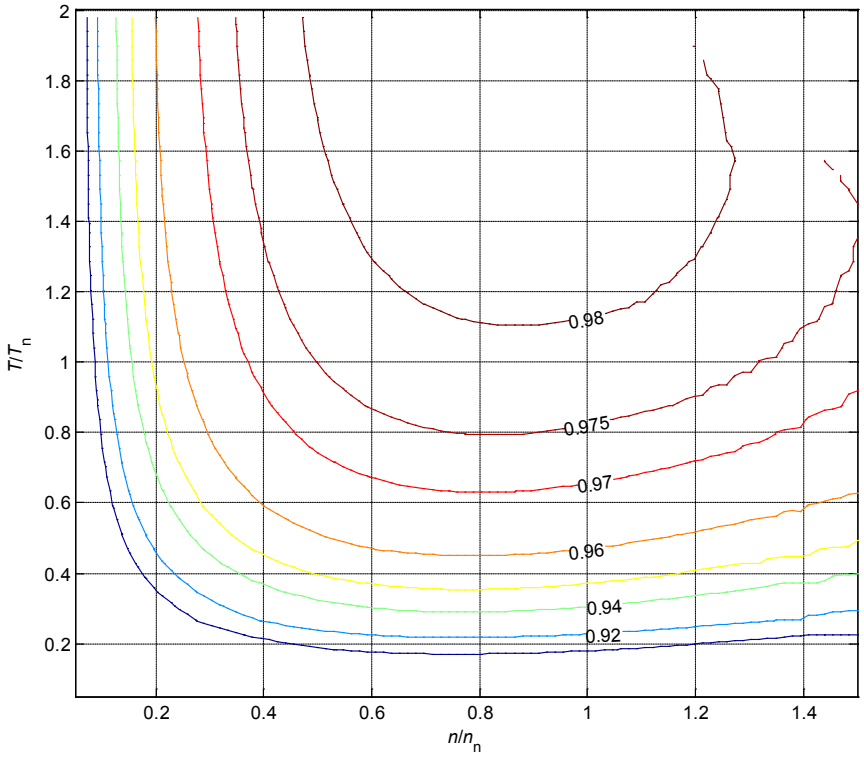


Fig. 2. Efficiency map of the machine illustrated in Fig. 1. Figure courtesy of Paula Immonen.

Nowadays, these machines are already widely used for instance in wind power applications [3]. Their high efficiency [22] at partial loads makes PMGs superior to induction generators because wind turbines usually operate at partial loads. However, their drawback is the price of the magnets [22]. Typically, the load factor is about 3000–4000 h.

Today, the most popular wind mill generator is based on the doubly-fed induction machine [3], [23], [24]. The drawback of the machine of this kind is that it always needs a gear with a high gear ratio (100:1), and at partial loads the machine efficiency decreases rapidly [25],

[26]. These drawbacks can be overcome by replacing the generator with a permanent magnet generator (PMG). The drawback of PMGs is the cost of the magnets [22]. At the moment, the typical price of NdFeB magnets is 100–150 $/kg, which is more than ten times the price of copper.

The effects of additional losses are extra heat and loss of torque production. The additional losses have to be removed by a cooling system. Every joule lost in the production is paid and repaid in the course of the machine lifetime [27].

The additional losses are produced by the saturation effects in the magnetic materials, the space harmonics, and the leakage fluxes. Additional losses result in a lower efficiency and derating of the machine rated power [28]. Thus, to get the most out of the machine, every opportunity to enhance the efficiency has to be considered.

In the literature, two terms are used for the undefined losses: additional losses and stray load losses [29]. In this doctoral thesis, the term ‘additional losses’ is used. Only those additional losses that concern PM machines are covered in this thesis, but they are also usually present in other types of machines.

## 1.1 Definition of additional losses

Historically, the definition, origin, and amount of additional losses have been debated. In principle, additional loss is the difference between the total measured loss and the sum of calculated losses: the stator and rotor resistive losses, the stator and rotor iron losses, and the mechanical losses. These losses are caused by several different phenomena. Some of them are easy to model but some very difficult to calculate. According to the IEC 60034-2-1 standard “Calculating the Efficiency of a Motor”, the joule losses are calculated by using the DC resistance of the winding, and therefore, the additional losses also include the losses caused by the skin effect in the conductors [30].

No-load iron losses can be reliably determined by the no-load test. They include the additional losses at no load, for example the eddy current losses that the air gap harmonics produce on the rotor surface, the stator and rotor tooth tips, and the windings; the iron losses in the clamping rings at the ends of the stator core; the iron losses in the frame and the end shields. Many of these loss components are small because the no-load current is small. In traditional machine design calculations, these loss components are normally evaluated empirically by using suitable correction coefficients [30].

In PM machines, the no-load test does not necessarily reveal the load-dependent losses as the no-load current can be very small. It is of course possible to use reactive current in the machine, but such a test does not correspond to the magnetic conditions in machines under load.

Over the recent years, modern FEM simulation tools have facilitated the identification of the additional losses. This has led to a greater understanding of the origins of the losses.

Most of the papers concerning additional losses concentrate on induction motors [4], [5], [27]–[29], [31]–[35]. The reason for this is that induction motors are the most commonly

used motors in the industry [5]. Only a few papers address additional losses in synchronous machines [36]–[38].

Additional losses occur mainly in the form of eddy currents in those parts of the machine that are subjected to the flux [34]. The rest of the additional losses comprise high-frequency hysteresis and rotating flux iron losses [39]–[49]. In other words, the additional load losses can be divided into losses that are not accounted for by the sum of friction and windage losses, the stator and rotor $I^2R$ loss, and the core loss [37], [50].

In PMGs, compared with induction motors, the additional losses are similar on the stator side but different on the rotor side. An induction motor has current-carrying conductors, which results in rotor $I^2R$ losses, whereas in PMGs the conductors are replaced by magnets. The eddy current losses in the magnets are much smaller than the losses in the rotor bars [6]. This is also the major reason why PMGs are more efficient than induction machines.

On the stator side, the losses comprise high-frequency eddy current and hysteresis losses in the stator iron, the frequency-dependent additional losses in the armature winding, the iron losses produced by the third field harmonic caused by the iron saturation [50], and the eddy current losses in the housing and the support structure (finger plate and clamping ring) [52]–[72].

In the early 20$^{th}$ century, the additional losses were defined as the losses measured in short circuit [73], and there were no methods to calculate these losses. At that time, it was acknowledged that flux density affects the iron losses. Therefore, the iron losses were regarded as additional losses because there were no tools to calculate them [73].

Rockwood [73] acknowledged in 1927 that it was difficult to develop an equation that could predict the short-circuit loss. Therefore, it would be better to divide the short-circuit losses into two distinct parts and develop an equation for each loss component. At that time, additional losses were defined to be the armature copper eddy current losses, the losses in the stator iron, the pole face loss, the end loss, and the loss in the armature copper caused by the armature reaction.

It was noticed that the AC losses are larger than the DC losses in the windings. A method to estimate the AC eddy current losses in the armature winding copper was developed in the early 1900s by Field [74], Lyon [75], and Gilman [76], [77]. Lyon developed an equation in 1921 to evaluate eddy current losses with hyperbolic functions. The equation did not get much attention until 40 years later in 1966 when Dowell [78] used the same equation for transformers. Today, the equation is widely known as Dowell's model or Dowell's equation, and his paper is cited frequently in a number of papers. Küpfmüller [79], Richter [80], [81], and Vogt [82] have also used the same equation in their analyses. The AC resistance factor $k_\mathrm{r}$ is defined by Dowell's equation as follows:

$$k_\mathrm{r} = \xi \frac{\sinh 2\xi + \sin 2\xi}{\cosh 2\xi - \cos 2\xi} + \frac{2\left(z_\mathrm{Q}^2 - 1\right)}{3} \frac{\sinh \xi - \sin \xi}{\cosh \xi + \cos \xi} \tag{1}$$

where

$$\xi = h_\mathrm{c} \sqrt{\frac{1}{2} \omega \mu_0 \sigma_\mathrm{C} \frac{b_\mathrm{c}}{b}} \tag{2}$$

and where $h_c$ is the solid conductor height (or the number of parallel strands on top of each other; $n_s \times$ strand height), $\omega$ is the radian frequency of the exciting sinusoidal current, $\sigma_C$ is the conductivity of the conducting material, $\mu_0$ is the permeability of vacuum, $z_Q$ is the number of turns in a slot, $b_c$ is the width of conductor, and $b$ is the slot width. The drawback of this equation is that it treats the conductor as a solid conductor; in other words, it does not take into consideration the number of strands and the length of the end winding.

In the 1940s, the losses in electrical machines were divided into two loss types: firstly, into losses that could be calculated with a reasonable accuracy, and secondly, into additional losses that could not be accurately determined in advance [37]. At the beginning of the 20$^{th}$ century, the additional losses were measured by a short circuit test [73], but in the 1940s, a reverse rotation test was introduced [37]. The reverse rotation test consists of two different measurements after the no-load current has been measured: firstly, the removed rotor test is performed to determine the power frequency additional losses, and secondly, the actual reverse rotation test is made to determine high-frequency additional losses [33], [84]. In the reverse rotation test, the rotor is rotated with a slip $s = 2$. In the 1960s, the reverse rotation method was questioned by Chalmers [32], [33]. According to Chalmers, the errors in the measurement are small only if the slot harmonics produce the major part of the additional losses. This method is inaccurate especially in the case of large motors.

Owing to the lack of knowledge in the 1950s, the clamping rings were made in some cases of copper, which is a highly conductive although nonmagnetic material [83]. The clamping ring made of copper had up to 3.4% losses of the input power, which is unacceptable nowadays. General Electric started experimenting with nonmagnetic metals in the support structures and reached promising results already in 1925 [38]. GE stated later that minimizing eddy current losses in the support structures of the machines is achieved by using nonmagnetic steel or a laminated structure. This was confirmed by measurements in the end region [38].

In 1959, Alger [35] divided additional load losses into six components: eddy current losses in the stator copper, losses in the end structure, high-frequency stator and rotor surface losses, high-frequency tooth pulsation and rotor $I^2R$ losses, six-times-frequency rotor $I^2R$ losses, and extra iron losses in motors with skewed slots.

By the 1960s, the general understanding of the principles of calculating the additional losses was established, at least to some extent [31]; however, there was still confusion about their origin and definition. Chalmers [33] divided additional losses into three categories: eddy current losses in the stator winding, losses in the end region, and losses resulting from skewing.

Schwarz [31] reclassified additional losses into two categories based on their origin: main flux variations and leakage fluxes. Before this, the losses were defined as stray no-load losses and stray load losses. Schwarz delineated the basic types of additional losses that were initially determined by Richter and Alger; concerning PM machines, surface losses fall into the first category, as they originate from the permeance variations (harmonic flux density components). In addition, there are tooth pulsation losses that result from the permeance variation caused by the relative tooth position. The second category includes surface losses in the iron, tooth pulsation losses in the iron, stator eddy current losses in the windings, and stator overhang losses (support structure).

In the 1960s, Stoll was one of the first to apply numerical methods to calculate eddy currents in copper conductors [52], [53] and in clamping rings [54].

In the 1980s, an agreement had not yet been reached about the definition of additional losses. For instance, the IEC defined the additional losses to be 0.5% of the input power. This has remained in the IEC standard until today. How the IEC decided to fix the additional losses to 0.5% is unknown because it is widely known that they vary significantly from design to design. Already in the 1980s, experimental results reported in the literature suggested that the additional losses were even up to 20 times 0.5% in some cases [1]. Almeida [4], [5] collected data of hundreds of squirrel cage induction motors, and according to his results, the IEC and IEEE standards underestimated additional losses by about 1 percentage point. Glew [27], [29] suggested that the standards underestimate the additional losses by fixing them to 0.5% of the input power (IEC 34-2). He presented a number of papers that suggested otherwise, always showing the additional losses to be more than 0.5%. He also argued that for decades millions of machines have been sold and designed according to the IEC 34-2 standard, implying that the efficiency has been overestimated [27]. Glew called for a reform of the calculation of additional losses. A fact supporting his point of view is that the amount of additional losses, for instance the value of 0.5%, cannot be fixed because many design factors may influence the additional losses. For example, the material of the support structure (finger plate and clamping ring) affects the losses, and also the winding design can have a significant effect on additional losses. Further, the stator iron material has an effect on the additional losses.

According to Jimoh [1], the effects of additional losses on the machine performance include heating, torque loss, and acceleration and deceleration effects, resulting in a decreased efficiency and derating. Jimoh also stated that there is no accurate method to measure additional losses in electrical machines, mostly because of inaccuracies in the measurements [1], [28]. Aoulkadi [84] has also observed inaccuracies especially in measurements made according to IEEE 112-B standard. Aoulkadi [84] even measured negative additional losses. In addition to the test method proposed by Jimoh, two additional measurements for the additional losses have been presented: the eh-star-method [84] and the equivalent no-load method [84]. Measurement inaccuracies are also discussed in [4], [5], [25], [85] regarding additional losses.

In 1992, Karmaker [36] investigated additional losses and compared FEM calculations and measurements made by a calorimetric method. The additional losses of the machine were very close to 0.5% of the input power determined either by the measurements or the FEM analysis.

Modern FEM programs started to enter the market in the 1990s, which made it possible to analyze the additional losses more precisely by numerical methods [87], [88].

There are also additional losses caused by the inverter [88], but they are excluded in this doctoral thesis. The thesis concentrates only on the additional losses that occur at a sinusoidal supply.

To sum up, additional losses are not easily defined by calculation. However, additional losses can be limited if the designer understands their origin and knows how to minimize the losses. In this thesis, the origins of some additional losses are observed and evaluated.

## 1.2 Additional losses in the stator iron

In particular, the estimation of iron losses is among the most challenging issues. Additional losses of iron have been identified as being caused mostly by the rotating flux [39]–[49], the high-frequency hysteresis losses, minor loop losses, and saturation effects [39]. Time harmonics are taken into account in a few papers [40], [44], [46], [47] when calculating the iron losses. In 1991, Bertotti [49] introduced an addition of excess losses to the classical analytical calculation method. In the classical analytical method, the losses are divided into eddy current and hysteresis losses. However, the estimation of the amount of additional losses is still challenging because of the lack of exact measurement techniques to verify the theoretical assumptions [4], [5], [25], [85].

Accurate measurement methods have been an issue also in the definition of the iron losses. Papers [40], [46], and [41] reported that the measurements deviated about 50% from the simulated ones. According to the authors, the reason for this was the losses caused by the rotational flux and the time harmonics in the stator iron. No measurement error was considered.

A loss surface (LS) model is used in this doctoral thesis and in the related publications to calculate the iron losses. The LS model aims to take into account the minor loop and high-frequency hysteresis losses [39]. Even though the additional losses are taken into account, there are still differences between the measurements and the FEM [46].

In this doctoral thesis and in Publication I, iron losses in load and no-load operation in a 1600 $min^{-1}$ permanent magnet wind power generator are investigated. The simulated machine is a 3 MW PMG equipped with embedded magnets. Such a design has inverse saliency ($L_q > L_d$). The quadrature axis flux increases the time harmonic content of the stator flux density under a load, and with low-height stator yokes the higher flux densities increase the iron losses. That is why the flux density of the stator yoke has to be kept below 1.5 T.

## 1.3 Additional losses in the supporting structures

Supporting structure losses are produced mainly by the eddy currents caused by the end-winding flux in the end region on the structural parts (clamping ring and finger plate, in Fig. 3), which hold the machine together. In addition, the housing may be subjected to additional losses if the stator yoke is saturating.

Clamping ring constructions can be found in different shapes and materials, and therefore, the losses of the clamping ring are highly dependent on the design. Therefore, to obtain accurate results, 3D finite element methods have to be used. Several papers treat the clamping ring and finger plate losses [52]–[72] mainly by applying 3D methods; some, however, use a combination of 2D and 3D [52], [72]. One paper even introduced a combination of analytical calculation and a 3D FEM [60], and finally, compared them with the measurements.

Finger plate and clamping ring losses can be minimized by replacing construction steel with stainless steel. The losses in the housing that surrounds the machine can be avoided by correct yoke dimensioning and by keeping the flux density of the stator yoke below 1.5 T. The housing losses are linked with the saturation effects as discussed in the next section on

additional losses in the windings. When saturation of iron takes place, many additional loss components will increase exponentially.

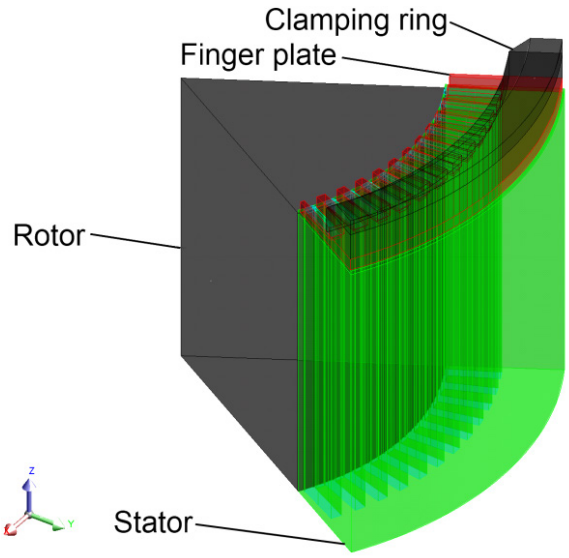


Fig. 3. One pole of the calculated machine with a finger plate and a clamping ring (Publication II).

According to Publication II, if construction steel is used, the losses in the clamping ring and the finger plate of a 3 MW 1600 $min^{-1}$ PM generator are close to 0.1%. Despite the seemingly small loss in efficiency, it should be noted that with a 4000 h annual load factor, the lost production is worth €770 in a year at the energy price of 80 €/MWh. This justifies the use of the expensive stainless steel. The payback time for the customer would be about five to six years if stainless steel were used instead of construction steel. It should be noted that even such a small improvement is of significance when pursuing highly efficient electrical machines.

## 1.4 Additional losses in the windings

Frequency converters have made it possible to use over 50 or 60 Hz frequencies in electrical machines. This leads to extra eddy current losses in the windings if losses are not minimized. The accurate evaluation of AC resistance losses in a machine is important [89], [90] especially in low-voltage high-speed (1500 rpm) multi-megawatt wind mill generators. In these generators, DC copper losses account for about 20–30% of all the losses (0.8–1% of the input power), and with an inappropriate design, AC copper losses are easily twice the DC copper losses when the power frequency is 80–100 Hz.

The reason for the above is the low number of turns. The conductor height is high (even 12–14 mm), which in turn attracts eddy currents if not reduced properly. Using preformed windings and a double-layer design naturally minimizes harmful eddy currents by transposing the winding at the end winding, but this may not suffice in all cases. Therefore, the use of Roebel bars or litz wires may come into question. In a Roebel bar the principle is about the same as in the litz wire, but a Roebel bar is made from square copper conductors

that are transposed ideally in the slot regime. The bars have to be connected in the end-winding area to complete the winding. In order to avoid the use of expensive Roebel bars and litz wires, an accurate analytical solution is needed to evaluate the losses of the form-wound windings. Analytical methods have been developed by Lyon [75], Richter [80], [81], Dowell [78], and Ferreira [91], [92]. Lyon and Richter concentrated on rotating electrical machines whereas Dowell and Ferreira focused on transformers. Papers [93]–[106] have developed and presented methods for more accurate calculation of eddy currents.

Figure 4 illustrates the main phenomena associated with the use of stranded conductors. Eddy currents are produced by the skin effect and the proximity effect. The skin effect is caused by the flux of the conductor, and the proximity effect is caused by the conductor next to it. Often, the proximity effect dominates. The skin effect and the proximity effect produce two currents; the strand-level eddy current that circulates mainly inside a solid conductor in slot-bound areas, and circulating currents that flow between the parallel strands. The proximity effect is always present in multilayered windings [104], [105].

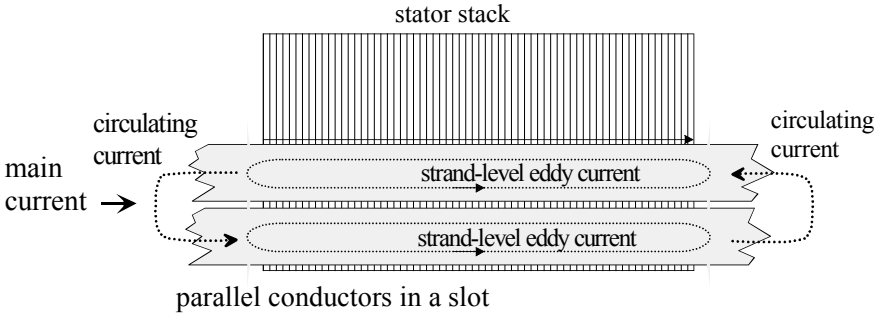


Fig. 4. Schematic illustrating the main current, the strand-level eddy current, and the circulating current in the case of two parallel nontransposed strands in a slot (Publication II).

Eddy currents can be minimized by dividing the conductor into smaller parallel and transposed conductors. In electrical machines with form-wound windings, this means placing the parallel strands on top of each other. With no transposing, this in turn produces circulating currents between the parallel strands as a result of skin and proximity effects. The circulating currents can be minimized by transposing the strands so that in an ideal case, every strand gets the same amount of flux. This will cancel out all the circulating currents but not the strand-level eddy currents. The drawback of all of these minimization methods is that the DC resistance increases because of the additional insulation between the strands.

Roebel bars are usually used in large multi-megawatt machines instead of form-wound windings if AC losses were otherwise too high. Now, high-power litz wires are available that could replace Roebel bars in some cases. Traditionally, a litz wire consists of insulated strands that travel everywhere in the slot cancelling out the circulating currents between the strands and leaving only the strand-level eddy currents. An ideal transposition also makes the winding slightly longer increasing the DC resistance. Now, a new type of litz wire has become available in the market. These litz wire with noninsulated strands are inexpensive enough to be used in multi-megawatt electrical machines. However, the favorable price comes at the expense of a lack of insulation between the strands. The idea of the litz wire with noninsulated strands is that the connection between the strands is weak. Xu measured that in the worst case, the interstrand resistivity in a litz wire with noninsulated strands was 1000 times the resistivity of solid copper [119]. Furthermore, litz wire makes the installation

of the wire inexpensive. The winding can be made without connections in the end-winding area, and therefore, does not require extra insulating work. The drawback is that it needs an extra support system to withstand the radial forces during operation.

Litz wires with insulated subconductors are used in high-frequency applications such as transformers [97]–[99], [107]–[113], induction cooking appliances [114], [115], and in HTS (high temperature superconductor) machines with superconducting excitation [116], [117]. There are several analytical calculation methods developed for litz wires [97]–[99], [107]–[113] and form-wound windings [75], [78], [80], [81] [91]–[106] to evaluate the AC resistance factor. Probably the most cited method concerning the AC resistance is Dowell's equation [78], which can be used to evaluate round wires [99], form-wound windings [78], and litz wires [118].

A drawback of all of these models is that they do not directly consider the end-winding effect on the AC resistance factor, even though it is acknowledged in [100]. Without ideal transposition, an end winding has mainly two current components flowing; a circulating current and the main current. That is, if the end-winding inductance and the strand-level eddy currents are neglected. Without knowing the amount of circulating current, the end-winding AC resistance factor is very difficult to calculate accurately in form-wound windings if ideal transposition is not satisfied. Although Richter [80], [81] has developed a model to take end winding effect into account afterwards, the model does not take the circulating currents into consideration. Furthermore, the number of parallel strands and the end-winding length affect the amount of circulating currents. This is demonstrated in Publication IV.

In Sullivan's litz wire model [107]

$$k_\mathrm{r} = 1 + \frac{\pi^3 \omega^2 \mu_0^2 z_\mathrm{Q}^2 n^2 d_\mathrm{s}^6}{3 \times 768 \rho^2 b_\mathrm{b}^2}, \tag{3}$$

where $\omega$ is the angular frequency of a sinusoidal current, $\rho$ is the resistivity of the conducting material, $\mu_0$ is the vacuum permeability, $z_\mathrm{Q}$ is the number of turns in a slot, $n$ is the number of strands, $d_\mathrm{s}$ is the diameter of each strand, and $b_\mathrm{b}$ is the slot width, the end winding can be taken into account quite easily because of the lack of circulating currents in

$$k_\mathrm{r} = \left( 1 + \frac{\pi^3 \omega^2 \mu_0^2 z_\mathrm{Q}^2 n^2 d_\mathrm{s}^6}{3 \times 768 \rho^2 b_\mathrm{b}^2} \right) \frac{l_\mathrm{stack}}{l_\mathrm{turn}} + \frac{l_\mathrm{end-winding}}{l_\mathrm{turn}}, \tag{4}$$

where $l_\mathrm{stack}$ is the length of the winding inside a stack, $l_\mathrm{end\text{-}winding}$ is the length of the end winding, and $l_\mathrm{turn}$ is the length of the turn.

## 1.5 Additional losses in the magnets

The previous additional loss component can be found in all electrical machines, but the eddy current losses in the magnets occur only in permanent magnet machines. These losses are not discussed in detail in this thesis, but are only described in brief below.

NdFeB magnets have made permanent magnet machines more desirable because of their high energy density [122]. Even though they were introduced already in the 1980s, their price and

availability have hindered their use in permanent magnet machines [122]. Nowadays, if a high-power permanent magnet machine is made, it is equipped with NdFeB magnets.

Eddy current losses in rotor surface permanent magnets are caused by permeance harmonics and winding harmonics [123]–[131]. Winding harmonics can be divided into space harmonics and time harmonics [125], [131]. Eddy current losses can also occur in the magnet retaining sleeve if fitted [128]. The eddy current losses in the sleeve depend highly on the material used. Two materials commonly used are stainless steel and carbon fiber. Stainless steel has a fairly low conductivity (in the range of 0.8–1.6 MS/m) and acceptable thermal properties. Carbon fiber sleeve, on the other hand, has a low axial conductivity but poor thermal properties.

The eddy current losses of the magnets are often neglected because they have only a slight effect on the efficiency but put the magnets in danger of demagnetization instead. Permanent magnets are usually difficult to cool, and the lack of sufficient cooling can lead to overheating and thereby demagnetization of the magnets [123]–[126], [128]–[132].

To get an accurate value for the eddy current losses, a 3D FEM simulation has to be performed [133]. However, if eddy current losses are to be analyzed analytically, many approximations have to be made [127]. The losses depend on the geometry and windings of the machine. Consequently, an exact analytical solution is difficult to establish (see e.g. [127]), and therefore, approximate models have been developed for the purpose [127] .

## 1.6 Outline of the thesis

The target of this doctoral thesis is to define the sources of some of the additional losses occurring in low-voltage high-power PM electrical machines and to find ways to minimize them.

The author of this doctoral thesis is the principal author and investigator in Publications I–IV, and is solely responsible for the scientific contribution in the papers and the introductory section of the thesis.

**Publication I** shows that if the iron losses of a permanent magnet machine with embedded magnets ($L_q$>$L_d$) are defined by applying a standard-based no-load test, the stator iron loss will be underestimated. When the machine is running at load, the quadrature-axis armature reaction modulates the air gap flux density thereby amplifying the 3$^{rd}$ and 5$^{th}$ harmonics. The basic idea of Publication I is that by dimensioning the stator yoke magnetically large enough, the iron loss caused by these harmonics can be minimized. In fact, the issue has not been analyzed for any traditional material so far, but the general guideline has only been to apply a low enough flux density in stator dimensioning. Hence, in this paper, the issue is now analyzed to such detail that even a person without in-depth knowledge in electrical machine design is able to comprehend the rationale behind the proposed guidelines.

**Publication II** is continuation of Publication I. It provides a detailed analytical approach to the problems associated with the calculation of losses in finger plates and clamp rings. The finger plate and clamp ring materials under study are S355 and nonmagnetic stainless steel used in the industry. If the target is to minimize the losses in the finger plates and the clamp rings, stainless steel has to be used for them both. The publication suggests that when

considering these two materials in particular, the use of different material combinations has to be calculated for each case individually; in other words, the calculation cannot be simplified or speeded up by applying values obtained from previous calculations. A high flux density in the stator yoke leads to a situation where the magnetic voltage of the support structure parts increases, and consequently, the iron parts of the support structures become an effective path for magnetic flux. This, again, leads to additional losses in the support structures. Hence, targeting cost-efficiency in the magnetic circuit design may have an adverse impact on the total machine efficiency.

**Publication III** addresses the resistance factor of the litz wire used in low-voltage PMGs. In this paper, measurements and a FEM simulation are made to evaluate different litz wires and their use in these kinds of applications. It is shown that modern litz wires can be successfully used in multi-megawatt low-voltage machines even up to 120 Hz to avoid the adverse effects of eddy currents and circulating currents.

**Publication IV** concentrates on the losses in form-wound windings and their analytical calculation. An accurate analytical model is developed for a single-layer form-wound winding with and without a 180 degree twist in the end winding.
This doctoral thesis consists of an introductory part, a summary of the journal publications, and four original journal publications. The introduction is divided into three chapters providing conclusions of the relevant publications.

Chapter 1: An introduction to the research topic is given. Then additional loss components are described in detail.

Chapter 2: Publication I, Publication II, Publication III, and Publication IV are analyzed in brief.

Chapter 3: The conclusions of this doctoral thesis are discussed, and suggestions are given for future work.

## 1.7 Scientific contribution

The main contribution of this doctoral thesis is the identification of additional losses in the support structure, the housing, the stator iron, and the windings. The scientific contributions of the thesis can be summarized as follows:

- The study analyzes and describes the mechanisms by which the quadrature-axis armature reaction of a salient pole permanent magnet machine and the stator yoke thickness affect the stator iron losses. Because of the $3^{rd}$ and $5^{th}$ harmonics, a thin stator yoke thickness results in significantly different losses measured at no load or under load.

- Losses in the clamping ring and the finger plate are modeled and simulated by the 3D FEM using either structural steel or stainless steel as construction materials. With construction steel the additional losses are 0.08% of the input power, whereas with stainless steel the losses are almost zero. If the stator yoke flux density exceeds 1.5 T,

also a significant amount of support housing losses will occur, thereby increasing the amount of additional losses.

- The use of litz wires in high-power, high-speed, low-voltage wind turbine generators is studied. Some improvements are suggested to the analytical calculation of litz wires to take end-winding resistance into account. A new equation to evaluate the AC resistance factor in litz wires is proposed. The measurement of the AC resistance factor is very sensitive to errors because of the very low resistance and the large inductance. Therefore, a simple measurement device is developed to measure the AC resistance factor.

- An analytical equation is developed to evaluate the AC resistance factor in a single-layer form-wound winding used in the frequency range of 0–200 Hz in electrical machines. A maximum error of 5% is achieved by incorporating the number of parallel strands and the end-winding length to Dowell's equation. Without these modifications, the errors could be as large as 150%.

# Chapter 2

# Publications

This chapter provides an overview of the four journal papers.

## 2.1 Publication I

A 3 MW salient pole PMG with embedded magnets and a nominal speed of 1600 $min^{-1}$ (Figs. 1 and 5) is studied in this paper. A re-evaluation of the traditional guideline value is made for the stator yoke dimensioning. Iron losses can be minimized by a correct selection of the no-load flux density in the yoke, and thus, by the correct dimensioning of the stator yoke height. With over 50 Hz machines, the use of a thinner material is preferred to a better-quality material. The study is made by varying the thickness of the stator yoke when all other dimensions remain unchanged. The machine is simulated in the Flux2D time stepping mode. Current sources are used to feed the external circuit that is coupled with the geometry. Iron losses are calculated by the Loss Surface (LS) model [48] and Bertotti's model [49] included in the Flux2D. In addition, the radial and tangential flux density components are analyzed with their harmonics in 11 points.

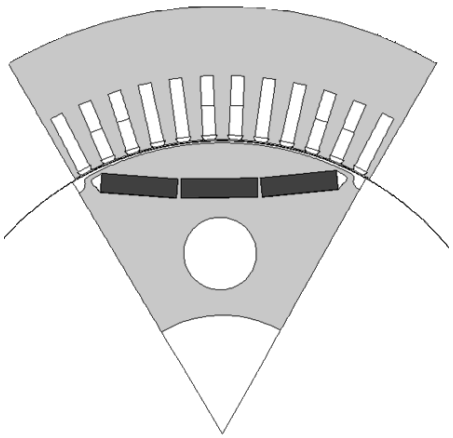

Fig. 5. Geometry of the investigated PMG (Publication I).

Table II (Publication II) shows the simulated iron losses calculated by the LS model that is included in the Flux2D program. The higher the height of the iron yoke is, the less high-frequency eddy current losses are produced. The dependency is nonlinear, and the influence

of the higher time harmonics plays a significant role in this kind of a salient pole machine with a large q-axis armature reaction. It can also be seen that the material thickness and the specific losses have a significant effect on the yoke losses. The M330 has higher losses than M400 probably because the M330 iron sheet is thicker, and therefore, produces more eddy current losses even though otherwise it is better than the M400 steel. This is possible when the frequency exceeds 50 Hz. The M330-65A has a 3.3W/kg maximum loss at 1.5 T and 50 Hz and M400-50A 4 W/kg in similar conditions. The hysteresis loss is typically smaller than the eddy current loss at 50 Hz. As the eddy current loss is proportional to the square of the lamination thickness, it is obvious that in the 0.65 mm thick M330-65A the proportion of the eddy current loss gets higher than in the 0.5 mm thick M400-50A. The hysteresis loss is directly proportional to the frequency while the eddy current loss is proportional to the square of the frequency. Therefore, a low-loss material can have more losses than a high-loss material at a higher frequency. The same conclusion is made also in [134].

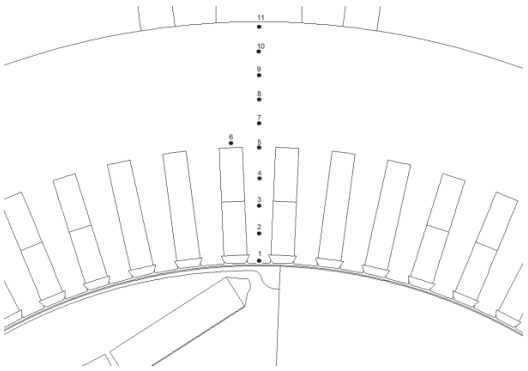

Fig. 6. Location of the points where the tangential and normal components of the flux are observed (Publication I).

TABLE II
STATOR IRON LOSSES WITH DIFFERENT STATOR DIAMETERS AND MATERIALS AT RATED LOAD (L) AND AT NO LOAD (NL), CALCULATED BY THE LS MODEL. THE AIR GAP DIAMETER OF THE 6 POLE MACHINE IS 3 MM AND THE TOTAL HEIGHT OF THE TEETH IS 67 MM (PUBLICATION I).

| Stator yoke height (mm) | 48 | 50.5 | 53 | 55.5 | 58 | 60.5 | 63 | 65.5 | 68 | 70.5 | 73 | 88 |
|---|---|---|---|---|---|---|---|---|---|---|---|---|
| Yoke material and yoke loss | | | | | | | | | | | | |
| L M330-65A (kW) | 14.1 | 14.1 | 14.0 | 14.0 | 13.9 | 13.7 | 13.4 | 13.1 | 12.7 | 12.3 | 12.0 | 11.2 |
| NL M330-65A (kW) | 11.0 | 11.0 | 11.5 | 11.9 | 12.5 | 12.7 | 12.8 | 12.7 | 12.7 | 12.3 | 12.0 | 10.5 |
| L M270-35A (kW) | 8.1 | 8.3 | 8.4 | 8.6 | 8.6 | 8.7 | 8.7 | 8.6 | 8.3 | 8.0 | 7.7 | 7.2 |
| NL M270-35A (kW) | 6.7 | 6.7 | 7.1 | 7.5 | 8.0 | 8.3 | 8.4 | 8.5 | 8.5 | 8.4 | 8.2 | 7.1 |
| L M400-50A (kW) | 12.0 | 12.0 | 12.0 | 12.1 | 12.1 | 12.0 | 11.8 | 11.6 | 11.3 | 11.0 | 10.8 | 10.1 |
| NL M400-50A (kW) | 9.7 | 9.7 | 10.1 | 10.5 | 11.1 | 11.3 | 11.4 | 11.3 | 11.3 | 11.1 | 10.9 | 9.9 |

Fig. 6 shows the location of the points where the radial and tangential flux densities are analyzed. Figures 7, 8, and 9 depict the total fundamental, tangential, and radial fundamental flux densities, respectively. The points from 1 to 5 are located in a tooth and points 6–11 in the stator yoke.

Instead, when a low-height stator yoke is used in comparison with a thicker stator yoke, the higher flux densities (Fig. 7) seem to be the reason for higher losses. The higher flux densities are mainly caused by a thinner yoke. With lower yoke heights, however, the harmonic flux densities under load become higher and the differences between the no-load and load iron losses in the yoke can get significantly higher. However, there is no direct link between the

harmonics and the losses. In particular, it would be misleading to differentiate the losses caused by different harmonics by superposition. However, the loss-surface model does not aim at evaluating the losses of different harmonics separately, but it is based on measurements and simulated flux densities.

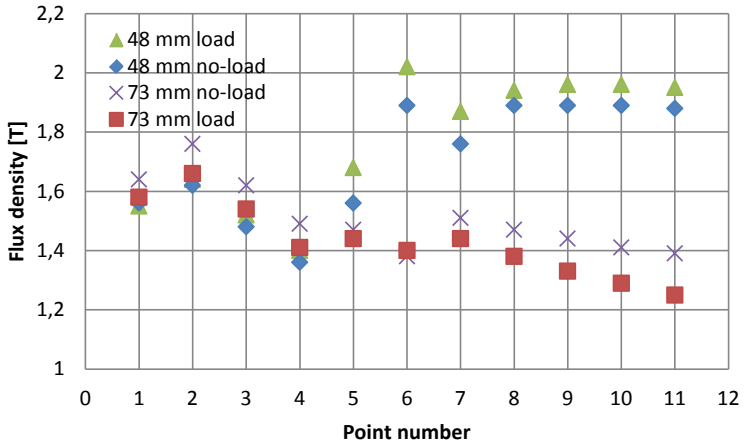


Fig. 7. Total fundamental flux density under load and at no load with the yoke thicknesses of 48 mm and 73 mm.

Figures 8 and 9 depict fundamental tangential and radial flux, respectively. The stator has mostly tangential flux (point 11), but towards point 6 the radial flux starts to increase gradually. This means that the flux is gets more rotational, thus causing more losses. Nevertheless, the radial flux is almost the same in all the cases and therefore does not explain the different losses between no load and load.

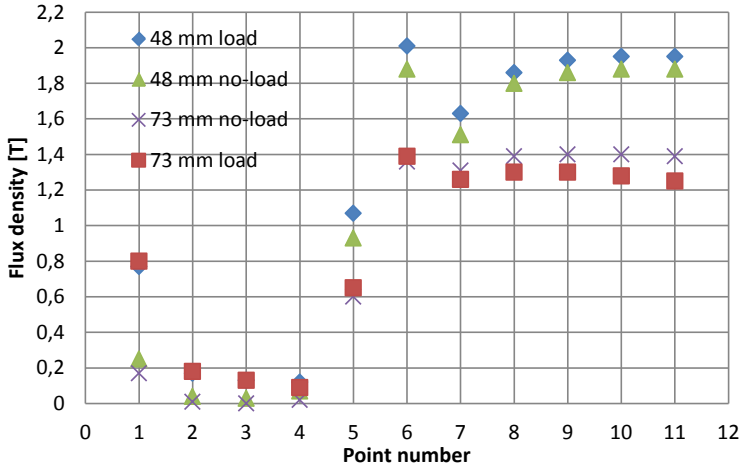


Fig. 8. Fundamental tangential flux density under load and at no load with the yoke thicknesses of 48 mm and 73 mm.

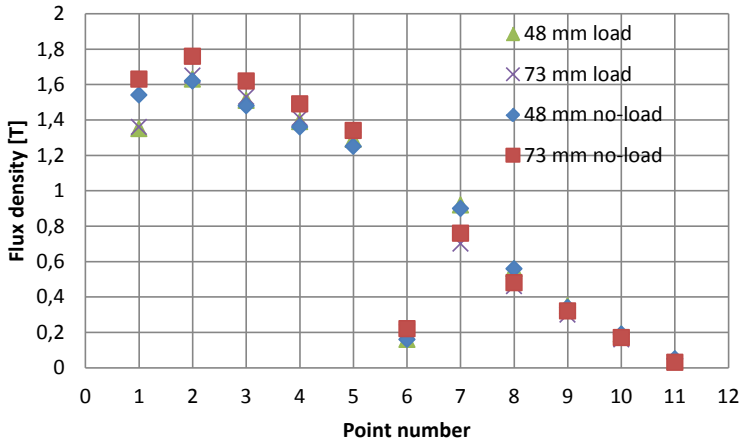


Fig. 9. Fundamental radial flux density under load and at no load with the yoke thicknesses of 48 mm and 73 mm.

Figures 10 and 11 demonstrate that under load the 3rd harmonics are much higher than at no load. This is caused by the quadrature-axis armature reaction and the modulating effect of the rotor construction. Even if the tangential harmonics are high in points 1–5, they affect the losses only slightly because the magnitudes of the flux densities are small. Hence, points 6–11 are of more importance because the flux densities are high (Fig. 8) and the load 3rd harmonic is high compared with no-load harmonics, which explains the difference between no load and load when the stator yoke thickness is the same.

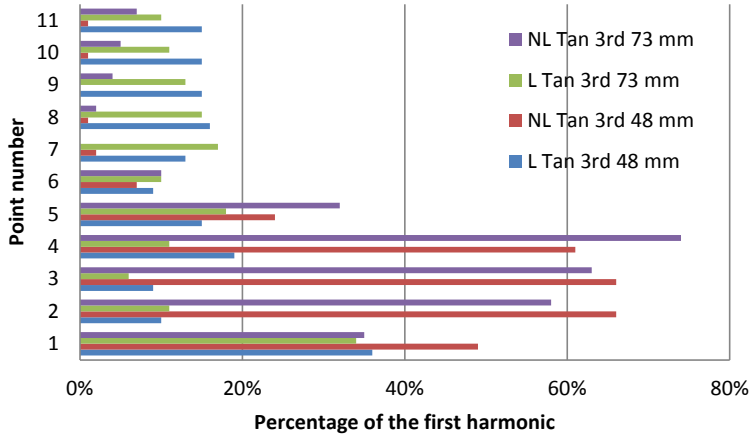


Fig. 10. Tangential flux density of the 3rd harmonic under load and at no load with the yoke thicknesses of 48 mm and 73 mm.

Based on the results given in Figs. 7 and 10 and Table II, it seems that when the stator yoke height is 48 mm at load, higher harmonics along with higher flux densities in the stator yoke compared with the no-load case are the main cause of additional losses in the iron. With the 73 mm yoke height instead, the higher harmonics (Fig. 10) and the lower flux densities (Fig. 7) at load in the stator yoke result in similar losses both at no load and under load.

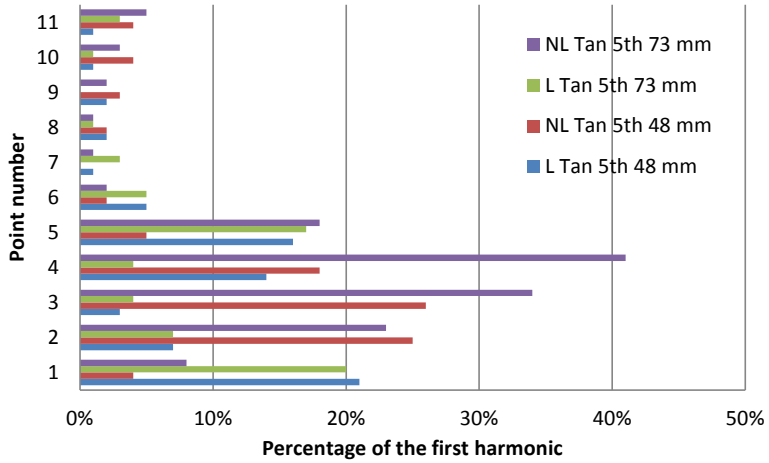


Fig. 11. Tangential flux density of the 5th harmonic under load and at no load with the yoke thicknesses of 48 mm and 73 mm.

Now, the radial flux densities are of more importance in points 1–5, because the teeth carry mostly radial flux (Fig. 9). In Figs. 12 and 13, the 3rd and 5th harmonics are much higher when the generator is loaded than at no load, which partly explains the differences between no load and load losses when the thickness remains the same. In Fig. 12 there is only a slight difference between the different yoke thicknesses.

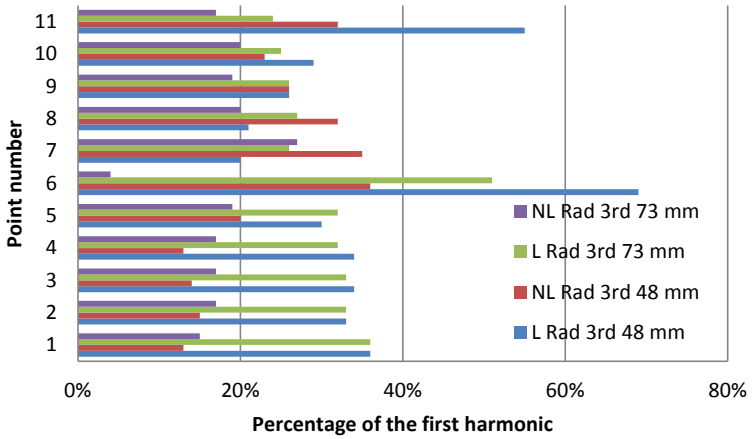


Fig. 12. Radial flux density of the 3rd harmonic under load and at no load with the yoke thicknesses of 48 mm and 73 mm.

In Fig. 13 there are some differences between different yoke thicknesses, which would contribute to different losses.

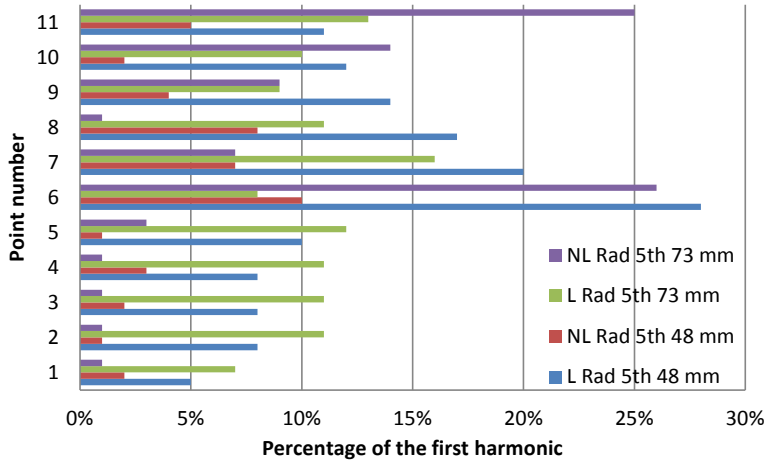


Fig. 13. Radial flux density of the 5th harmonic at load and no load with the yoke thicknesses of 48 mm and 73 mm.

Figures 14 and 15 illustrate radial against tangential components. With a lower stator yoke height (48 mm), the flux path is more rotational, and when the stator yoke height is increased to 73 mm, the flux path becomes more elliptical. The rotational flux also contributes to the additional losses around point 5, but in every other point the ratio of radial and tangential flux densities remains almost the same.

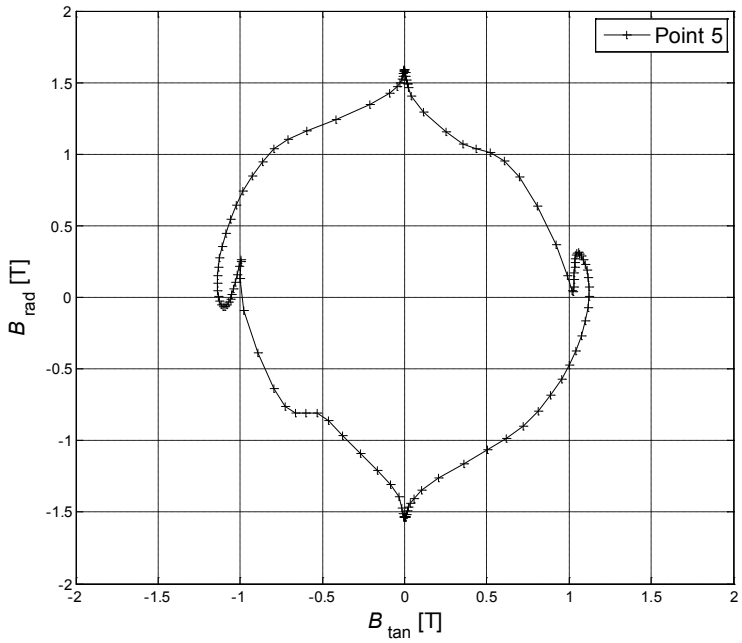


Fig. 14. Flux density rotational behavior over one period with 48 mm as the stator yoke height.

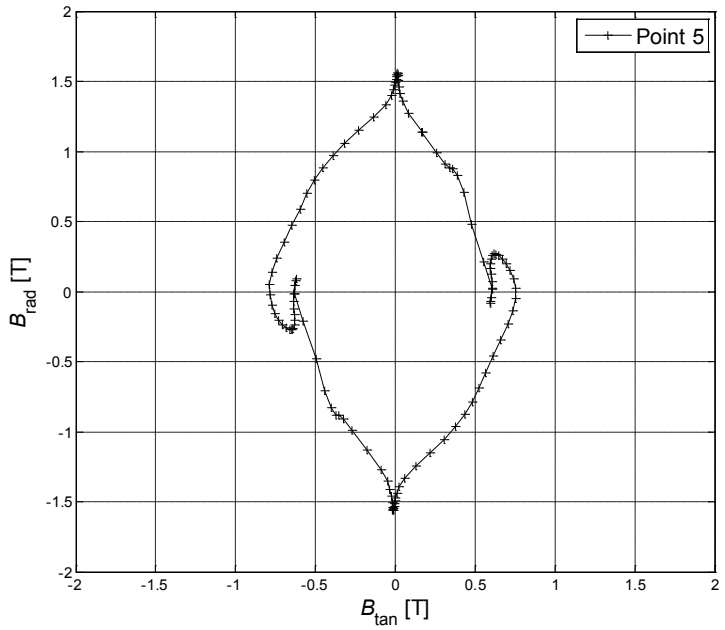


Fig. 15. Flux density rotational behavior over one period with 73 mm as the stator yoke height.

As a conclusion, the quadrature-axis armature reaction increases the 3rd and the 5th harmonics in the teeth and the 3rd harmonic in the stator yoke, and mainly accounts for the additional losses in the stator iron. This explains along with the higher flux densities the differences between the losses under load and at no load. The loss differences between the materials mainly result from the thickness of the iron sheets (lower eddy current losses) and less from the material quality (M330, M400). In general, the losses are higher with low-height yokes, which is a natural result of higher flux densities. With a correct dimensioning, the load and no-load iron losses are almost the same. Then iron losses can be measured also at no load.

## 2.2 Publication II

In this paper, the stator support structure of the same 3 MW PMSG (Fig. 3) is studied. The support structure that holds the stator stack consists of a clamping ring and a finger plate at both ends of the stator stack (Fig. 3). In 50 Hz machines, the finger plate and the clamping ring are usually made of construction steel, for instance S355JO/EN 10025 or nonmagnetic stainless steel. The end-winding field produces eddy current losses in the clamping ring and the finger plate. The machine frame structure (housing) is also used to fasten the machine to the base plate. Eddy current losses may also occur if the main flux can penetrate the housing from the stator yoke. According to the results, the losses start to increase if the flux density of the stator yoke exceeds 1.5 T (Table III, Publication II).

TABLE III
POWER LOSS IN THE HOUSING AND IN THE WELDED PARTS WITH DIFFERENT STATOR DIAMETERS (PUBLICATION II).

| Stator diameter [mm] and yoke height [mm] | Maximum flux density at the stator yoke [T] | Housing power loss [W] | Percentage of the output power [%] |
|---|---|---|---|
| 850, 48 | 1.85 | 4275 | 0.14 |
| 855, 50.5 | 1.79 | 2094 | 0.07 |
| 860, 53 | 1.75 | 1885 | 0.06 |
| 865, 55.5 | 1.72 | 1029 | 0.03 |
| 870, 58 | 1.67 | 538 | 0.02 |
| 875, 60.5 | 1.62 | 249 | 0.01 |
| 880, 63 | 1.56 | 101 | 0.00 |
| 885, 65.5 | 1.52 | 35 | 0.00 |
| 890, 68 | 1.44 | 11 | 0.00 |
| 895, 70.5 | 1.38 | 3 | 0.00 |
| 900, 73 | 1.27 | 2 | 0.00 |
| 910, 78 | 1.18 | 1 | 0.00 |
| 920, 83 | 1.09 | 1 | 0.00 |
| 930, 88 | 0.97 | 0 | 0.00 |

Clamping ring and finger plate losses are studied by the Flux3D program. To obtain reliable results from the finite element loss analysis, there have to be at least two element layers in the skin depth. A fine mesh is built to accurately analyze the losses in the clamping ring and the finger plate. The results show that the losses are approx. 0.08% of the output power if construction steel is used and nearly zero with nonmagnetic stainless steel. Even such a small loss has to be considered when pursuing highly efficient machines.

## 2.3 Publication III

New heavy-duty litz wires offer an interesting alternative to low-voltage, high-power machine windings. Such a material might be very suitable to be used in 3 MW 690 V wind power generators as they have very few conductors in a slot and are, therefore, vulnerable to problems caused by skin and proximity effects.

In this paper, several litz wires are measured and compared both with an analytical model and 2DFEM results. A motorette was built to test the losses in the laboratory. It is difficult to measure the AC resistance from litz wires; the test motorette is very inductive and the phase angle between the current and the voltage is about 87 degrees. Thus, the results are very sensitive to measurement errors. Measurement errors may result for instance from a weak connection close to the measuring point and from inappropriate (imprecise) measurement equipment. The requirement for the measurement accuracy is 0.1 degrees in the angle between current and voltage, which is achieved by building a simple measurement device. The accuracy requirement is because of 0.5 degree error would result in AC resistance factor about 0.25 error at 50 Hz, which is quite a large error. In addition, end-winding resistance is included in the analytical model in Eq. (4).

From the easy manufacturing point of view, perhaps the most interesting target is the litz wire with noninsulated strands. Two different litz wires of this kind are analyzed. It is also studied whether the impregnation has an effect on the AC resistance of a litz wire with noninsulated strands. Therefore, the samples are measured both before and after the VPI process. One litz wire shows a reduction in the AC resistance after impregnation while the other did not. Even

though the results are only indicative, they show that in some cases the impregnation affects the resistance, and hence, further research is needed.

Further, an oxidation-insulated litz wire was measured, and according to the results, it performed better than the litz wire with noninsulated strands, which was expected. Finally, the results also show that when comparing the FEM results of the form-wound winding with the measured litz wire with noninsulated strands used in the actual machine, there is a small difference in the AC resistance factor. This indicates that litz wires with noninsulated strands can be used instead of a form-wound winding, if needed. Such a winding material is, from the viewpoint of practical winding work, very efficient as there is no need to remove any insulation from the numerous conductor surfaces when preparing joints.

## 2.4 Publication IV

In this publication, an accurate analytical model to calculate the AC resistance factor is developed for single-layer form-wound windings used in the frequency range of 0–200 Hz in electrical machines. There is a need to propose such an approach, because in the literature, ideal transposition along several slots is usually assumed meaning that there are no circulating currents in the winding. However, circulating currents often cause problems in form-wound windings, which are not necessarily suitable for ideal transposition and therefore, suffer from circulating currents.

The model in question is also based on Dowell's model [78]. Dowell's model is used to calculate the strand-level eddy currents and the circulating current separately and to add them up with the DC losses to get the total winding losses. A maximum error of 5% is achieved by incorporating the number of parallel strands and the end-winding length into Dowell's equation. Without these modifications, the errors could be even as large as 150%.

In order to accurately calculate the AC resistance factor, the amount of circulating currents in the windings has to be known. The circulating currents travel through the whole winding whereas strand-level eddy current travels, in practice, only on the slot length.

Also the end winding significantly affects the total AC resistance factor and, therefore, has to be included in the model. In addition, the number of parallel strands affects the amount of circulating currents.

The proximity effect in Dowell's model is corrected with an equation that includes the end-winding resistance and the number of parallel strands. The proximity effect has to be adjusted because the circulating currents differ in different winding configurations, which in turn seem to affect the proximity effect the most.

The results are obtained by calculating a circulating current factor $k_{\mathrm{circ}}$ and a strand-level eddy current factor $k_{\mathrm{strand}}$ from the 2D FEM results. The total eddy current factor is then calculated by the following equation

$$k_{\mathrm{total}} = k_{\mathrm{strand}} + k_{\mathrm{circ}} + 1. \qquad (5)$$

Then, analytical equations are obtained by a curve fitting method. The results for different strand numbers and different end-winding lengths are matched with the corresponding FEM

results. Additions to Dowell's model are $r_{\text{circ}}$ and $r_{\text{strand}}$, which are used to calculate the circulating current factor and the strand-level eddy current factor separately. The developed analytical equations are presented in Publication III and in the following equations.

$$k_{\text{strand}} = \xi\left[\frac{\sinh 2\xi + \sin 2\xi}{\cosh 2\xi + \cos 2\xi} + r_{\text{strand}}\frac{2(z_{\text{Q}}^2 - 1)}{3}\frac{\sinh \xi + \sin \xi}{\cosh \xi + \cos \xi}\right] - 1 \tag{6}$$

where

$$r_{\text{strand}} = n_{\text{s}}\left(-\frac{l_{\text{stack}}}{l_{\text{turn}}}0.1 + 0.4\right) + \frac{l_{\text{stack}}}{l_{\text{turn}}}1.065 \tag{7}$$

where $n_{\text{s}}$ is the number of parallel strands in a turn, $l_{\text{stack}}$ is the length of the copper conductor in a slot in a turn, and $l_{\text{turn}}$ is the length of the turn.

$$k_{\text{circ}} = \xi\left[\frac{\sinh 2\xi + \sin 2\xi}{\cosh 2\xi + \cos 2\xi} + r_{\text{circ}}\frac{2(z_{\text{Q}}^2 - 1)}{3}\frac{\sinh \xi + \sin \xi}{\cosh \xi + \cos \xi}\right] - 1 \tag{8}$$

where

$$r_{\text{circ}} = n_{\text{s}}\frac{l_{\text{stack}}}{l_{\text{turn}}}0.06 + \frac{l_{\text{stack}}}{l_{\text{turn}}} - 0.38\,. \tag{9}$$

In addition, a model for a transposed winding is developed. When the winding is transposed in the other end of the winding, every strand is subjected to an equal amount of stray flux, and therefore, the circulating current factor becomes zero. With Eq. (7) the first term of the equation is related to the circulating currents, and can therefore be neglected. After the changes, the transposed winding can be calculated as follows:

$$k_{\text{total}} = k_{\text{strand}} + 1\,, \tag{10}$$

$$r_{\text{strand-180}} = \frac{l_{\text{stack}}}{l_{\text{turn}}}1.065\ . \tag{11}$$

# Chapter 3

# Conclusions and future work

## 3.1 Conclusions

In this doctoral thesis, some additional load losses were studied in a 3 MW permanent magnet wind power generator with embedded magnets, and thereby, with significant saliency. Three key topics were under study:

- The effects of flux density modulation on the stator losses and especially on the stator yoke losses, caused by the rotor construction.
- Losses of the stator stack supporting elements that are caused by the end region flux and the losses in the stator housing caused by the stator yoke saturation.
- Joule losses produced in the stator windings in form-wound windings and in litz windings; the effects of transposing, circulating currents, eddy currents and the proportion of the end winding.

Publication I showed that the flux density of the stator yoke has to be kept below 1.5 T in salient pole machines to avoid excess losses in the yoke and in the housing. Higher losses in the stator iron under load compared with no-load are produced because of the $3^{rd}$ and $5^{th}$ spatial harmonics. Furthermore, eddy current losses seem to dominate over hysteresis losses in the stator iron. This is explained by the fact that the lower-quality thin lamination material (M400-50A) has lower losses than the higher-quality (M330-65A) with thicker laminations. Therefore, thin sheets are recommended in the design process of salient pole machines over a higher-quality material to minimize stator iron losses in over 50 Hz machines.

In this study, the additional losses in the stator yoke varied significantly. However, the additional load loss in the case of a thin stator yoke (48 mm) compared with a thick stator yoke (88 mm) and the M330-65A material was 3.1 kW corresponding to 0.1% of the output power of the generator. Furthermore, additional load losses were also found in the stator stack support system. The analysis on the stator stack support structure indicated that the losses can be significant in the clamping rings and the finger plates, in this case about 0.08% of the output power when using construction steel. This loss can be removed almost completely by using nonmagnetic stainless steel. The information can be used as a guideline in the machine design process while estimating support structure losses.

The measurement of AC resistance in electrical machines is a complicated task. Because of the low voltage (0.2 V at minimum), the connections have to be solid. The measurement accuracy of the phase between the voltage and the current has to be below 0.1% owing to the

highly inductive load, where the phase is close to 90 degrees. This can be achieved with an accurate current shunt that minimizes the phase shift error in the current measurement. Further, the measurement also had a poor signal-to-noise ratio that was caused by the electromagnetic interference coupled to the measurement via the physically large inductor. This was overcome by developing a simple measurement device. According to the results for large electrical machines, litz wire with 630×0.5 mm thick noninsulated strands can be used as a winding material instead of double-layer form-wound windings. In the litz winding design of the 3 MW generator, the additional load loss was at the same level with the form-wound winding at the nominal frequency.

An improvement to the analytical evaluation of litz wires was achieved, and an addition to the existing model was suggested taking into account the end-winding resistance in the calculation of the AC resistance factor.

Finally, an accurate analytical calculating model was developed for the evaluation of losses in single-layer form-wound windings. A modification to the existing model was proposed with an inclusion of the number of strands and the end-winding length. The existing model was only valid for the active length of the machine, and because of the circulating currents between the strands, it is extremely difficult and inaccurate to include the end-winding losses separately in the model. Circulating currents pass through the whole winding, which means that the strand-level eddy current losses and circulating current losses have to be calculated separately and summed with the DC losses to obtain the total winding loss factor.

According to the results in these four journal papers, the additional losses of a machine cannot be fixed to a certain percentage of the input power as the IEC-34 has been suggesting since the 1980s [27]. This is because the additional losses depend on many aspects in the design process such as the material, saturation effects, and the winding design. Therefore, it would be incorrect to assume that a certain fixed value is always valid. The results achieved in this doctoral thesis support this argument: In Publication I, the losses depend on the stator yoke thickness (saturation effect). Again, in Publication II, the housing losses depend on the stator yoke thickness (saturation effect), while the clamping ring and finger plate losses depend on the material selection. Finally, in Publications III and IV, the winding losses depend on the design of the winding. A fixed value could be introduced if the machine design were standardized, but as long as it is not, the amount of additional losses are design-dependent losses. However, with the modern design methods, the losses can be kept at a very low level (<0.5% of the output power).

This doctoral thesis provides suggestions and guidelines as well as a modified analytical model in order to better estimate and minimize additional losses in electrical machines.

## 3.2 Suggestions for future work

The results from the impregnation effect tests were indicative only, and further research is needed to determine the optimal insulation construction to achieve the optimum AC resistance factor. It would be interesting to study how the impregnation affects the resistance in litz wires with noninsulated strands. This would require more samples with different strand sizes and insulation constructions.

A model to evaluate the AC resistance factor in a single-layer form-wound winding could be developed further by constructing a model for a double-layer form-wound winding.

# References


[1] A.A. Jimoh, R.D. Findlay, and M. Poloujadoff, "Stray Losses in Induction Machines: Part I, Definition Origin and Measurement," *IEEE Trans. Power App. Syst.,* vol. PAS-104 , no. 6, pp. 1500–1505, 1985.

[2] F. Iov, M. Ciobotaru, and F. Blaabjerg, "Power electronics control of wind energy in distributed power systems," in *the 11th Int. Conf. Optimization of Electr. and Electronic Equip.*, *OPTIM 2008*, pp. XXIX–XLIV.

[3] H. Li and Z. Chen, "Overview of different wind generator systems and their comparisons," *IET Renewable Power Generation*, vol. 2, no. 2, pp. 123–138, 2008.

[4] A.T. de Almeida, F.J.T.E. Ferreira, and J.A.C. Fong, "Standards for Super-Premium Efficiency class for electric motors," in *IEEE Tech. Conf. Ind. & Commercial Power Systems*, 2009, pp. 1–8.

[5] A.T. de Almeida, F.J.T.E. Ferreira, and J.A.C. Fong, "Standards for Efficiency of Electric Motors," *IEEE Ind. Appl. Mag.*, vol. 17, no. 1, pp. 12–19, 2011.

[6] I. Hofman, P. Sergeant, and A. Van den Bossche, "Influence of Soft Magnetic Material in a Permanent Magnet Synchronous Machine With a Commercial Induction Machine Stator," *IEEE Trans. Magn.,* vol. 48, no. 4, pp. 1645–1648, 2012.

[7] *IEEE Criteria for Class IE Electric Systems,* IEEE Standard 308, 1969. Rotating Electrical Machines—Part 2: Methods for Determining Losses and Efficiency of Electrical Machinery From Tests (Excluding Machines for Traction Vehicles) With Amendments 1: 1995 and 2: 1996, IEC Std 60 034-2, 1972.

[8] T. Bratoljic, "Currents induced in the inner Stator frame of large turbogenerators by the end-Zone field," *IEEE Trans. Energy Convers.*, vol. EC-1, no. 4, pp. 108–114, 1986.

[9] D.C., Hanselman and W.H., Peake, "Eddy-current effects in slot-bound conductors," In *IEE Proc. Electric Power App.*, vol. 142, no. 2, 1995, pp. 131–136.

[10] H. Seok-Hee, T.M. Jahns, and Z.Q. Zhu, "Analysis of Rotor Core Eddy-Current Losses in Interior Permanent-Magnet Synchronous Machines," *IEEE Trans. Ind. App.*, vol. 46, no. 1, pp. 196–205, 2010.

[11] H. Jussila, P. Salminen, M. Niemelä, A. Parviainen, and J. Pyrhönen, "Torque and inductances of concentrated wound permanent magnet machines," *Int. Review of Elect. Eng. (IREE)*, vol. 2, no. 5, pp. 704–710, Oct. 2007.

[12] R. Bharanikumar, A. Nirmal Kumar, and K.T. Maheswari, "Novel MPPT Controller for Wind Turbine Driven Permanent Magnet Generator with Power Converters," *Int. Review of Elect. Eng. (IREE)*, vol. 5, no. 4, Part A, pp. 1555–1562, Aug. 2010.

[13] R. Melicio, V. M. F. Mendes, and J.P.S. Catalao, "Modeling, Control and Simulation of Full-Power Converter Wind Turbines Equipped with Permanent Magnet Synchronous Generator," *Int. Review of Elect. Eng. (IREE)*, vol. 5, no. 5, Part A, pp. 397–408, Apr. 2010.

[14] S. M. Muyeen, R. Takahashi, T. Murata, and J. Tamura, "Miscellaneous Operations of Variable Speed Wind Turbine Driven Permanent Magnet Synchronous Generator," *Int. Review of Elect. Eng. (IREE)*, *vol. 3, no. 5*, pp. 912–921, Oct. 2008.

[15] M. Pinilla and S. Martinez, "Selection of Main Design Variables for Low-Speed Permanent Magnet Machines Devoted to Renewable Energy Conversion," *IEEE Trans. Energy Convers.*, vol. 26, no. 3, pp. 940–945, 2011.

[16] K. Atallah and W. Jiabin, "A Brushless Permanent Magnet Machine With Integrated Differential," *IEEE Trans. Magn.*, vol. 47, no. 10, pp. 4246–4249, 2011.

[17] N. Shuangxia, S.L. Ho, and W.N. Fu, "A Novel Direct-Drive Dual-Structure Permanent Magnet Machine," *IEEE Trans. Magn.*, vol. 46, no. 6, pp. 2036–2039, 2010.
[18] J. Aubry, H. Ben Ahmed, and B. Multon, "Sizing Optimization Methodology of a Surface Permanent Magnet Machine-Converter System Over a Torque-Speed Operating Profile: Application to a Wave Energy Converter," *IEEE Trans. Ind. Electron.,* vol. 59, no. 5, pp. 2116–2125, 2012.
[19] Pinilla, M., "Performance Improvement in a Renewable Energy Direct Drive Permanent Magnet Machine by means of Soft Magnetic Composite Interpoles," *IEEE Trans. Energy Convers.*, vol. 27, no. 2, pp. 440–448, 2012.
[20] L. Kaiyuan and E. Ritchie, "Torque Analysis With Saturation Effects for Non-Salient Single-Phase Permanent-Magnet Machines," *IEEE Trans. Magn.*, vol. 47, no. 6, Part: 2, pp. 1732–1738, 2011.
[21] J.A. Kinnunen, J. Pyrhonen, M. Niemelä, O. Liukkonen, and P. Kurronen, "Design of damper windings for permanent magnet synchronous machines," *Int. Review of Elect. Eng. (IREE)*, vol. 2, no. 2, pp. 260–272, Apr. 2007.
[22] M. Liserre, R. Cárdenas, M. Molinas, and J. Rodriguez, "Overview of Multi-MW Wind Turbines and Wind Parks," *IEEE Trans. Ind. Electron.*, vol. 58, no. 4, pp. 1081–1095, Apr. 2011.
[23] A. Mullane and M. O'Malley, "The Inertial Response of Induction-Machine-Based Wind Turbines," *IEEE Trans Power Syst.*, vol. 20, no. 3, pp.1496–1503, Aug. 2005.
[24] D. Baohua, S. Asgarpoor, and Q. Wei, "Voltage analysis of distribution systems with DFIG wind turbines," *IEEE Power Electron. and Machines in Wind Appl.*, *PEMWA 2009*, pp.1–5.
[25] M. Andriollo, M. De Bortoli, and A. Tortella, "Procedures for the additional losses assessment and analysis in high-efficiency induction machines," *International Conf. Clean Elect. Power (ICCEP)*, 2011, pp. 389–394.
[26] H. Polinder, F.F.A. van der Pijl, G.-J. de Vilder, and P.J. Tavner, "Comparison of direct-drive and geared generator concepts for wind turbines," *IEEE Trans. Energy Convers.*, vol. 21, no. 3, pp.725–733, Sept. 2006.
[27] N. Glew, "Stray load losses in induction motors: a challenge to academia," *Power Eng. J.,* vol. 12, no. 1, pp. 27–32, 1998.
[28] A.A. Jimoh, R.D. Findlay, and M. Poloujadoff, "Stray Losses in Induction Machines: Part II, Calculation and Reduction," *IEEE Trans. Power App. Syst.*, vol. PAS-104, no. 6, pp. 1506–1512, 1985.
[29] N. Glew, "Stray losses in induction motors-if only I knew where to start!," *IEE Half Day Colloquium on Testing of Elect. Machines* (Ref. no. 1999/161), 1999, pp. 1/1–1/3.
[30] Pyrhönen, J., Jokinen, T., and Hrabovcova, V., *Design of rotating electrical machines*, Chichester, UK: John Wiley & Sons, Ltd., 2008.
[31] K.K. Schwarz, "Survey of basic stray losses in squirrel-cage induction motors," Proc. Institution of Electrical Engineers, vol. 111, no. 9, pp. 1565–1574, September 1964.
[32] B.J. Chalmers, and A.C. Williamson, "Stray losses in squirrel-cage induction motors," *J. the Inst. Elect. Eng.*," vol. 9, no. 106, 1963.
[33] B.J. Chalmers, and A.C. Williamson, "Stray losses in squirrel-cage induction motors. Validity of the reverse-rotation test method," In *Proc. Inst. of Elect. Eng.*, vol. 110, no. 10, 1963, pp. 1773–1777.
[34] T.H Barton, V. Ahmad, "The measurement of induction-motor stray loss and its effect on performance," *Proc. IEE - Part C: Monographs*, vol. 105, no. 7, 1958, pp. 69–75.

[35] P. L. Alger, G. Angst, E. John Davies, "Stray-Load Losses in Polyphase Induction Machines," *Trans. the American Inst. Elect. Eng. Power App. and Syst., Part III.* vol. 78, no. 3, pp. 349–355, 1959.
[36] H.C. Karmaker, "Stray losses in large synchronous machines," *IEEE Trans. Energy Convers.,* vol. 7, no. 1, pp. 148–153, 1992.
[37] P. Richardson, "Stray losses in synchronous electrical machinery," *Journal of the Institution of Electrical Engineers - Part II: Power Engineering*, vol. 92, no. 28, pp. 291–301, 1945.
[38] R. L. Winchester, "Stray Losses in the Armature End Iron of Large Turbine Generators," *Trans. the American Inst. Elect. Eng. Power App. and Syst., Part III*. vol. 74, no. 3, pp. 381–391, 1955.
[39] A. Krings and J. Soulard, "Overview and Comparison of Iron Loss Models for Electrical Machines," *Int. Conf. and Exhibition Ecological Vehicles and Renewable Energies,* 2009.
[40] G. Diaz, C. Gonzalez-Moran, P. Arboleya, and J. Gomez-Aleixandre, "Analytical Interpretation and Quantification of Rotational Losses in Stator Cores of Induction Motors," *IEEE Trans. Magn.*, vol. 43, no. 10, pp. 3861–3867, 2007.
[41] M. Ranlof, A. Wolfbrandt, J. Lidenholm, and U. Lundin, "Core Loss Prediction in Large Hydropower Generators: Influence of Rotational Fields," *IEEE Trans. Magn.,* vol. 45, no. 8, pp. 3200–3206, 2009.
[42] A. Boglietti, A. Cavagnino, D.M. Ionel, M. Popescu, D.A. Staton, and S. Vaschetto, "A General model to predict the iron losses in inverter fed induction motors," in *Energy Convers. Congress and Exposition*, *ECCE 2009*, pp. 1067–1074.
[43] C.A. Hernandez-Aramburo, T.C. Green, and A.C. Smith, "Estimating rotational iron losses in an induction machine," *IEEE Trans. Magn*., vol. 39, no. 6, pp. 3527–3533, 2003.
[44] L. Yujing S.K. Kashif, and A.M. Sohail, "Engineering considerations on additional iron losses due to rotational fields and sheet cutting," in *the 18th International Conf. on Electrical Machines*, *ICEM 2008*, pp.1–4.
[45] A. Boglietti, A. Cavagnino, T.L. Mthombeni, and P. Pillay, "Comparison of lamination iron losses supplied by PWM voltages: US and European experiences," in *IEEE Int. Conf. Electric Machines and Drives*, 2005, pp. 1431–1436.
[46] M. Lei Ma Sanada, S. Morimoto, and Y. Takeda, "Prediction of iron loss in rotating machines with rotational loss included," *IEEE Trans. Magn.,* vol. 39, no. 4, Part: 2, pp. 2036–2041, 2003.
[47] Jian Guo Zhuand and V.S. Ramsden, "Improved formulations for rotational core losses in rotating electrical machines," *IEEE Trans. Magn.,* vol. 34, no. 4, Part: 2, pp. 2234–2242, 1998.
[48] T. Gautreau, *Estimation des pertes fer dans les machines électriques. Model d'hysteresis loss surface et application aux machines synchrones a aimants*, Doctoral thesis, http://hal.archives-ouvertes.fr/docs/00/16/99/03/PDF/these_TGautreau.pdf, 1999.
[49] G. Bertotti, A. Boglietti, M. Chiampi, D. Chiarabaglio, F. Fiorillo, and M. Lazzari, "An improved estimation of iron losses in rotating electrical machines," *IEEE Trans. Magn.*, vol. 27, no. 6, Part 2, pp. 5007–5009, 1991.
[50] H. Köfler, "Stray Load Losses in Induction Machines A Review of Experimental Measuring Methods and a Critical Performance Evaluation," in *Int. Conf. Renewable Energies and Power Quality (ICREPQ'03),* Vigo, 2003.

[51] A.R. Hagen, A. Binder, M. Aoulkadi, T. Knopik, and K. Bradley, "Comparison of measured and analytically calculated stray load losses in standard cage induction machines," in *the 18th Int. Conf. Electrical Machines*, *ICEM 2008*, pp. 1–6.

[52] R.L. Stoll and P. Hammond, "Calculation of the magnetic field of rotating machines. Part 5: Field in the end region of turbogenerators and the eddy-current loss in the end plates of stator cores," in *Proc. Inst. of Elect. Eng.*, vol. 113, no. 11, 1966, pp. 1793–1804.

[53] R.L. Stoll and P. Hammond, "Calculation of the magnetic field of rotating machines. Part 5: Field in the end region of turbogenerators and the eddy-current loss in the end plates of stator cores," in *Proc. Inst. Elect. Eng.*, vol. 113, no. 11, 1966, pp. 1793–1804.

[54] R.L. Stoll, "Solution of linear steady-state eddy-current problems by complex successive overrelaxation," in *Proc. Inst. Elect. Eng.*, vol. 117, no. 7, 1970, pp. 1317–1323.

[55] Y. Liang, H. Huang, and G. Hu, "Numerical calculation of end region electromagnetic field of large air-cooled turbogenerator," *World Automation Congr.*, *WAC 2008*, pp. 1–5.

[56] M. Fujita, T. Ueda, T. Tokumasu, K. Nagakura, M. Kakiuchi, and T. Otaka, "Eddy current analysis in the stator end structures of large capacity turbine generators," in *Int. Conf. Elect. Machines and Syst.*, *ICEMS 2009,* pp. 1–6.

[57] Y. Yao, H. Xia, G. Ni, X. Liang, S. Yang, and P. Ni, "3-D eddy current analysis in the end region of a turbogenerator by using reduced magnetic vector potential," *IEEE Trans. Magn.*, vol. 42, no. 4, pp. 1323–1326, 2006.

[58] L. Jinxiang, S. Yutian, and Y. Guijie, "Calculation and analysis of 3D magnetic field for end region of large turbogenerators," in *Proc. Eighth Int. Conf. Elect. Machines and Syst.*, *ICEMS 2005,* vol. 3, pp. 2079–2082.

[59] K. Takahashi, K. Hattori, A. Nakahara, and M. Saeki, "Three dimensional harmonic field and eddy Current analysis for rotor end region of turbine generator," *IEEE Int. Conf. Electric Machines & Drives, 2007. IEMDC '07.* vol. 1, pp. 477–481.

[60] G.K.M. Khan, G.W. Buckley, R.B. Bennett, and N. Brooks, "An integrated approach for the calculation of losses and temperatures in the end-region of large turbine generators," *IEEE Trans. Energy Convers.*, vol. 5, no. 1, pp. 183–194, 1990.

[61] R. Lin, A. Haavisto, and A. Arkkio, "Validation of a Time-Harmonic Numerical Model for Solving Magnetic Field in End Region of a Radial-Flux Machine," *IEEE Trans. Magn.,* vol. 45, no. 12, pp. 5360–5367, 2009.

[62] R. Lin and A. Arkkio, "Calculation and Analysis of Stator End-Winding Leakage Inductance of an Induction Machine," *IEEE Trans. Magn.,* vol. 45, no. 4, pp. 2009–2014, 2009.

[63] R. Lin, A. Haavisto, and A. Arkkio, "Analysis of Eddy-Current Loss in End Shield and Frame of a Large Induction Machine," *IEEE Trans. Magn.*, vol. 46, no. 3, Part 2, pp. 942–948, 2010.

[64] R. Lin, A. Haavisto, and A. Arkkio, "Axial Flux and Eddy-Current Loss in Active Region of a Large-Sized Squirrel-Cage Induction Motor," *IEEE Trans. Magn.*, vol. 46, no. 11, pp. 3933–3938, 2010.

[65] S.L. Ho, H.L. Li, and W.N. Fu, "Inclusion of interbar currents in a network-field coupled time-stepping finite-element model of skewed-rotor induction motors," *IEEE Trans. Magn.*, vol. 35, no. 5, Part 3, pp. 4218–4225, 1999.

[66] V.C. Silva, Y. Marechal, and A. Foggia, "Surface impedance method applied to the prediction of eddy currents in hydrogenerator stator end regions," *IEEE Trans. Magn.*, vol. 31, no. 3, pp. 2072–2075, 1995.

[67] V.C. Silva, G. Meunier, and A. Foggia, "A 3D finite-element computation of eddy currents and losses in the stator end laminations of large synchronous machines," *IEEE Trans. Magn.*, vol. 32, no. 3, Part 1, pp. 1569–1572, 1996.

[68] E. Schmidt, G. Traxler-Samek, and A. Schwery, "Comparison of Time-Harmonic and Transient Finite Element Analyses for Eddy Currents in the Stator Clamping System of Synchronous Generators," in *Canadian Conf. on Elect. and Computer Eng., CCECE 2007,* pp. 260–263.

[69] E. Schmidt, G. Traxler-Samek, and A. Schwery, "Influence of higher harmonics in the end region magnetic field on eddy currents in the stator clamping system of hydro generators," in *IEEE Int. Conf. Electric Machines and Drives*, 2005, pp. 1268–1274.

[70] K. Takahashi, K. Hattori, A. Nakahara, and M. Saeki, "Three dimensional harmonic field and eddy current analysis for rotor end region of turbine generator," *IEEE Int. Conf. Electric Machines & Drives, IEMDC '07,* vol. 1, 2007, pp. 477–481.

[71] R. De Weerdt and R. Belmans, "Squirrel cage induction motor end effects using 2D and 3D finite elements," in *the Seventh Int. Conf. Elect. Machines and Drives*, Conf. Publ. no. 412, 1995, pp. 62–66.

[72] A. El-Refaie, M. Shah, J. Alexander, S. Galioto, K. Huh, and W. Gerstler, "Rotor end losses in multi-phase fractional-slot concentrated-winding permanent magnet synchronous machines," *IEEE Trans. Ind. Appl.*, vol. 47, no. 5, pp. 2066–2074, 2011.

[73] G. H. Rockwood, "Calculation of stray load losses," *Trans. the American Inst. Elect. Eng.*, vol. XLVI, pp. 1139–1147, 1927.

[74] A. B. Field, "Eddy Currents in Large Slot-Wound Conductors," *Trans. the American Inst. Elect. Eng.*, vol. XXIV, pp. 761–788, 1905.

[75] W. V. Lyon, "Heat Losses in the Conductors of Alternating-Current Machines," *Trans. the American Inst. Elect. Eng.*, vol. XL, pp. 1361–1409, 1921.

[76] R. E. Gilman, "Eddy Current Losses in Armature Conductors," *Trans. the American Inst. Elect. Eng.*, vol. XLIII, pp. 246–251, 1924.

[77] R. E. Gilman, "Eddy Current Losses in Armature Conductors," *Trans. the American Inst. Elect. Eng.*, vol. XXXIX, no. 1, 1920, pp. 997–1056.

[78] P. L. Dowell, "Effects of eddy currents in transformer winding," in *Proc. Inst. Elect. Eng.*, vol. 113, no. 8, Aug. 1966, pp. 1387–1394.

[79] K. Küpfmüller, *Introduction to Theoretical Electrical Engineering (Einführung in die theoretische Elektrotechnik),* Springer Verlag, Berlin, 6th rev., 1959.

[80] R. Richter, *Electrical machines: Induction machines (Elektrische Maschinen: Die Inductionsmaschinen)*, Basle and Stuttgart: Birkhäuser Verlag, vol. IV, 2nd edn, 1954.

[81] R. Richter, *Electrical machines: General calculation elements. DC machines (Elektrische Maschinen: Allgemeine Berechnungselemente. Die Gleichstrommaschinen),* Basle and Stuttgart: Birkhäuser Verlag, vol. I, 3rd edn, 1967.

[82] Vogt, K., *Design of Electrical Machines (Berechnung elektrischer Maschinen*), Weinheim, Wiley-VHC Verlag GmbH, 1996.

[83] J. Baird, "Eddy-Current Losses in Induction Motor End-Turn Clamping Rings," *Trans. the American Inst. Elect. Eng. Power App. and Syst. Part III*, vol. 73, no. 1, Part: III-A, pp. 660–664, 1954.

[84] M. Aoulkadi and A. Binder, "When loads stray: Evaluation of Different Measurement Methods to Determine Stray Load Losses in Induction Machines," *IEEE Ind. Electron. Magn.*, vol. 2, no. 1, pp. 21–30, 2008.

[85] A.I. de Almeida, F.J.T.E. Ferreira, J.F. Busch, and P. Angers, "Comparative analysis of IEEE 112-B and IEC 34-2 efficiency testing standards using stray load losses in low-voltage three-phase, cage induction motors," *IEEE Trans. Ind. Appl.,* vol. 38, no. 2, pp. 608–614, 2002.

[86] S.L. Ho and W.N. Fu, "Computation of harmonic stray losses of induction motors using adaptive time stepping finite element method together with externally coupled circuits," in *Seventh Int. Conf. Elect. Machines and Drives, (Conf. Publ. No. 412)*, 1995, pp. 93–97.

[87] S.L. Ho, W.N. Fu, and H.C. Wong, "Estimation of stray losses of skewed rotor induction motors using coupled 2-D and 3-D time stepping finite element methods," *IEEE Trans. Magn.*, vol. 34, no. 5, Part: 1, 1998, pp. 3102–3105.

[88] E. Schmidt, F. Mullner, and H. Neudorfer, "Modelling and precalculation of additional losses of inverter fed asynchronous induction machines of traction drives," *IEEE Int. Electric Machines & Drives Conf. (IEMDC)*, 2011, pp. 533–538.

[89] N. Shuangxia S.L. Ho, W.N. Fu, and Z. Jianguo, "Eddy Current Reduction in High-Speed Machines and Eddy Current Loss Analysis With Multislice Time-Stepping Finite-Element Method," *IEEE Trans. Magn.,* vol. 48, no. 2, pp. 1007–1010, 2012.

[90] A. Bellara, H. Bali, R. Belfkira, Y. Amara, and G. Barakat, "Analytical Prediction of Open-Circuit Eddy-Current Loss in Series Double Excitation Synchronous Machines," *IEEE Trans. Magn.,* vol. 47, no. 9, pp. 2261–2268, 2011.

[91] J.A. Ferreira, "Analytical computation of AC resistance of round and rectangular litz-wire windings," *IEE Proc. B Electric Power Appl.,* vol. 139, no. 1, pp. 21–25, 1992.

[92] J. A. Ferreira, "Improved analytical modeling of conductive losses in magnetic components," *IEEE Trans. Power Elect.*, vol. 9, no. 1, pp. 127–131, 1994.

[93] E. A. Hanney, "Heat losses due to load current in direct-current armature windings," *J. the Inst. Elect. Eng.*, vol. 71, no. 427, pp. 263–283, 1932.

[94] M. P. Perry, "Multiple Layer Parallel Connected Air-Core Inductor Design," *IEEE Trans. Power App. and Syst.*, vol. PAS-98, no. 4, pp. 1387–1393, 1979.

[95] M. P. Perry, "Multiple Layer Series Connected Winding Design for Minimum Losses," *Trans. Power App. and Syst.*, vol. PAS-98, no. 1, pp. 116–123, 1979.

[96] C. R. Sullivan, "Computationally efficient winding loss calculation with multiple windings, arbitrary waveforms, and two-dimensional or three-dimensional field geometry," *IEEE Trans. Power Elect.,* vol. 16, no. 1, pp. 142–150, 2001.

[97] N. Xi and C. R. Sullivan, "Simplified high-accuracy calculation of eddy-current loss in round-wire windings," *IEEE 35th Annual Power Electron. Specialists Conf.,* vol. 2, 2004, pp. 873–879.

[98] N. Xi and C. R. Sullivan, "An improved calculation of proximity-effect loss in high-frequency windings of round conductors," in *IEEE 34th Annu. Power Electron. Specialist Conf.*, *PESC '03*, vol. 2, pp. 853–860.

[99] R. Wojda and M. Kazimierczuk, "Analytical Optimization of Solid-Round Wire Windings," *IEEE Trans. Ind. Electron.*, vol. 60, no. 3, pp. 1033–1041, 2013.

[100] R. Wrobel, A. Mlot, and P. H. Mellor, "Contribution of End-Winding Proximity Losses to Temperature Variation in Electromagnetic Devices," *IEEE Trans. Ind. Electron.,* vol. 59, no. 2, pp. 848–857, 2012.

[101] W. G. Hurley, E. Gath, and J. G. Breslin, "Optimizing the AC resistance of multilayer transformer windings with arbitrary current waveforms," *IEEE Trans. Power Electron.,* vol. 15, no. 2, pp. 369–376, 2000.

[102] L. J. Wu, Z. Q. Zhu, D. Staton, M. Popescu, and D. Hawkins, "Analytical Model of Eddy Current Loss in Windings of Permanent-Magnet Machines," *IEEE Trans. Accounting for Load Magn.*, vol. 48, no. 7, pp. 2138–2151, 2012.

[103] I. Boldea and S.A. Nasar, *The Induction Machine Handbook*, Boca Raton, CRC Press LLC, 2001.

[104] J. Gyselinck, P. Dular, N. Sadowski, P. Kuo-Peng, and R. V. Sabariego, "Homogenization of Form-Wound Windings in Frequency and Time Domain Finite-

Element Modeling of Electrical Machines," *IEEE Trans. Magn.,* vol. 46, no. 8, pp. 2852–2855, 2010.
[105] G. S. Dimitrakakis and E. C. Tatakis, "High-Frequency Copper Losses in Magnetic Components With Layered Windings," *IEEE Trans. Magn.*, vol. 45, no. 8, pp. 3187–3199, 2009.
[106] M. J. Islam, J. Pippuri, J. Perho, and A. Arkkio, "Time-harmonic finite-element analysis of eddy currents in the form-wound stator winding of a cage induction motor," *IET Electric Power Appl.*, vol. 1, no. 5, pp. 839–846, 2007.
[107] C.R. Sullivan, "Optimal choice for number of strands in a litz-wire transformer winding," *IEEE Trans. Power Electron.,* vol. 14, no. 2, pp. 283–291, 1999.
[108] A.W. Lotfi, P.M. Gradzki, and F.C. Lee, "Proximity effects in coils for high frequency power applications," *IEEE Trans. Magn.*, vol. 28, no. 5, pp. 2169–2171, Sep. 1992.
[109] N. Xi and C.R. Sullivan, "An Equivalent Complex Permeability Model for litz-wire Windings," *IEEE Trans. Ind. Appl.*, vol. 45, no. 2, pp. 854–860, 2009.
[110] A.W. Lotfi and F.C. Lee, "A high frequency model for litz-wire for switch-mode magnetics," in *IEEE Conf. Ind. Appl. Society Annu. Meeting,* vol. 2, 1993, pp. 1169–1175.
[111] F. Tourkhani and P. Viarouge, "Accurate analytical model of winding losses in round litz-wire windings," *IEEE Trans. Magn.,* vol. 37, no. 1, Part: 2, pp. 538–543, 2001.
[112] M.K. Kazimierczuk, *High-Frequency Magnetic Components,* Chichester, UK: John Wiley & Sons, 2009.
[113] M. Bartoli, N. Noferi, A. Reatti, and M.K. Kazimierczuk, "Modeling litz-wire winding losses in high-frequencies power inductors," in *Proc. IEEE Power Electron. Spec. Conf.,* Baveno, Italy, Jun. 23–27, 1996, pp. 1690–1696.
[114] J. Acero, R. Alonso, J.M. Burdio, L.A. Barragan, and D. Puyal, "Frequency-dependent resistance in litz-wire planar windings for domestic induction heating appliances," *IEEE Trans. Power Electron.,* vol. 21 , no. 4, pp. 856–866, 2006.
[115] G. Cerri, S.A. Kovyryalov, and V.M. Primiani, "Modelling of a litz-wire planar winding," *IET Measurement & Technology Science*, vol. 4, no. 4, pp. 214–219, 2010.
[116] W. Nick, M. Frank, G. Klaus, J. Frauenhofer, and H.-W. Neumuller, "Operational Experience With the World's First 3600 rpm 4 MVA Generator at Siemens," *IEEE Trans. Appl. Supercond.,* vol. 17, no. 2, Part: 2, pp. 2030–2033, 2007.
[117] D. Wu and E. Chen, "Stator Design for a 1000 kW HTSC Motor With Air-gap Winding," *IEEE Trans. Appl. Supercond.,* vol. 21 , no. 3 , Part 2, pp. 1093–1096, 2010.
[118] R.P. Wojda and M.K. Kazimierczuk, "Winding resistance of litz-wire and multi-strand inductors," *IET Power Electron.,* vol. 5, no. 2, pp. 257–268, Feb. 2012.
[119] T. Xu and C.R. Sullivan, "Stranded wire with uninsulated strands as a low-cost alternative to litz-wire," in *IEEE 34th Annual Power Electronics Specialist Conf.,* vol. 1, 2003, pp. 289–295.
[120] T. Xu and C.R. Sullivan, "Optimization of subconductored-wire windings and comparison with litz-wire on the basis of cost and loss," in *IEEE 35th Annu. Power Electron. Specialist Conf.*, vol. 2, 2004, pp. 854–860.
[121] C.R. Sullivan, "Cost-constrained selection of strand diameter and number in a litz-wire transformer winding," *IEEE Trans. Power Electron.*, vol. 16, no. 2, pp. 281–288, 2001.
[122] B. Semones, "Volumetric improvements in high energy magnet motors," *IEEE Trans. Magn.*, vol. 21, no. 5, 1985, pp. 1948–1951.

[123] A. Bettayeb, X. Jannot, and J. Vannier, “Analytical calculation of rotor magnet eddy-current losses for high speed IPMSM,” in *the XIX Int. Conf. Elect. Machines (ICEM)*, 2010, pp. 1–6.
[124] H. Polinder and M.J. Hoeijmakers, “Electric Eddy-current losses in the segmented surface-mounted magnets of a PM machine,” *IEE Proc. Power Appl.*, vol. 146, no. 3, 1999, pp. 261–266.
[125] R. Deeb, M. Janda, and Z. Makki, “Prediction of eddy current losses of surface mounted permanent magnet servo motor,” in *the XXth International Conf. on Electrical Machines (ICEM)*, 2012, pp. 1797–1802.
[126] J. Pyrhönen, H. Jussila, Y. Alexandrova, P. Rafajdus, and J. Nerg, “Harmonic Loss Calculation in Rotor Surface Permanent Magnets—New Analytic Approach,” *IEEE Trans. Magn.*, vol. 48, no. 8, pp. 2358–2366, 2012.
[127] M. Markovic and Y. Perriard, “A simplified determination of the permanent magnet (PM) eddy current losses due to slotting in a PM rotating motor,” in *Int. Conf. Elect. Machines and Syst.*, *ICEMS 2008*, pp. 309–313.
[128] Z. Nannan, Z.Q. Zhu, and L. Weiguo, “Rotor Eddy Current Loss Calculation and Thermal Analysis of Permanent Magnet Motor and Generator,” *IEEE Trans. Magn.*, vol. 47 , no. 10, pp. 4199–4202, 2011.
[129] H. Vansompel, P. Sergeant, and L. Dupre, “Effect of segmentation on eddy-current loss in permanent-magnets of axial-flux PM machines using a multilayer-2D — 2D coupled model,” in *the XXth Int. Conf. Elect. Machines (ICEM),* 2012, pp. 228–232.
[130] M. Nakano, H. Kometani, and M. Kawamura, “A study on eddy-current losses in rotors of surface permanent-magnet synchronous machines,” *IEEE Trans. Ind. Appl.*, vol. 42, no. 2, pp. 429–435, 2006.
[131] J. Alexandrova, H. Jussila, J. Nerg, and J. Pyrhönen, “Comparison between models for eddy-current loss calculations in rotor surface-mounted permanent magnets,” in *the XIX International Conf. on Electrical Machines (ICEM),* 2010, pp. 1–6.
[132] J. Nerg, M. Niemelä, J. Pyrhonen, and J. Partanen, “FEM calculation of rotor losses in a medium speed direct torque controlled PM synchronous motor at different load conditions,” *IEEE Trans. Magn.*, vol. 38, no. 5, Part: 1, pp. 3255–3257, 2002.
[133] T. Okitsu, D. Matsuhashi, G. Yanhui, and K. Muramatsu, “Coupled 2-D and 3-D Eddy Current Analyses for Evaluating Eddy Current Loss of a Permanent Magnet in Surface PM Motors,” *IEEE Trans. Magn.*, vol. 48, no. 11, pp. 3100–3103, 2012.
[134] P.L. Sergeant and A. Van den Bossche, “Reducing the permanent magnet content in fractional-slot concentrated-windings permanent magnet synchronous machines,” in *the XXth International Conference on Electrical Machines (ICEM)*, 2012, pp. 1405–1411.

**Publication I**



H. Hamalainen, J. Pyrhonen, J. Nerg, Effect of Quadrature Axis Armature Reaction on Magnetic Circuit Time Harmonics and Stator Iron Losses in Permanent Magnet Synchronous Generator with Embedded Magnets, *International Review of Electrical Engineering (I.RE.E.),* vol. 5, no. 5 part A, pp. 2057-2062, Oct. 2010.

International Review of Electrical Engineering (I.R.E.E.), Vol. 5, N. 5
September-October 2010

# Effects of Quadrature Axis Armature Reaction on Magnetic Circuit Time Harmonics and Stator Iron Losses in a Permanent Magnet Synchronous Generator with Embedded Magnets

H. Hamalainen, J. Pyrhonen, J. Nerg

**Abstract** – *In permanent magnet machines with inverse saliency and relatively large quadrature axis inductance, the armature reaction causes stator teeth to saturate under load. The phenomenon cannot be observed in no-load tests. Therefore, determining the iron losses in a normal no-load test does not suffice, as the iron losses under load may be considerably higher than the no-load iron losses. Losses are compared between different stator yoke thicknesses, and also different iron materials are used. Time harmonics are taken from 11 different points in the stator iron. Variations in the time harmonics are detected between different stator yoke thicknesses. This results in different losses at no load and at load. Iron loss results are obtained by using a loss surface (LS) model.* 

***Keywords***: *Additional Losses, Iron Losses, Quadrature Axis Inductance, Time Harmonics*

## Nomenclature

| | |
|---|---|
| PMG | Permanent Magnet Generator |
| FEM | Finite Element Method |
| LS | Loss Surface |
| $p_{hyst}$ | static hysteresis losses, |
| $p_{ec}$ | the dynamic eddy current losses |
| $p_{exc}$ | excess losses |
| $P(t)$ | instant power loss |
| $k_h$ | hysteresis loss coefficient |
| $B_m$ | peak value of magnetic flux density |
| $f$ | frequency |
| $\sigma$ | the conductivity of the iron material |
| $d$ | thickness of lamination |
| $k_e$ | excess loss coefficient |
| $dP_{average}$ | volume density of average power loss |
| $P_{average}$ | average power loss dissipated in volume region |

## I. Introduction

Permanent magnet generators have been under extensive research in recent years [1]–[5], and they are gaining stronger and stronger position for instance in wind power applications [6]. Especially geared PMGs with full-scale power converters are a very attractive solution because of their low maintenance costs and higher efficiency compared with induction generators. More precisely, their high efficiency at partial loads makes PMGs superior to induction generators.

One of the most important tasks when designing an electrical machine is the proper estimation of losses.

In particular, estimation of iron losses is among the most challenging issues. Several authors have attempted to take time harmonics into account [7]–[10] when calculating the iron losses. In some papers, the losses are evaluated with analytical methods, while another approach is to calculate the losses by FEM; one of the first papers on the topic was published by Bertotti *et al.* [11] in 1991. Papers [7], [9], and [12] reported in parallel that iron loss errors were in the range of 50 % between simulations and measurements. In these papers, the authors assumed that the errors resulted from the rotational flux and time-harmonics-caused losses in the stator iron. It is extremely difficult to separate iron losses from other losses because there is no absolute measurement technique to measure iron losses separately in an actual machine, especially in a PM machine, where the flux cannot be turned off during the measurement. In machines with embedded magnets, the iron losses cannot be measured accurately at no load as the quadrature armature reaction in such a case is insignificant. It has been acknowledged that in electrical machines additional losses caused by the rotational flux and harmonics make the calculation results deviate from the measured ones [9].

This paper studies the dependency of iron losses on the magnetic circuit geometry and the stator steel material in a high-speed (1600 $min^{-1}$), 3 MW PMG equipped with embedded magnets, Fig. 1. Such a design has inverse saliency, and the quadrature axis flux increases the time harmonic content of the stator flux density under heavy load. In particular, the third harmonic is added to the time dependency of the teeth

flux densities and the yoke flux density. The quadrature axis armature reaction also considerably increases the stator teeth flux densities under load. In salient pole machines, the recommended stator yoke maximum flux densities [13] should not be exceeded because of the adverse effects of the quadrature armature reaction on the stator iron losses. In traditional designs, losses caused by the quadrature armature reaction are taken into account by calculating additional losses proportional to the machine rated power. According to [13], additional losses in salient pole synchronous machines vary between 0.1 and 0.2 % of the machine rated power.

The target is to provide different aspects for designers to consider when designing an electrical machine and in particular, a PMG. The selected magnetic material also has a significant effect on the iron losses and, therefore, on the efficiency.

The results show that the stator iron losses in an embedded magnet machine can be significantly affected by changing the thickness of the stator yoke. In addition, the yoke material has an essential effect on machine efficiency. The rotor geometry may have a major influence on the stator losses. In a rotor surface magnet machine, the armature reaction does not modulate the flux densities in the time domain similarly as in a machine with embedded magnets. In rotor surface magnet machines, the time dependency of the stator flux density remains mainly sinusoidal, and hence, the losses can be smaller than in machines with embedded magnets. Embedding the magnets is, however, a beneficial solution from mechanical engineering and cooling points of view and is a good choice in large permanent magnet machines. In large rotor surface magnet machines, different bands must be used to fasten the magnets to the rotor surface, as a result of which the cooling of the rotor is significantly degraded. In embedded magnet machines the rotor surface remains bare and the cooling of the rotor is efficient.

## II. Method of Analysis

None of the several methods to calculate iron losses presented in [14] fully complies with the measurement results. Bertotti's equation and the loss surface (LS) model are used with the voltage-driven time stepping 2D finite element method to compare the iron loss behavior with different stator yoke thicknesses and iron sheet qualities. A calculation of scalar iron losses is carried out with Bertotti's equation also in the Flux2D program by Cedrat. The program calculates the iron losses based on the flux density in the node and with a parameter that the user has given. The iron loss equation that the Flux2D uses is

$$p_{\mathrm{Fe}} = p_{\mathrm{hyst}} + p_{\mathrm{ec}} + p_{\mathrm{exc}} . \tag{1}$$

Then, according to equation (1), the average power loss can be calculated by equations (2), (3) and (4):

$$dP(t) = k_{\mathrm{h}} B_{\mathrm{m}}^2 f + \sigma \frac{d^2}{12}\left(\frac{dB}{dt}(t)\right)^2 + k_{\mathrm{e}}\left(\frac{dB}{dt}(t)\right)^{3/2} \tag{2}$$

$$dP_{\mathrm{average}} = \frac{1}{T}\int_0^T dP(t)dt \tag{3}$$

$$P_{\mathrm{average}} = \iiint dP_{\mathrm{average}} dv . \tag{4}$$

Parameters for Bertotti's equation are obtained by using the manufacturer's data sheets. Data sheets usually give measurement results for 50 and 100 Hz. For 75 Hz, a curve is generated between these two frequencies by applying $f^{1.5}$ overall loss dependency. The curve fitting toolbox of Matlab is used to obtain parameters for Bertotti's equation. When a ferromagnetic material gets saturated, the domain walls disappear and excess losses reduce to zero [10]. A more accurate method is to use the LS model, which is based on thousands of measurements [15]. In this paper, the iron loss results are derived with Flux2D by using the LS model. The LS model approximates the rotating losses by adding losses produced independently by the major and minor axis components of the flux density [15]. We acknowledge that the LS model does not fully take the rotational losses into account but overestimates them [16]. It still gives an estimation of the rotational losses with an error in the range of 10 % [15]. When comparing the results of Bertotti's equation and the LS model, Bertotti's equation gives higher losses than the LS model [15], [16]. The LS model, however, also takes the time harmonics more accurately into account.

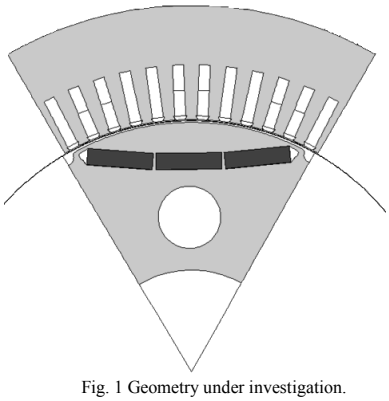

Fig. 1 Geometry under investigation.

Tangential and radial components of the flux density are investigated in 11 different points. Points 1 through 6 are at the same place for all investigated outer diameters (850 mm to 900 mm), while because of the change in the thickness of the yoke, points 7 through 11 are divided equally along the yoke's thickness. The places of the observed points are depicted in Fig 2.

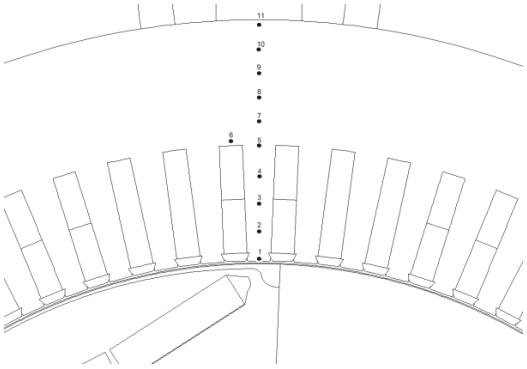

Fig. 2. Location of the points where tangential and normal components of the flux are observed.

## III. Structure under investigation

A high-speed permanent magnet wind turbine generator with embedded magnets is investigated in the paper. In Fig. 1, the geometry of the machine is depicted. The machine is equipped with a double-layer form-wound winding. The investigated stator outer diameters are 850, 855, 860, 865, 870, 875, 880, 885, 890, 895, 900, and 930 mm. An actual 3.15 MW machine with a 850 mm stator outer diameter was tested to get physical evidence for the calculation results.

TABLE I
SPECIFICATIONS OF THE HIGH-SPEED PERMANENT MAGNET MACHINE

| High-speed permanent magnet generator | |
|---|---|
| $L_d$ | 0.73 p.u. |
| $L_q$ | 1.36 p.u. |
| Rated power (kW) | 3150 |
| Rated torque (kNm) | 21.1 |
| Rated frequency (Hz) | 73 |
| Outer diameter of stator iron core (mm) | 850–930 |
| Inner diameter of stator iron core (mm) | 622 |
| Number of pole pairs | 3 |
| Number of stator slots | 72 |
| Number of turns in series in a stator coil | 2 |
| Stator core material | M330–65A |

## IV. Results

The research reported in this paper aims at finding an explanation for the results obtained in the measurements, where the no-load iron losses deviate from the load iron losses. A similar tendency can be observed in the simulations in Table II.

The most interesting observation in Table II is that when the stator yoke is designed to be narrow (850 mm in stator diameter), the losses may look appropriate at no load, but become much worse under load, and the efficiency of the machine suffers from extra iron losses. When the stator yoke is designed 'too' wide (930 mm), the results are smallest as expected. By performing the measurements according to the standard IEEE 112, one may find contradiction with no-load and load measurements.

In Tables II and III, the calculation results given by the LS model and Bertotti's equation are presented. Comparison of the tables shows that Bertotti's equation gives considerably higher losses than the LS model. This observation is also acknowledged in other papers [15], [16].

### *IV.1. Time Harmonics*

Time harmonics are among the factors that cause difference when comparing losses at no load and load. The third space harmonic can be seen in the air gap flux density at no load, Fig. 3 (a) and (b). This means that some of the third harmonic comes naturally from the geometry of the machine, and one would expect to find the third harmonic as a time harmonic also in the stator iron. In Fig. 4 (a) and (b), the third and fifth harmonics increase under load compared with the no load.

Rotational losses are yet another concern [8], [9], [10], [17] in addition to the time harmonics of the flux. By using the flux density tangential and radial components in time, flux density loci can be plotted; these loci show whether the flux is rotating or alternating. When the ratio of the radial and tangential components is 1, the flux density is totally rotating, but usually in the flux density, one of the components is dominating.

Tables IV and V show the tangential and radial components, where the first harmonic is given in teslas and the third and fifth harmonics in percentages of the first harmonic. The places of the points are depicted in Fig 2. In the stator yoke (points 7–11), the tangential flux density component is dominating, and in the teeth (points 1–5), the radial flux density component is dominating. In this paper, we concentrate only on the time harmonics of the major component, that is, where the most of the losses are generated.

The losses of the 850 mm and 900 mm stators are compared by investigating Table II. Both stators are made of M330-65A iron sheets. The 900 mm stator has 1 kW higher losses at no load, which is due to the third harmonic in the stator in points 7–11. Under load, the situation is different: the losses of the 850-mm stator are 14.1 kW, while the 900-mm stator has 12 kW of losses.

In Table II, an explanation as to why the stator made of M330-65A has higher losses than the M400-50A one is that the latter is thinner and therefore has smaller eddy current losses.

In Table V, the percentage of the third harmonic decreases from point 7 to 11 under load. The difference is largest in point 11, where the third harmonic is 5 percent units lower with the 900 mm stator compared with the 850 mm one.

TABLE II
STATOR IRON LOSSES WITH DIFFERENT STATOR DIAMETERS AND MATERIALS AT RATED LOAD (L) AND AT NO LOAD (NL), CALCULATED WITH THE LS MODEL.

| Stator diameter (mm) | 850 | 855 | 860 | 865 | 870 | 875 | 880 | 885 | 890 | 895 | 900 | 930 |
|---|---|---|---|---|---|---|---|---|---|---|---|---|
| L M330-65A (kW) | 14.1 | 14.1 | 14.0 | 14.0 | 13.9 | 13.7 | 13.4 | 13.1 | 12.7 | 12.3 | 12.0 | 11.2 |
| NL M330-65A (kW) | 11.0 | 11.0 | 11.5 | 11.9 | 12.5 | 12.7 | 12.8 | 12.7 | 12.7 | 12.3 | 12.0 | 10.5 |
| L M270-35A (kW) | 8.1 | 8.3 | 8.4 | 8.6 | 8.6 | 8.7 | 8.7 | 8.6 | 8.3 | 8.0 | 7.7 | 7.2 |
| NL M270-35A (kW) | 6.7 | 6.7 | 7.1 | 7.5 | 8.0 | 8.3 | 8.4 | 8.5 | 8.5 | 8.4 | 8.2 | 7.1 |
| L M400-50A (kW) | 12.0 | 12.0 | 12.0 | 12.1 | 12.1 | 12.0 | 11.8 | 11.6 | 11.3 | 11.0 | 10.8 | 10.1 |
| NL M400-50A (kW) | 9.7 | 9.7 | 10.1 | 10.5 | 11.1 | 11.3 | 11.4 | 11.3 | 11.3 | 11.1 | 10.9 | 9.9 |

TABLE III
STATOR IRON LOSSES CALCULATED WITH BERTOTTI'S EQUATION WITH DIFFERENT STATOR DIAMETERS AND MATERIALS AT RATED LOAD.

| Stator diameter (mm) | 850 | 855 | 860 | 865 | 870 | 875 | 880 | 885 | 890 | 895 | 900 |
|---|---|---|---|---|---|---|---|---|---|---|---|
| M330-65A (kW) | 18.8 | 18.6 | 19 | 18.6 | 18.3 | 18.2 | 18 | 17.7 | 17.4 | 17.1 | 17 |

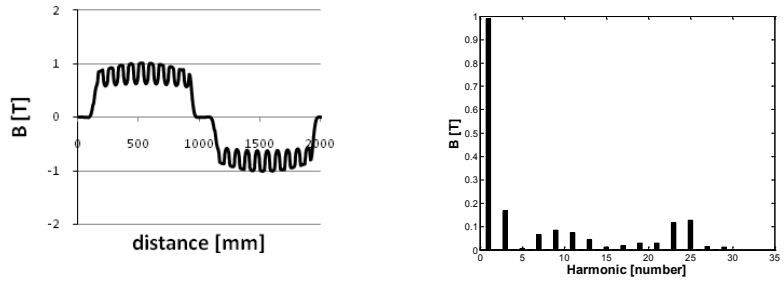


(a) (b)

Fig. 3. (a) Air gap flux density over one pole pitch and (b) analysis of the spatial harmonics at no load.

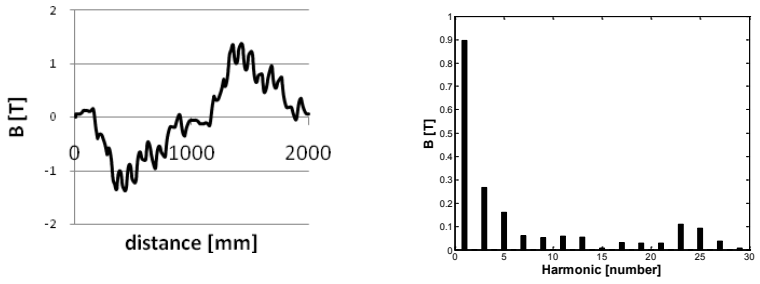


(a) (b)

Fig. 4 (a) Air gap flux density over pole pitch in and (b) analysis of the spatial harmonics under load.

This explains quite well the differences in losses with different diameters. By increasing the stator yoke, the no-load losses can even increase slightly, but more importantly, the load iron losses decrease by 15 %.

A significant increase in the third and fifth harmonics is caused by the large q-axis inductance, which is one of the consequences of the embedded magnets. This is illustrated very well in the tables. The q-axis inductance is the same with the 850 mm and 900 mm diameters. However, by varying the stator yoke thickness, we can modulate the harmonics so that the load losses are significantly lower compared with the worst-case scenario (850 mm). At the same time, the no-load losses are slightly higher. Changing of the height of the stator yoke does not affect the relative harmonic contents of the flux, but the flux densities start to saturate in the stator yoke when the yoke thickness is reduced. In the case of the 850 mm and M330-65A stator, loading of the machine increases the stator iron losses from 11 kW to 14.1 kW. 3.1 kW is 0.1 % of the machine rated power. If, however, Bertotti's equation is used, the losses increase from 11 kW to 18.8 kW when loading the

machine. 7.8 kW is 0.25 % of the machine rated load. As additional losses also take place in other machine parts, a 0.1–0.25 % increase in the iron losses seems large in the light of traditional knowledge. If the 900 stator diameter is used instead, the stator iron losses seem not to increase at all from the no-load values.

A generator manufacturer measured a prototype machine with a 850 mm stator outer diameter. The machine no-load losses were measured to be 36 kW. The no load friction loss was 19 kW. Hence, 17 kW of the electrical losses were present at no load. The rotor iron no-load losses were calculated to be 2 kW. Now, we have 15 kW of no-load stator losses, and hence, we can be satisfied with the no-load losses calculated by the LS model, giving 14.1 kW stator iron loss for the machine. Under load, the measured efficiency of the machine supports the study according to which the iron losses increase during loading of the machine.

TABLE IV
AMPLITUDES OF FLUX TIME HARMONICS WITH THE STATOR DIAMETER 850 MM UNDER LOAD (L) AND NO LOAD (NL).

| 850mm | *L B* [T] | *NL B* [T] | Tan 1st [T] | NL Tan 1st [T] | L Tan 3rd* | NL Tan 3rd* | L Tan 5th* | NL Tan 5th* | L Rad 1st [T] | NL Rad 1st [T] | L Rad 3rd* | NL Rad 3rd* | L Rad 5th* | NL Rad 5th* |
|---|---|---|---|---|---|---|---|---|---|---|---|---|---|---|
| Point 1 | 1.55 | 1.56 | 0.77 | 0.25 | 36 % | 49 % | 21 % | 4 % | 1.35 | 1.54 | 36 % | 13 % | 5 % | 2 % |
| Point 2 | 1.64 | 1.62 | 0.17 | 0.04 | 10 % | 66 % | 7 % | 25 % | 1.63 | 1.62 | 33 % | 15 % | 8 % | 1 % |
| Point 3 | 1.52 | 1.48 | 0.13 | 0.03 | 9 % | 66 % | 3 % | 26 % | 1.51 | 1.48 | 34 % | 14 % | 8 % | 2 % |
| Point 4 | 1.4 | 1.36 | 0.12 | 0.07 | 19 % | 61 % | 14 % | 18 % | 1.39 | 1.36 | 34 % | 13 % | 8 % | 3 % |
| Point 5 | 1.68 | 1.56 | 1.07 | 0.93 | 15 % | 24 % | 16 % | 5 % | 1.29 | 1.25 | 30 % | 20 % | 10 % | 1 % |
| Point 6 | 2.02 | 1.89 | 2.01 | 1.88 | 9 % | 7 % | 5 % | 2 % | 0.16 | 0.16 | 69 % | 36 % | 28 % | 10 % |
| Point 7 | 1.87 | 1.76 | 1.63 | 1.51 | 13 % | 2 % | 1 % | 0 % | 0.92 | 0.9 | 20 % | 35 % | 20 % | 7 % |
| Point 8 | 1.94 | 1.89 | 1.86 | 1.8 | 16 % | 1 % | 2 % | 2 % | 0.56 | 0.56 | 21 % | 32 % | 17 % | 8 % |
| Point 9 | 1.96 | 1.89 | 1.93 | 1.86 | 15 % | 0 % | 2 % | 3 % | 0.35 | 0.34 | 26 % | 26 % | 14 % | 4 % |
| Point 10 | 1.96 | 1.89 | 1.95 | 1.88 | 15 % | 1 % | 1 % | 4 % | 0.19 | 0.19 | 29 % | 23 % | 12 % | 2 % |
| Point 11 | 1.95 | 1.88 | 1.95 | 1.88 | 15 % | 1 % | 1 % | 4 % | 0.04 | 0.05 | 55 % | 32 % | 11 % | 5 % |

* Percentages of the first harmonic; the first tangential harmonic in point 1 under load is 0.77 and the third harmonic is 36 % of 0.77 (0.2772 T)
** Fundamental magnitude of flux

TABLE V
AMPLITUDES OF FLUX TIME HARMONICS WITH THE STATOR DIAMETER 900 MM UNDER LOAD (L) AND NO LOAD (NL).

| 900mm | *L B* [T]** | *NL B* [T]** | L Tan 1st [T] | NL Tan 1st [T] | L Tan 3rd | NL Tan 3rd | L Tan 5th | NL Tan 5th | L Rad 1st [T] | NL Rad 1st [T] | L Rad 3rd | NL Rad 3rd | L Rad 5th | NL Rad 5th |
|---|---|---|---|---|---|---|---|---|---|---|---|---|---|---|
| Point 1 | 1.58 | 1.64 | 0.8 | 0.17 | 34 % | 35 % | 20 % | 8 % | 1.36 | 1.63 | 36 % | 15 % | 7 % | 1 % |
| Point 2 | 1.66 | 1.76 | 0.18 | 0.01 | 11 % | 58 % | 7 % | 23 % | 1.65 | 1.76 | 33 % | 17 % | 11 % | 1 % |
| Point 3 | 1.54 | 1.62 | 0.13 | 0 | 6 % | 63 % | 4 % | 34 % | 1.53 | 1.62 | 33 % | 17 % | 11 % | 1 % |
| Point 4 | 1.41 | 1.49 | 0.09 | 0.02 | 11 % | 74 % | 4 % | 41 % | 1.41 | 1.49 | 32 % | 17 % | 11 % | 1 % |
| Point 5 | 1.44 | 1.47 | 0.65 | 0.6 | 18 % | 32 % | 17 % | 18 % | 1.29 | 1.34 | 32 % | 19 % | 12 % | 3 % |
| Point 6 | 1.4 | 1.38 | 1.39 | 1.36 | 10 % | 10 % | 5 % | 2 % | 0.2 | 0.22 | 51 % | 4 % | 8 % | 26 % |
| Point 7 | 1.44 | 1.51 | 1.26 | 1.31 | 17 % | 0 % | 3 % | 1 % | 0.7 | 0.76 | 26 % | 27 % | 16 % | 7 % |
| Point 8 | 1.38 | 1.47 | 1.3 | 1.39 | 15 % | 2 % | 1 % | 1 % | 0.46 | 0.48 | 27 % | 20 % | 11 % | 1 % |
| Point 9 | 1.33 | 1.44 | 1.3 | 1.4 | 13 % | 4 % | 0 % | 2 % | 0.3 | 0.32 | 26 % | 19 % | 9 % | 9 % |
| Point 10 | 1.29 | 1.41 | 1.28 | 1.4 | 11 % | 5 % | 1 % | 3 % | 0.16 | 0.17 | 25 % | 20 % | 10 % | 14 % |
| Point 11 | 1.25 | 1.39 | 1.25 | 1.39 | 10 % | 7 % | 3 % | 5 % | 0.03 | 0.03 | 24 % | 17 % | 13 % | 25 % |

** Fundamental magnitude of flux

## V. Conclusion

The embedded rotor magnet geometry contributes to large quadrature axis armature reaction, which results in time harmonics in the stator magnetic circuit. Significant losses are generated because of the presence of the time harmonics in the magnetic circuit. Correct dimensioning of the yoke helps tackling the problem. In a tooth, the third harmonic is the major loss-causing component with its over 30 % amplitude compared with the fundamental.

Varying the thickness of the stator yoke affects the losses more when using a more lossy material. With a better material, a thinner stator yoke can be used. When comparing Bertotti's equation with the LS model, Bertotti's equation tends to overestimate losses compared with the LS model. Adding rotational losses to the classical equation will take it further away from the truth. The measurement results from an actual machine support the idea of increased iron losses in the core. This paper gives a new perspective to where to look for losses when simulations and measurements do not match.

## References


[1] Jussila, H., Salminen, P., Niemelae, M., Parviainen, A., Pyrhoenen, J., Torque and inductances of concentrated wound permanent magnet machines, *International Review of Electrical Engineering (IREE)*, *vol. 2 n. 5*, October 2007, pp. 704 – 710.

[2] Kinnunen, J. A., Pyrhonen, J., Niemela, M., Liukkonen, O., Kurronen, P., Design of damper windings for permanent magnet synchronous machines, *International Review of Electrical Engineering (IREE)*, *vol. 2 n. 2*, April 2007, pp. 260 – 272.

[3] R. Bharanikumar, A. Nirmal Kumar, Maheswari K. T., Novel MPPT Controller for Wind Turbine Driven Permanent Magnet Generator with Power Converters, *International Review of Electrical Engineering (IREE)*, *vol. 5 n. 4*, Part A, August 2010, pp. 1555 – 1562.

[4] Melicio, R., Mendes, V. M. F., Catalao, J. P. S., Modeling, Control and Simulation of Full-Power Converter Wind Turbines Equipped with Permanent Magnet Synchronous Generator, *International Review of Electrical Engineering (IREE)*, *vol. 5 n. 5*, Part A, April 2010, pp. 397 – 408.

[5] Muyeen, S. M., Takahashi, R., Murata, T., Tamura, J., Miscellaneous Operations of Variable Speed Wind Turbine Driven Permanent Magnet Synchronous Generator *International Review of Electrical Engineering (IREE)*, *vol. 3 n. 5*, October 2008, pp. 912 – 921.

[6] Li, H., Chen, Z., Overview of different wind generator systems and their comparisons, *IET Renewable Power Generation*, *Volume: 2* , N. 2 , Publication Year: 2008 , Pp. 123 – 138

[7] G. Gonzalez-Moran Diaz, , C. Arboleya, P. Gomez-Aleixandre, J., Analytical Interpretation and Quantification of Rotational Losses in Stator Cores of Induction Motors, *IEEE Transactions on Magnetics, Vol. 43 n. 10*, Publication Year: 2007, pp. 3861 - 3867

[8] Yujing Liu Kashif, S.K. Sohail, A.M., Engineering considerations on additional iron losses due to rotational fields and sheet cutting, *ICEM 2008 18th International Conference on Electrical Machines*, Publication Year: 2008 , pp. 1 - 4

[9] Lei Ma Sanada, M. Morimoto, S. Takeda, Y., Prediction of iron loss in rotating machines with rotational loss included, *IEEE Transactions on Magnetics, Vol. 39 n. 4* , Part: 2, Publication Year: 2003 , pp. 2036 - 2041

[10] Jian Guo Zhu Ramsden, V.S., Improved formulations for rotational core losses in rotating electrical machines, *IEEE Transactions on Magnetics*, *Vol. 34 n. 4*, Part: 2 Publication Year: 1998 , pp. 2234 - 2242

[11] G. Bertotti, A. Boglietti, M. Chiampi, D. Chiarabaglio, F. Fiorillo, M. Lazzari, An improved estimation of iron losses in rotating electrical machines, *IEEE Transactions on Magnetics, Vol. 27 n. 6*, Part 2, Publication Year: 1991 , pp. 5007 - 5009

[12] M. Ranlof, A. Wolfbrandt, J. Lidenholm, U. Lundin, Core Loss Prediction in Large Hydropower Generators: Influence of Rotational Fields', *IEEE Transactions on Magnetics, Vol. 45 n. 8,* Publication Year: 2009 , pp. 3200 - 3206

[13] Pyrhönen, J., Jokinen, T., Hrabovcova, V., *Design of rotating electrical machines*, (John Wiley & Sons, Ltd., 2008)

[14] A. Krings, J. Soulard, Overview and Comparison of Iron Loss Models for Electrical Machines, *Ecological Vehicles and Renewable Energies, International Conference and Exhibition*, Publication Year: 2009.

[15] G. Thierry, *Estimation des pertes fer dans les machines électriques. Model d'hysteresis loss surface et application aux machines synchrones a aimants*, Ph.D. dissertation, Institut National Polytechnique de Grenoble, 2005.

[16] C.A Hernandez-Aramburo, T.C. Green, A.C. Smith, Estimating rotational iron losses in an induction machine, *IEEE Transactions on Magnetics, Vol. 39 n. 6,* Publication Year: 2003 , pp. 3527 - 3533

[17] A. Boglietti, A. Cavagnino, D.M. Ionel, M. Popescu, D.A. Staton, S. Vaschetto, A General model to predict the iron losses in inverter fed induction motors, *ECCE 2009, Energy Conversion Congress and Exposition*, Publication Year: 2009 , pp. 1067 - 1074


## Authors' information


Lappeenranta University of Technology
LUT-Energy, Laboratory of electrical Drives technology
PL 20, 53851 Lappeenranta


**H. Hämäläinen** received the M.Sc. degree in electrical engineering from Lappeenranta University of Technology (LUT), Lappeenranta, Finland, in 2009.
In 2009 he started his post-graduate studies concerning permanent magnet generators and their additional losses.
E-mail: henry.hamalainen@lut.fi

**J. Pyrhönen** received the M.Sc. degree in electrical engineering, the Licentiate of Science (Technology) degree, and the D.Sc. (Technology) degree from Lappeenranta University of Technology (LUT), Lappeenranta, Finland, in 1982, 1989, and 1991, respectively.
In 1993, he became an Associate Professor in electric engineering with LUT, where since 1997, he has been a Professor in electrical machines.
E-mail: juha.pyrhonen@lut.fi

**J. Nerg** received the M.Sc. degree inelectrical engineering, the Licentiate of Science(Technology) degree, and the D.Sc. (Technology)degree from Lappeenranta University of Technology (LUT), Lappeenranta, Finland, in 1996, 1998, and 2000, respectively.
He is currently a Senior Researcher with the Laboratory of Electrical Drives Technology, Department of Electrical Engineering, LUT
E-mail: janne.nerg@lut.fi

**Publication II**



H. Hamalainen, J. Pyrhonen, J. Nerg, J. Puranen,"3D Finite Element Method Analysis of Additional Load Losses in the End Region of Permanent Magnet Generators," *Transactions on Magnetics,* Vol. 48, no. 8, Aug. 2012.

# 3-D Finite Element Method Analysis of Additional Load Losses in the End Region of Permanent-Magnet Generators

Henry M. Hämäläinen[1], Juha Pyrhönen[1], Janne Nerg[1], and Jussi Puranen[2]

[1]Lappeenranta University of Technology, Lappeenranta, Finland
[2]The Switch Drive Systems Oy, Lappeenranta, Finland

**Machine design typically concentrates on the main magnetic and electric circuits while various additional losses are evaluated only by simple empirical equations. The objective of this paper is to examine the importance of the additional losses in the stator end region and in the housing of a 3.1 MW permanent-magnet wind generator. Stator stack clamping ring and finger plate losses are investigated using a 3-D finite element method. 2-D FEM analysis of the stator supporting housing losses is also performed. Two common mechanical component materials are analyzed in the 3-D studies; construction steel and stainless steel. The results show that failure to consider stator end areas and stator supporting constructions at the design stage can result in unwanted additional losses and affect machine efficiency. Indirect verification of the results is provided by efficiency measurements of different versions of the real 3.1 MW machine.**

*Index Terms*—**Clamping ring, eddy currents, finger plate, skin effect, stator end region losses, 3-D FEM.**

## I. Introduction

MOST electromagnetic loss mechanisms in an electrical machine are well-known design factors and can be calculated with acceptable accuracy. Additional losses, however, are only assumed to be some percentages of the total losses, according to IEC 34-2 [1], and they are generally not identified more accurately. Additional losses occur, for instance, in the supporting structures of the machine [2], in the windings (skin effect) [3], or in the laminated iron core of the stator or the rotor [4]. Finger plates and clamping rings in particular are subject to additional load losses as they are located close to the armature end windings. Losses in the finger plate and in the clamping ring are most difficult to calculate or measure. Modern simulation tools permit more accurate identification of these losses, making their minimization possible.

Clamping ring constructions are different in different machines, and consequently, the losses vary depending on the shape and current of the machine. Analysis of clamping ring losses is therefore best approached with 3-D finite element methods. 3-D calculations of the end region magnetic field have been presented in several papers [5]–[23]. Two of these papers [6], [23] apply a 2.5-D method, that is, an approach that combines 2-D and 3-D methods.

Three papers [8], [11], [23] treat the losses of the clamping ring and the stator stack supporting finger plates. However, in all of these three cases, the mesh was not fine enough to accurately calculate the Joule losses caused by eddy currents.

In [8], the magnetic field in the end region is calculated using reduced magnetic vector potential. No losses of the machine were reported; the method is only used to calculate the end region flux. Flux density and eddy current distributions were shown. Higher flux density was achieved with no load than with load. However, no explanation was presented for this finding. Furthermore, the mesh density utilized in the study did not allow accurate loss calculation on the clamping ring and the finger plate.

In [11], the calculation of clamping ring losses was done by defining them analytically and then inserting them into a FEM program, calculating temperatures, and comparing them to measurements of the real machine. A 3-D method was not used to calculate the clamping losses because of the lack of computing power when the research was done in the beginning of the nineties. 3-D was only used to solve the end region field.

A permanent-magnet machine with non-metallic and metallic clamping rings has been investigated by measurement and 2.5-D finite element methods [23]. The PMSM analyzed was a very small automotive machine, and the study focused on losses at the maximum speed, which is five times the rated speed, rather than losses at the nominal point. Therefore, exact information was not given on the proportion of losses of the rated power at the nominal point. Nevertheless, the paper gives a good indication of losses in machines used in automotive applications.

In this paper, the additional losses of a 1650 $\mathrm{min}^{-1}$ 3.1 MW permanent-magnet wind generator (PMG) in the stator stack supporting finger plate and the clamping ring are analyzed by 3-D FEM. A very fine mesh is built where the skin effect is pronounced. As a result, accurate losses are obtained. The results show that normal construction steel material S355JO/EN 10025 can be used with moderate losses in both the finger plates and the clamping rings; however, an efficiency improvement of about 0.075% can be achieved by using austenitic stainless steel in large permanent-magnet wind turbine generators instead of ferromagnetic steel. Losses in the stator housing are analyzed by a 2-D finite element method.

## II. Methods

The finger plate and clamping ring are located at the stator core ends. Fig. 1 depicts the location of the finger plate and clamping ring, one pole, and half of the machine. Finger plate and clamping ring are found from the both ends of the machine and are used to keep the laminated stator core together.

Manuscript received November 16, 2011; revised February 23, 2012; accepted March 05, 2012. Date of publication March 13, 2012; date of current version July 20, 2012. Corresponding author: (e-mail: henry.hamalainen@lut.fi).

Color versions of one or more of the figures in this paper are available online at http://ieeexplore.ieee.org.

Digital Object Identifier 10.1109/TMAG.2012.2190741

TABLE I
MATERIAL DATA FOR 3-DFEM FINGER PLATE AND CLAMPING RING SIMULATION

| Linear isotropic | Construction steel: S355JO/EN 10025 | Stainless steel 304 |
|---|---|---|
| Relative Permeability $\mu_r$ | 1000 | 1.04 |
| Resistivity μΩm | 0.267 | 0.73 |

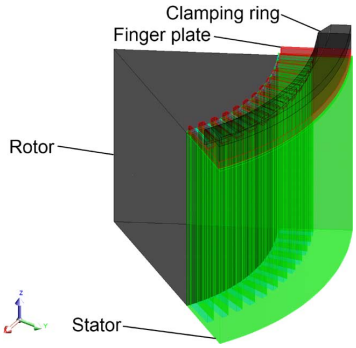


Fig. 1. One pole of the calculated machine.

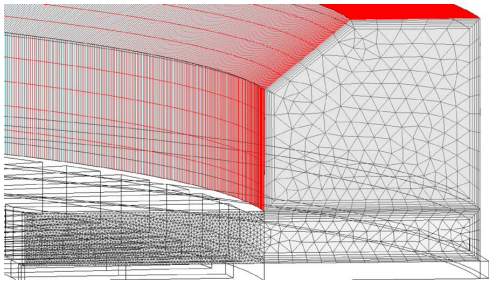

Fig. 2. Stator clamping ring and finger plate area dense mesh in areas where the skin effect is pronounced.

A 3-D steady-state AC magnetic finite element method was applied to analyze the clamping ring and finger plate losses using Flux 3D software. The main problem in building the model is the mesh; it must be known where the skin effect is pronounced and the number of mesh elements minimized accordingly. The mesh of the cross section of the clamping ring and the finger plate is depicted in Fig. 2. As the clamping ring can be extruded, a very accurate mesh can be achieved in the clamping ring and the yoke part of the finger plate, in which case mapped meshing can be used in the volumes. Using mapped faces makes the elements rectangular, and the mesh can be made fine near the surface, where the skin effect is pronounced. When using construction steel, the mesh does not have to be dense in the middle of the clamping ring because the skin depth is only 1 mm. The mesh is dense enough for stainless steel, as stainless steel has a skin depth of 50 mm with a nominal frequency of 82.5 Hz. To obtain sufficient accuracy in the eddy current losses there needs to be at least two elements in the skin depth [24]. The Flux 3D software uses second order interpolation and in order to model this kind of a problem correctly there needs to be at least two second order elements in the skin depth range.

When considering the tooth of the finger plate, the same accuracy cannot be achieved in the case of construction steel because the teeth cannot be extruded in Flux3D and the mapped mesh is unusable in the volumes. It is therefore not possible to generate an accurate mesh, i.e. the two elements in the skin depth are not achieved in every place where the skin effect is pronounced. Therefore, less accurate results have to be accepted in the finger plate. For stainless steel, the accuracy is, however, very good because the skin depth is large compared with construction steel and there are always more than two elements in the skin depth.

Modelling was carried out with various meshes. When the finger plate was calculated with a sparse mesh, the results with stainless steel were 10 times too large, illustrating the importance of correct mesh size for accurate results.

Material data for 3-D simulation are presented in Table I. Eddy current calculation is always a complex problem especially in 3-D, and sometimes convergence is not achieved. The material used was isotropic linear material because when using a saturating material the calculation did not converge. Using linear material means that the flux densities near the surface are higher than in reality. The unsaturated material thus adds some losses to the calculation but the results suggest that such losses are not high. The losses in reality should be somewhat smaller than those presented in this paper, indicating that it should be possible to use construction steel in the clamping rings and finger plates.

In addition to end region losses calculated with 3-D FEM, losses in the stator housing were studied by 2-D FEM calculation. The housing losses can be studied by 2-D FEM because the field is not 3-dimensional. The thickness of the yoke was varied and the maximum flux density in the yoke and the losses in the housing were recorded. When the losses in the housing start to occur can be seen from these results. This information is very useful for designers. In Fig. 3, the squares on the top of the yoke are welded to the stator stack. They are used to bolt the finger plate and the clamping ring to the stator and they are also included in the losses of the housing.

In the simulation, there are 200 $\mu$m air gaps between the iron parts and the stator yoke. In the actual machine there is always some air between the supporting structure and the stator yoke.

## III. RESULTS

### A. Stator Stack End Finger Plate and Clamping Ring Losses

In this section, 3-D FEM results are first presented for losses in the clamping ring and the finger plate with two different materials. In the second part, 2-D FEM is used to assess when losses start to occur in the housing.

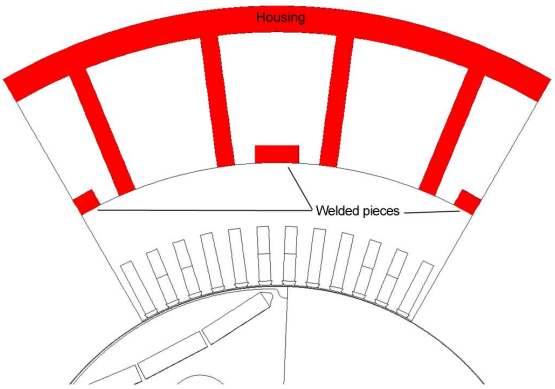


Fig. 3. Supporting steel structure of the machine.

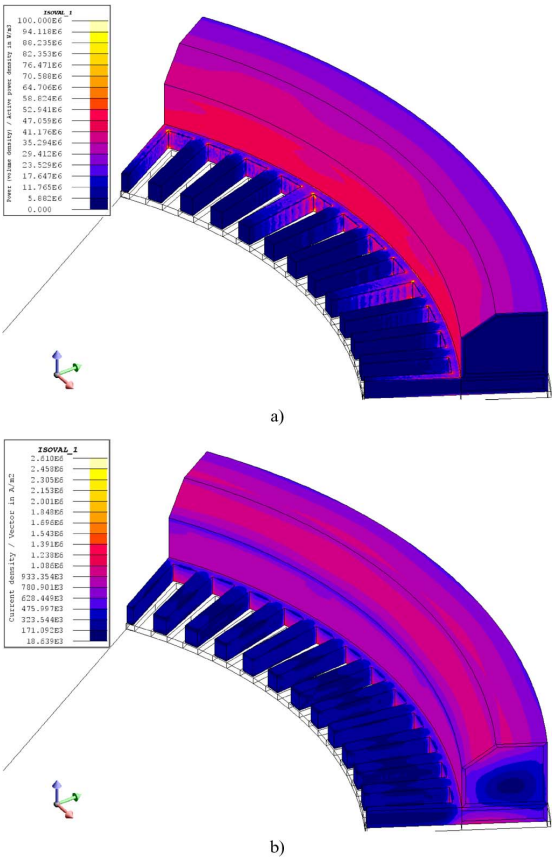


Fig. 4. Eddy current density when a) the finger plate and the clamping ring are made of construction steel and b) when the finger plate and the clamping ring are made of stainless steel.

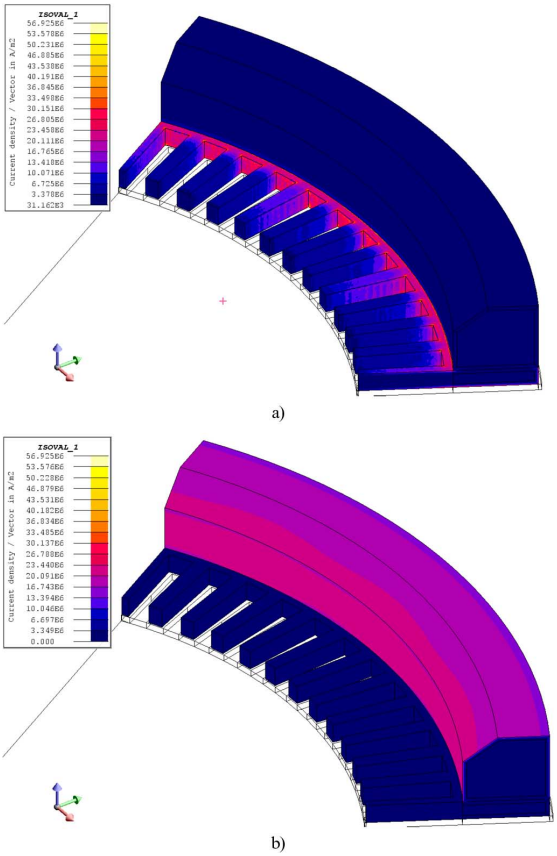


Fig. 5. Eddy current densities when a) the finger plate is made of construction steel and the clamping ring of stainless steel; b) the finger plate is made of stainless steel and the clamping plate of construction steel.

At correct voltage with no load, the armature current of a PM generator is practically close to zero and the load-dependent additional losses approach zero in these mechanical parts. However, at load the armature current linkage tries to excite also the finger plate and the clamping ring areas. Figs. 4 and 5 illustrate the current densities of the finger plate and clamping ring of the 3.1 MW six-pole machine used in this study. The thickness of the finger plates is 15 mm and the thickness of the clamping ring is 55 mm. A 3-D simulation was used where the current linkages produced by the armature currents travel axially before proceeding into the tangential parts of the end winding. In the calculation, the rated armature current (2800 $\mathrm{A_{rms}}$) was used at the rated frequency of 82.5Hz.

3-D FEM simulation results for the two different materials are presented in Table II. The losses are given for both ends of the machine.

Fig. 4 presents cases where the materials are the same in both the clamping ring and the finger plate. It was expected that the losses would differ significantly; the small size of the losses when using construction steel was somewhat surprising. Nevertheless, 2.3 kW savings in losses were obtained when using stainless steel instead of construction steel, signifying a 0.075% improvement in the efficiency. The eddy current density distribution in construction steel can be seen clearly in Fig. 6. Most

TABLE II
SIMULATION RESULTS IN 3-D FEM FOR THE CLAMPING RINGS AND THE FINGER PLATES MADE OF EITHER CONSTRUCTION STEEL OR STAINLESS STEEL

| Finger plate material | Clamping ring material | Finger plate losses [W] | Clamping ring losses [W] | Total losses [W] |
|---|---|---|---|---|
| Construction steel | Construction steel | 1220 | 1300 | 2520 |
| Stainless steel | Stainless steel | 70 | 140 | 210 |
| Construction steel | Stainless steel | 2640 | 280 | 2920 |
| Stainless steel | Construction steel | 140 | 1650 | 1790 |

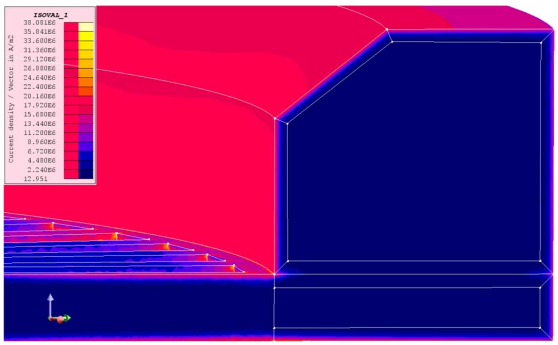

Fig. 6. Eddy current density when the finger plate and the clamping ring are made of construction steel.

of the eddy currents are concentrated on the edges of the ring and the plate, as expected.

The case was also studied where the clamping ring and the finger plate are made of different materials. Fig. 5 shows the eddy current density distribution when the clamping ring and finger plate materials are different. When the finger plate is made of construction steel and the clamping ring is made of stainless steel, the total losses are almost twofold compared with the case where the materials are vice versa.

When the finger plate is made of construction steel and the clamping ring is made of stainless steel, the losses seem to be bigger compared with the case where both are made from construction steel.

The results indicate that there is interaction between the finger plate and the clamping ring when different materials are used. Therefore, if one material is replaced by some other material, previous results cannot be considered to be fully valid even if the other supporting ring or plate in the new configuration is made of the same material. The losses need to be completely recalculated with new material data. When stainless steel is used instead of construction steel, a 0.075% increase in the rated point efficiency is attained.

It can be seen in Fig. 6 that when construction steel is used, the eddy currents are very much concentrated on the edges of the finger plate and the clamping ring. Consequently, a very dense mesh is needed at the edges. In Figs. 4(a) and 5(a), the current is not equal at every finger, which is due to the mesh not being dense enough in the finger plate. In Figs. 4(b) and 5(b), where stainless steel is used, the mesh density gives accurate results because two elements in the skin depth are enough to give accurate results and there are more than two elements in the skin depth throughout. The same mesh can be used for both materials.

In the case of the ferromagnetic material, the skin depth is limited because of the low resistivity ($\rho = 25\ \mu\Omega\text{cm}$) and high permeability. However, the ferromagnetic material experiences high flux densities because of the linear properties of the material, and significant eddy current losses are generated. Therefore, losses when the construction steel is used are higher than in reality. On the other hand, when the non-ferromagnetic material was used, the flux density remained low, and losses are therefore quite close to what they are in reality.

When looking at Fig. 5(b), one can see that the current density is higher in the inner circle of the clamping ring than the outer circle. This happens because flux penetrates the clamping ring radially and generates eddy currents that just circle tangentially in the surface of the inner circle. As far as the outer circle is concerned, the flux is only tangential and does not create any current tangential to the outer circle of the clamping ring.

### *B. Losses in the Support Structure*

Saturation in the stator yoke may result in losses in the stator supporting material. In this study, the stator external diameter was varied between 850 mm and 930 mm to adjust the saturation level. Variation of stator diameter was done by changing the stator yoke thickness. All other dimensions were kept unchanged. The results were derived with Flux2D. The results show that the additional losses in the housing can be prevented by correctly dimensioning the thickness of the stator yoke.

In Table III, the losses of the supporting parts of the machine are listed with maximum stator yoke flux densities excluding previously calculated finger plate and clamping ring losses. When the stator diameter is reduced from 930 mm to 850 mm, the additional losses in the supporting structure increase by 4 kW. The reason for this is that the stator yoke is close to saturation, and the magnetic voltage across the supporting parts starts to increase when the supporting iron becomes an attracting route for the flux.

As Table III shows, when the stator diameter is 880 mm and above, the losses in the support structure are close to nonexistent. It may be concluded that in cases when the stator yoke is

TABLE III
POWER LOSS IN THE HOUSING AND IN THE WELDED PARTS WITH DIFFERENT STATOR DIAMETERS

| Stator diameter [mm] | Maximum flux density at stator yoke [T] | Housing power loss [W] | Percentage of the output power [%] |
|---|---|---|---|
| 850 | 1.85 | 4275 | 0.14 |
| 855 | 1.79 | 2094 | 0.07 |
| 860 | 1.75 | 1885 | 0.06 |
| 865 | 1.72 | 1029 | 0.03 |
| 870 | 1.67 | 538 | 0.02 |
| 875 | 1.62 | 249 | 0.01 |
| 880 | 1.56 | 101 | 0.00 |
| 885 | 1.52 | 35 | 0.00 |
| 890 | 1.44 | 11 | 0.00 |
| 895 | 1.38 | 3 | 0.00 |
| 900 | 1.27 | 2 | 0.00 |
| 910 | 1.18 | 1 | 0.00 |
| 920 | 1.09 | 1 | 0.00 |
| 930 | 0.97 | 0 | 0.00 |

TABLE IV
PERMITTED FLUX DENSITIES AT THE STATOR YOKE FOR DIFFERENT TYPES OF ELECTRICAL MACHINES [26]

| Machine type | Stator yoke flux density $B$/T |
|---|---|
| Squirrel-cage motor | 1.4–1.7 |
| DC machine | 1.1–1.5 |
| Salient pole synchronous machine | 1.0–1.5 |
| Non-salient pole synchronous machine | 1.0–1.5 |

Fig. 7. 3.1 MW PMGs in back-to-back efficiency test setup.

designed to be thin, the designer may unintentionally add losses to the supporting structure. The flux densities given in Table IV can provide guidelines for design of the stator yoke thickness.

It should be noted that the thickness of the yoke not only affects losses in the housing but can also influence losses in other iron parts of the machine, as shown in [25].

### C. Efficiency Measurement of 3.1 MW 1650 rpm PMG

Efficiency measurements were carried out on 3.1 MW PMGs. The test setup is depicted in Fig. 7. The efficiency measurement was done by using two identical machines connected back-to-back and using IEC 34-2 [1] to calculate the efficiency. In the first measurement, the finger plates and clamping rings were made from construction steel and the efficiency was measured to be 97.4%. In the second measurement, the finger plates and clamping rings were made from stainless steel and the efficiency was measured to be 97.5%.

Taking the margin of error of the measurements into consideration, the data indicate that the FEM calculation results are within the correct range.

## IV. CONCLUSION

In 3-D FEM eddy current problems, a dense mesh has to be built in areas where the skin effect is pronounced. The mesh has to be denser near the surface of the investigated object to obtain accurate results. In this paper, a very accurate mesh was built and the losses with a non-ferromagnetic and a ferromagnetic material were calculated. According to the simulation results, a loss that reduces the efficiency by 0.075% takes place in the finger plates and the clamping rings when using a ferromagnetic material. This loss value can be reduced almost to zero by switching to a non-ferromagnetic material. The result was verified by efficiency measurements of 3.1 MW PMGs that had finger plates and clamping rings made either of construction steel or stainless steel. With low-loss material, a clear improvement in the machine efficiency was measured.

Based on the results of this paper, designers can easily estimate the importance of additional losses in these types of

machines. The designer can choose from two different and common materials used in the end region support structure. Even construction steel can be used without compromising the efficiency too much.

Despite the seemingly small loss in efficiency, it should be noted that with a 4000 h annual load factor the lost production is worth euro 750–1000 p.a. at an energy price of 80 euro/MWh. Losses can also be generated in the stator supporting structure if there is too high a flux density in the stator yoke, that is, if the stator yoke starts to saturate. If the peak stator yoke flux density is limited to 1.5 T in the stator yoke, there will be no significant losses in the housing of a machine at a low operating frequency. This result supports traditional guidelines for generator stator yokes.

In conclusion, it should be noted that even such a small improvement as found in this study is of significance when pursuing highly efficient electrical machines.

## ACKNOWLEDGMENT

The authors would like to thank The Switch Drive Systems for their assistance.

## REFERENCES

[1] *IEEE Criteria for Class IE Electric Systems (Standards Style)*, IEEE Standard 308, 1969, Rotating Electrical Machines-Part 2: Methods for Determining Losses and Efficiency of Electrical Machinery From Tests (Excluding Machines for Traction Vehicles) With Amendments 1: 1995 and 2: 1996, IEC Std 60 034-2, 1972.

[2] T. Bratoljic, "Currents induced in the inner stator frame of large turbogenerators by the end-zone field," *IEEE Trans. Energy Convers.*, vol. EC-1, no. 4, pp. 108–114, Dec. 1986.

[3] D. C. Hanselman and W.H. Peake, "Eddy-current effects in slot-bound conductors," *IEE Proc.–Elect. Power Appl.*, vol. 142, no. 2, pp. 131–136, Mar. 1995.

[4] H. Seok-Hee, T. M. Jahns, and Z. Q. Zhu, "Analysis of rotor core eddy-current losses in interior permanent-magnet synchronous machines," *IEEE Trans Ind. Appl.*, vol. 46, no. 1, pp. 196–205, Jan./Feb. 2010.

[5] R. L. Stoll and P. Hammond, "Calculation of the magnetic field of rotating machines. Part 5. Field in the end region of turbogenerators and the eddy-current loss in the end plates of stator cores," *Proc. Inst. Elect. Eng.*, vol. 113, no. 11, pp. 1793–1804, Nov. 1966.

[6] Y. Liang, H. Huang, and G. Hu, "Numerical calculation of end region electromagnetic field of large air-cooled turbogenerator," in *World Automation Congress, WAC 2008*, 2008, pp. 1–5.

[7] M. Fujita, T. Ueda, T. Tokumasu, K. Nagakura, M. Kakiuchi, and T. Otaka, "Eddy current analysis in the stator end structures of large capacity turbine generators," in *Int. Conf. Electrical Machines and Systems, ICEMS 2009*, 2009, pp. 1–6.

[8] Y. Yao, H. Xia, G. Ni, X. Liang, S. Yang, and P. Ni, "3-D eddy current analysis in the end region of a turbogenerator by using reduced magnetic vector potential," *IEEE Trans. Magn.*, vol. 42, no. 4, pp. 1323–1326, Apr. 2006.

[9] L. Jinxiang, S. Yutian, and Y. Guijie, "Calculation and analysis of 3D magnetic field for end region of large turbogenerators," in *Proc. Eighth Int. Conf. Electrical Machines and Systems, ICEMS 2005*, 2005, vol. 3, pp. 2079–2082.

[10] K. Takahashi, K. Hattori, A. Nakahara, and M. Saeki, "Three dimensional harmonic field and eddy current analysis for rotor end region of turbine generator," in *IEEE Int. Conf. on Electric Machines & Drives, IEMDC '07*, 2007, vol. 1, pp. 477–481.

[11] G. K. M. Khan, G. W. Buckley, R. B. Bennett, and N. Brooks, "An integrated approach for the calculation of losses and temperatures in the end-region of large turbine generators," *IEEE Trans. Energy Convers.*, vol. 5, no. 1, pp. 183–194, Mar. 1990.

[12] R. Lin, A. Haavisto, and A. Arkkio, "Validation of a time-harmonic numerical model for solving magnetic field in end region of a radial-flux machine," *IEEE Trans. Magn.*, vol. 45, no. 12, pp. 5360–5367, Dec. 2009.

[13] R. Lin and A. Arkkio, "Calculation and analysis of stator end-winding leakage inductance of an induction machine," *IEEE Trans. Magn.*, vol. 45, no. 4, pp. 2009–2014, Apr. 2009.

[14] R. Lin, A. Haavisto, and A. Arkkio, "Analysis of eddy-current loss in end shield and frame of a large induction machine," *IEEE Trans. Magn.*, vol. 46, no. 3, pt. 2, pp. 942–948, Mar. 2010.

[15] R. Lin, A. Haavisto, and A. Arkkio, "Axial flux and eddy-current loss in active region of a large-sized squirrel-cage induction motor," *IEEE Trans. Magn.*, vol. 46, no. 11, pp. 3933–3938, Nov. 2010.

[16] S. L. Ho, H. L. Li, and W. N. Fu, "Inclusion of interbar currents in a network-field coupled time-stepping finite-element model of skewed-rotor induction motors," *IEEE Trans. Magn.*, vol. 35, no. 5, pt. 3, pp. 4218–4225, Sep. 1999.

[17] V. C. Silva, Y. Marechal, and A. Foggia, "Surface impedance method applied to the prediction of eddy currents in hydrogenerator stator end regions," *IEEE Trans. Magn.*, vol. 31, no. 3, pp. 2072–2075, May 1996.

[18] V. C. Silva, G. Meunier, and A. Foggia, "A 3D finite-element computation of eddy currents and losses in the stator end laminations of large synchronous machines," *IEEE Trans. Magn.*, vol. 32, no. 3, pt. 1, pp. 1569–1572, May 1996.

[19] E. Schmidt, G. Traxler-Samek, and A. Schwery, "Comparison of time-harmonic and transient finite element analyses for eddy currents in the stator clamping system of synchronous generators," in *Canadian Conf. Electrical and Computer Engineering, CCECE 2007*, pp. 260–263.

[20] E. Schmidt, G. Traxler-Samek, and A. Schwery, "Influence of higher harmonics in the end region magnetic field on eddy currents in the stator clamping system of hydro generators," in *IEEE Int. Conf. Electric Machines and Drives*, 2005, pp. 1268–1274.

[21] K. Takahashi, K. Hattori, A. Nakahara, and M. Saeki, "Three dimensional harmonic field and eddy current analysis for rotor end region of turbine generator," in *IEEE Int. Conf. Electric Machines & Drives, IEMDC '07*, 2007, vol. 1, pp. 477–481.

[22] R. De Weerdt and R. Belmans, "Squirrel cage induction motor end effects using 2D and 3D finite elements," in *Seventh Int. Conf. Electrical Machines and Drives*, 1995, pp. 62–66, Conf. Publ. No. 412.

[23] A. El-Refaie, M. Shah, J. Alexander, S. Galioto, K. Huh, and W. Gerstler, "Rotor end losses in multi-phase fractional-slot concentrated-winding permanent magnet synchronous machines," *IEEE Trans. Ind. Appl.*, vol. 47, no. 5, pp. 2066–2074, Sep./Oct. 2011.

[24] V. Ardon, J. Aime, O. Chadebec, E. Clavel, J.-M. Guichon, and E. Vialardi, "EMC modeling of an industrial variable speed drive with an adapted PEEC method," *IEEE Trans. Magn.*, vol. 46, no. 8, pp. 2892–2898, Aug. 2010.

[25] H. Hamalainen, J. Pyrhonen, and J. Nerg, "Effects of quadrature axis armature reaction on magnetic circuit time harmonics and stator iron losses in a permanent magnet synchronous generator with embedded magnets," *IREE, Int. Rev. Elect. Eng.*, vol. 5, no. 5, pt. A, p. 6, 2010.

[26] J. Pyrhönen, T. Jokinen, and V. Hrabovcova*, Design of Rotating Electrical Machines*. New York: Wiley, 2008, p. 283, 459.

**Publication III**



H. Hämäläinen, J. Pyrhönen, J. Nerg, J. Talvitie, “Ac resistance Factor of Litz-Wire Windings Used in Low-Voltage Generators,” *IEEE Transactions on Industrial Electronics,* forthcoming.

# AC Resistance Factor of Litz-Wire Windings Used in Low-Voltage High-Power Generators

Henry Hämäläinen, Juha Pyrhönen, *Member, IEEE,* Janne Nerg, *Member, IEEE, and* Joonas Talvitie, *Member, IEEE*

***Abstract*— New types of heavy litz wires with noninsulated or insulated strands are offered for high-power low-voltage electrical machines, where skin and proximity effects can cause serious problems if traditional windings are used. This paper evaluates the ac resistance of a litz-wire and its usability in MW range low-voltage electrical machines. The evaluation is made by finite element analysis and by resistance measurements with an experimental test setup. A simple amplifier configuration was used to minimize current and voltage phase shift errors, which are critical in this kind of low impedance and low frequency measurement. A simple measurement device based on the above-mentioned configuration was prepared to ensure a precise measurement result. Tests were done in a frequency range of 50 Hz to 200 Hz, to cover a wide range of practical high-power low-voltage electrical machines. It is found that the measured litz wire with originally noninsulated strands can be used in large electrical machines up to about 120 Hz if about 50% increase in ac-resistance compared to the dc-resistance is allowed. Impregnation of the originally noninsulated litz wire with VPI improved the ac resistance in one test case, and in the other case, it seemed to have no effect on the ac resistance.**

***Index Terms*—Eddy currents, skin effect, proximity effect, litz wire, low-voltage, generator**

## I. INTRODUCTION

Minimizing eddy current losses in electrical machines is an important task when improving efficiency [1]. Utilization of new types of heavy litz wires now offers a practical approach to mitigate the skin effect and harmful circulating currents in rotating electrical machines, especially, in multi-megawatt low-voltage applications.

Litz wires with insulated subconductors have for decades been widely used in high frequency applications such as transformers [2]-[10] and induction cooking heating appliances [11] [12]. They have also been proposed for HTS (high temperature superconductor) machines [13] [14] where the flux densities are high and pass through the conductors.

Traditionally, high-frequency litz wires have been manufactured of very thin insulated strands and have not been considered applicable in high-power rotating machines because of high costs and a poor space factor for copper $k_{\mathrm{Cu}}$ .

Manuscript received August 14, 2012; revised November 23, 2012 and January 11, 2013; accepted February 20, 2013. This work is supported in part by Von Roll and in part by The Switch Drive Systems.

The Authors are with Lappeenranta Univertsity of Technology, 53850, Lappeenranta, Finland (e-mail:henry.hamalainen@lut.fi; juha.pyrhonen@lut.fi; janne.nerg@lut.fi; joonas.talvitie@lut.fi).

Color versions of one or more of the figures in this paper are available online at http://ieeexplore.ieee.org.

Digital Object Identifier 10.1109/TIE.2013.2251735

The trend of using low-voltage multi-megawatt generators for full power converter applications, especially in wind power generation, has increased problems associated with avoidance of high Joule losses, as the number of turns in a slot usually remains very low, sometimes just one turn per slot. In such windings, the skin effect and circulating current problems are obvious at normal generator frequencies, if full transposition of the subconductors cannot be arranged. Such a transposition with traditional form wound windings easily leads, in practice, to the use of Roebel bars, which are very expensive.

A completely new range of heavy litz wires has now become available on the marketplace. Such litz wires with noninsulated subconductors are cheap enough to be used in multi-megawatt electrical machines. However, the advantageous price comes at the cost of a lack of insulation between the subconductors. The underlying idea of litz wire with noninsulated strands is that the galvanic connections between subconductors in the slot area, especially after winding impregnation, are assumed to be weak enough so that the wire can be used at moderate machine frequencies without the large Joule losses which are present in bulky conductors.

Litz wire, by definition, has insulated subconductors and thus litz with noninsulated strands should maybe not be called litz wire but rather a bunched wire [2]. This paper, however, shall use the term litz wire also for stranded and transposed wires dedicated for use in low-voltage electrical machines even when the strands are originally noninsulated.

The advantages of using these novel litz wires for low voltage high-power machines are that: 1) the Joule losses remain low because of a good transposition, meaning that each strand is, in practice, linked by the same amount of slot leakage flux, and therefore, no circulating currents between parallel strands are formed, 2) manufacturing of the winding is easy, as the non-impregnated litz wire is very easy to bend, 3) the whole phase winding can be made without any joints between coils, and 4) as a result of the lack of joints, there is no need to make extra insulations at the coil ends.

The low rigidity of litz wire creates a need for extra support systems for the end-windings, which can be regarded as an adverse effect of using these novel litz wires.

Analytical methods have been developed to evaluate litz wire losses in transformers [2]-[9] [15]-[21]. Probably the most cited work concerning the ac resistance is Dowell's formula, which can be used to evaluate round-wires [10], form wound windings [22] and litz wires [18].

The resistance in a noninsulated and oxidized litz wire depends on how tightly the wire is packed into the slot. Xu and

Sullivan [5] has measured the resistance between parallel non-insulated subconductors and has found that the conductivity between strands changes as a function of wire packing pressure until 80 kPa. Although the data were inconsistent, even in the worst case, the measured resistivity was 1000 times the resistivity of copper conductor material. Xu's model is complex and its use requires knowledge of the resistance between subconductors. For this reason, usage of the model has been precluded in our paper.

In this paper, we shall study if the assumption of low losses of impregnated litz wire with originally noninsulated strands in rotating machines is valid. Two actual 3 MW permanent magnet (PM) generators (PMG) were manufactured; one using litz wire with noninsulated subconductors and the other using form wound windings. No difference between the two versions was observed in the efficiency measurements, which supports the idea that a low loss winding can be manufactured using heavy litz wires. The aims of this paper are to assess whether this result is correct and, furthermore, to determine until which approximate frequency the technology can be used in large low-voltage electrical machines. Other litz wires were also measured to increase the amount and reliability of data. For the difficult measurement of very low ac-resistance, a simple operational-amplifier-based measurement device was developed to minimize the effect of phase shift error, which is a critical factor in this kind of low resistance and high inductance measurement.

## II. EDDY CURRENTS

An equation for calculating the dc resistance in a litz wire has been developed, e.g., in [5], as:

$$R_{\mathrm{DC,litz}} = \frac{4\rho_{\mathrm{Cu}} l}{\pi n d_{\mathrm{s}}^2}\left(1+\frac{\pi^2 n d_{\mathrm{s}}^2}{4k_{\mathrm{Cu}} l_{\mathrm{p}}^2}\right), \qquad (1)$$

where $\rho_{\mathrm{Cu}}$ is the resistivity of copper, $k_{\mathrm{Cu}}$ is the copper space factor (typically around 0.6), $l$ the total length of the wire, $d_{\mathrm{s}}$ is the diameter of the sub-conductor, $n$ is the number of subconductors, and $l_{\mathrm{p}}$ is the pitch of the litz wire arrangement.

The resistance also depends on the temperature

$$\rho_{\mathrm{Cu}} = \rho_{\mathrm{Cu(20°C)}}(1+\Delta T\alpha_{\mathrm{Cu}}), \qquad (2)$$

where $\rho_{\mathrm{Cu(20°C)}}$ is the resistivity of copper at 20 degrees Celsius, $\Delta T$ is the temperature difference to 20 degrees Celsius, and $\alpha_{\mathrm{Cu}}$ the temperature coefficient of resistivity. The resistivity of a standard commercial copper, according to the international annealed copper standard (IACS) at room temperature (+20 °C) is $\rho_{\mathrm{Cu(20°C)}} = 1.724\cdot10^{-8}$ Ωm. The resistivity of higher-purity copper can be a few percents lower than that of the IACS value. The temperature coefficient of the resistivity for copper is $\alpha_{\mathrm{Cu}} = 3.81\cdot10^{-3}$ 1/K.

When a current carrying conductor with a finite cross-sectional area carries an alternating current, according to Faraday's induction law, an electric field strength $\boldsymbol{E}$ curl is induced in the internal paths of the conductor

$$\nabla\times E = -\frac{\partial B}{\partial t}, \qquad (3)$$

which in turn creates an eddy current density vector $\boldsymbol{J}$

$$J = \frac{1}{\rho_{\mathrm{Cu}}}E \quad . \qquad (4)$$

Based on (3) and (4), the current density $J$ is dependent on the conductor inductance and the physical properties of the conducting material.

The depth of penetration $\delta$ for a plane conductor is

$$\delta = \sqrt{\frac{\rho}{\mu\pi f}}, \qquad (5)$$

where $f$ is the supply frequency, and $\mu$ is the conductor permeability.

A formula for calculating losses in a litz wire with insulated strands has been developed in [2] as

$$k_{\mathrm{r}} = 1+\frac{\pi^3\omega^2\mu_0^2 z_{\mathrm{Q}}^2 n^2 d_{\mathrm{s}}^6}{3\times768\rho^2 b_{\mathrm{b}}^2} \quad , \qquad (6)$$

where $\omega$ is the angular frequency of a sinusoidal current, $\rho$ is the resistivity of the conducting material, $\mu_0$ is the vacuum permeability, $z_{\mathrm{Q}}$ is the number of turns in a slot, $n$ is the number of strands, $d_{\mathrm{s}}$ is the diameter of each strand, and $b_{\mathrm{b}}$ is the slot width. Eq. (6) has been derived based on the assumption that each strand is thin compared to the depth of penetration and, therefore, it assumes that the field is uniform inside a conductor [4]. It also assumes that there is equal current sharing between the strands, which means that the construction of the litz wire is done in such a way that it minimizes the bundle-level skin and proximity effects correctly [4], i.e., there is ideal transposition in the wire, which, in practice is not fully true. Eq. (6) only applies for 1-D field. The formula does not take into account the end winding in any way. End winding resistance, however, still plays a big part in the total resistance factor because the longer the end winding, the greater is the resistance faced by the circulating currents and the smaller will be the effect of the slot bound area on the total resistance factor. The skin effect and proximity effect originate mostly in the slot area [23]. The total increase in the ac resistance is the average effect in the whole winding. If only the effects in the slot area are taken into consideration, the effect seems to be high, but when the end winding is taken into account, the total winding resistance factor gets smaller. In the test stack in this study, the amount of copper in a slot is set to be 50 % of the total copper amount. In the actual 3 MW PM machine, where noninsulated litz with 0.5 mm diameter subconductors were used, the length ratio between the slot-bound conductor and end-winding conductor is about 65 % and 35 % respectively. If the end winding resistance is taken into account using (2) the result is:

$$k_{\mathrm{r}} = \left(1+\frac{\pi^3\omega^2\mu_0^2 N^2 n^2 d_{\mathrm{s}}^6}{3\times768\rho^2 b_{\mathrm{b}}^2}\right)\frac{l_{\mathrm{stack}}}{l_{\mathrm{turn}}}+\frac{l_{\mathrm{end-winding}}}{l_{\mathrm{turn}}}, \qquad (7)$$

where $l_{\mathrm{stack}}$ is the length of the winding inside a stack, $l_{\mathrm{end\text{-}winding}}$ is the length of the end winding, and $l_{\mathrm{turn}}$ is the length of the turn.

Most of the stray flux crosses the slot near the slot opening and for solid or non-transposed stranded conductors it seems to force most of the current to travel as close to the slot opening as possible. The proximity effect amplifies the phenomena in such a way that the other side of the conductor, nearer the slot bottom, also seems to acquire a large current density, leaving the centre of the conductor with lower current density. The proximity effect is always present in multi-layered windings [24], [25].

Eddy currents flow in two ways in windings; 1) by the skin effect that is caused by the conductor's own field, and 2) by the proximity effect that is caused by the field of the conductors adjacent to the conductor in question. From these effects, two physical eddy currents are built. Firstly, inside a solid conductor, eddy currents flow in the slot bound areas. This can also be called strand-level eddy current loss. Secondly, if there are parallel conductors, a circulating current will flow through the whole winding in the parallel conductors.

Eddy currents inside a solid conductor can be minimized by dividing the conductors into smaller subconductors (parallel strands). However, when subconductors are used, circulating currents start to occur between them. The circulating currents go from one coil end to another where the subconductors are in galvanic contact. A transposition can be used to minimize the circulating currents between the subconductors. A double-layer form-wound winding partly cancels out the circulating current since the sub-conductor at the top of the slot is at the bottom of the slot on the other coil side. To minimize circulating currents further, the subconductors should be equally placed in every position in the slot depth. Since this is not possible with form-wound winding, litz wires or Roebel bars can be used. In a litz wire, ideally, each sub-conductor travels thorough the slots via all possible magnetic conditions averaging the slot leakage flux effects to be the same in all insulated strands, thus preventing circulating currents between parallel subconductors connected galvanically together at machine terminals. However, if eddy currents are minimized, there is the drawback of increased dc-resistance of the wire, caused by the addition of insulation between the subconductors and a small length increase as the strands are twisted together. In multi-megawatt low-voltage permanent magnet windmill generators, the space factor for copper $k_{Cu}$ of a form-wound machine, based on our experience, is about 0.6. With noninsulated litz wire, the space factor reached in our test machines is about 0.58. Thus, with noninsulated litz wire, the dc-resistance was increased by 3%.

## III. Measurement Setup and Analysis Method

Four types of litz wires were measured and compared when preparing this paper. Two of the tested litz wires are shown in Fig. 1. The wire on the left-hand side of Fig. 1 has subconductors of 0.5 mm in diameter. The number of subconductors is 631 and the dimensions of the whole conductor are 12 mm × 14 mm ($w \times h$). The wire on the right-hand side of Fig. 1 has 1 mm diameter round noninsulated subconductors. The dimensions of the whole conductor are 10.5 mm × 18 mm ($w \times h$) and it consists of 180 noninsulated subconductors. The third litz wire consists of 176 grade 0 insulated 1-mm-diameter subconductors. Grade 0 is used by Von Roll in their standard for litz wires [26]. Grade 0 has one layer of enamel on it. Also litz wire that consists of 179 oxidized 1-mm-diameter subconductors was measured and compared.

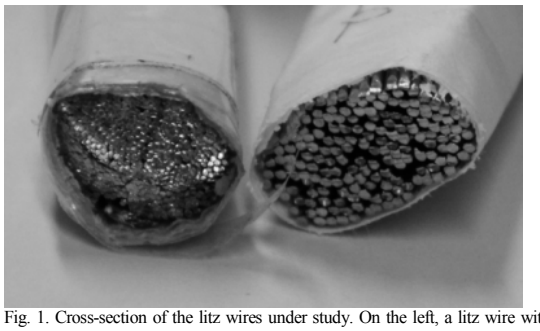

Fig. 1. Cross-section of the litz wires under study. On the left, a litz wire with 630 noninsulated subconductors, and on the right, a litz wire with 180 noninsulated subconductors. Both wires originally have rectangular form but are deformed because of cutting.

TABLE I
LITZ WIRE CONFIGURATION.

| No. | Litz wire type | Centre bundle | Outer bundle | Insulated strands | Pitch [mm] |
|---|---|---|---|---|---|
| 1 | 6×11+11×10 (176× 1mm) | 6×10 | 6×11+ 5×10 | Yes | 310 |
| 2 | 8×10+9×11 (179 × 1mm) | 6×10 | 2×10+ 9×11 | Oxidized | 310 |
| 3 | 10×11×7x10 (180 × 1mm) | 5 × 11 | 5×11+ 7×10 | No | 310 |
| 4 | 5×45+10×36 (631 × 0.5mm) | 11×32 | 2×32+ 5×43 | No | 160 |

The bundle configurations are presented in Table I. The wires have been given a label used later in the figures. The measured litz wires are constructed in a way that the centremost bundles are twisted together and then other bundles twisted around the centre bundles. In Table I, for example, the first number set (6×11) means that there are in total 6 bundles with 11 strands in each bundle and the latter (+11×10) shows that there are 11 more bundles with 10 strands in each bundle. Such a litz does not represent ideal transposition because the centremost bundles will never pass through the edges of the wire but stay in the centre.

For each wire, the dc resistance is measured and used to calculate the resistance factor according to (8) and (9).

The wires with noninsulated strands were measured before and after the impregnation. The impregnation was done with the vacuum pressure impregnation (VPI) method. The resin used is polyester CC1105 and the impregnation was repeated twice. The VPI method ensures good penetration of resin between individual subconductors and, to some extent, seems – according to our results – to lessen the galvanic connections between the subconductors with noninsulated litz.

Finite-Element (FE) Method (FEM) analysis was used to evaluate the ac resistance factor in a single conductor in the litz wire with 1 mm thick insulated subconductors and also to compare the double-layer form-wound winding and its

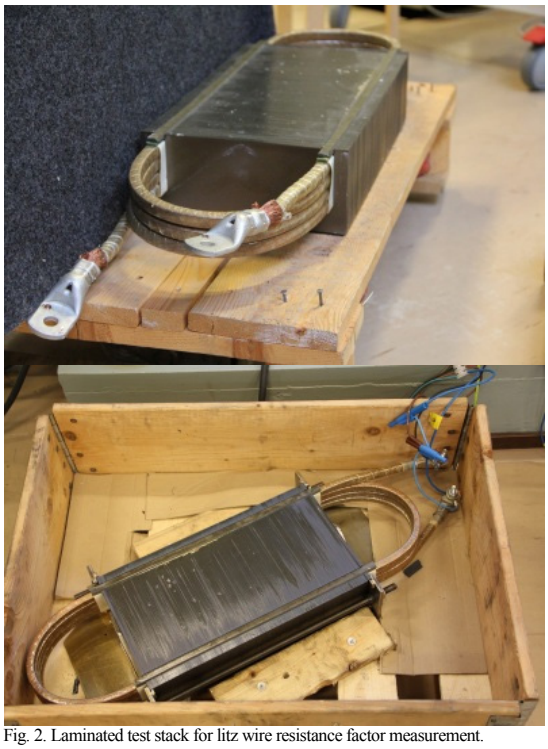

Fig. 2. Laminated test stack for litz wire resistance factor measurement.

usability compared with litz wire with 0.5 mm noninsulated subconductors.

The losses were measured on two 3-MW 6-pole PM machines equipped either with form-wound windings or with litz wire windings (0.5 mm subconductors). The measurement was performed in a back-to-back connection of two machines, the first one having a litz wire winding and the second one having a form wound winding. There were several PT-100 sensors inserted in the windings. No substantial difference was observed in the winding temperatures of the machines at a nominal frequency of 82 Hz, which would indicate that the copper losses should be quite close to each other. However, it should be borne in mind that the stator copper losses in this kind of a machine constitute only 25 % of the total losses (according to the efficiency measurements) and small changes in losses are not observed easily at operational temperatures.

The concept underlying the litz wire is that small enough parallel subconductors are transposed as ideally as possible so that the circulating currents are, in practice, eliminated. Additionally, each single sub-conductor should be thin enough that no significant eddy currents are formed inside a single conductor. The concept of the well-impregnated litz wire with originally noninsulated strands, on the other hand, presupposes that the galvanic contacts between the subconductors are sufficiently weak as to make actual insulation unnecessary.

A test arrangement was planned in which a test stack would simulate the real machine using representative slots.

The test stack designed is shown in Fig. 2. The test stack was made from M400-50A iron and was 400 mm in length. The stack has rectangular, actual-sized slots that emulate the slots of an actual machine, causing a transverse flux density across the

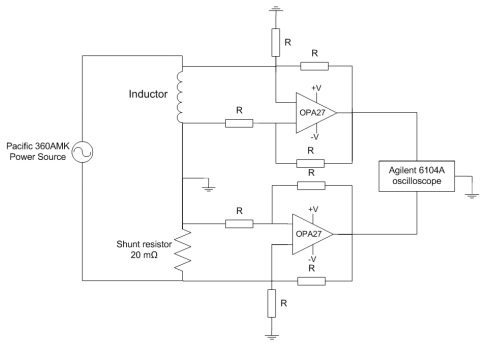


Fig. 3. Measurement instrumentation using two identical differential operational amplifier circuits.

slot and encouraging the skin effect and proximity effect to take place. The stack support structure is made from non-magnetic stainless steel to avoid additional losses. The non-magnetic stainless steel bars used to tighten the stack are insulated at the ends.

The coil has four turns and the end windings are as long as the conductors inside the iron slot (400 mm). Thus, the total length of the coil is 6400 mm. The dc resistance is in the range of 1 mΩ.

### *A. Measurement setup*

The dc resistances were measured using a Hewlett Packard 34420A micro-ohm meter. A Pacific 360-AMX ac power source was used with frequencies 50–200 Hz. 50 Hz is the lower limit for the device. The current shunt used in current measurement was a Hilo-Test ISM 5P/20. An Agilent DSO6104A oscilloscope was used to obtain voltage and current measurements.

In the ac resistance measurement, we are operating near 90° of phase shift between voltage and current phasors, which makes the measurement sensitive to error. This error is usually known in measurement devices as *Q*-factor error. A 1° error between the phase difference of voltage and current would mean that the resistance factor is 50 % higher than it should be. The total impedance is in the range of 20 mΩ at 50 Hz, which means that impedance measurement devices are unusable in this frequency range.

To obtain accurate measurement, one has to make sure that connections are solid. Voltage probes of type 10074D by Agilent were also used, but the result had a poor signal-to-noise ratio and, therefore, measurements with the probes only were unusable. We believe that the poor signal-to-noise ratio was caused by the electromagnetic interference coupled to the measurement via the physically large inductor. To overcome the noise problem, a simple application-specific measurement device was built to reduce the bandwidth of the measurement. The measurement amplifier was prepared using OPA27 operational amplifiers with 0.1 dB bandwidth of 35 kHz. The schematics of the measurement are depicted in Fig. 3.

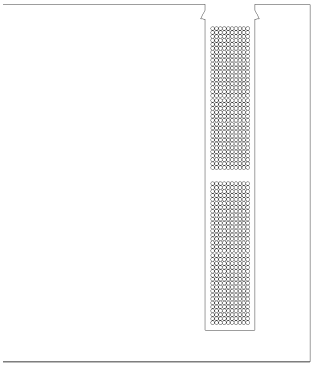

Fig. 4. Geometry of the FEA. There are 720 insulated solid conductors in a slot. Therefore, no galvanic connections between adjacent wires are modelled in the FEA.

A low measurement current was used in the measurements to avoid excessive iron losses. This approach was used because any iron loss would sum up to the result and the conductor Joule losses would seem higher than they really are. The low iron losses were confirmed with Flux 2-D's loss surface model, which is a scalar and dynamic hysteresis model [27]. Only the third decimal in the losses changed and this had no noticeable effect on the result.

Temperature was not measured but we concluded that the temperature would not rise significantly because of the low measurement current (7 A) and the large cross-section area (124–141 mm$^2$) of the litz wire.

The basic approach was to measure the coil current and voltage and calculate the active power by integration of multiplication of the current and voltage instantaneous values. The ac-resistance can then be written

$$R_{\mathrm{ac}} = \frac{P}{I_{\mathrm{rms}}^2}. \qquad (8)$$

The resistance factor is calculated as

$$k_{\mathrm{r}} = \frac{R_{\mathrm{ac}}}{R_{\mathrm{dc}}} \ . \qquad (9)$$

## IV. FEM ANALYSIS

There are two physical eddy current components which originate from the skin effect and proximity effect, mostly in the slot area." In this analysis, we however assume that eddy currents are only originated from slot area because of simplification. This means that the resistance factor for the end-winding area is assumed to be 1.00 in the FEM and in (7). This was confirmed with FE analysis (FEA) for the geometry depicted in Fig. 4. The simulation showed that when iron was changed to air, the losses at 200 Hz were 4.4 ‰ bigger than at 5 Hz. Based on these results, we can assume that the end winding ac resistance factor with originally insulated 1 mm subconductors is $k_{\mathrm{r}} = 1$. FEM analysis was also used to get additional confirmation data for the comparison.

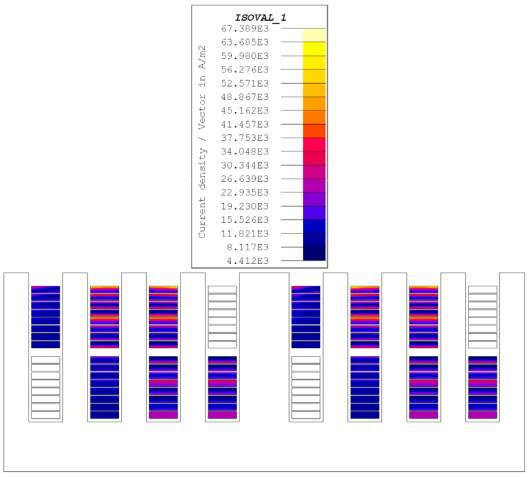


Fig. 5. FEA results of the form-wound winding. Current density distribution is illustrated with nominal frequency.

The geometry of the FEA is presented in Fig. 4. There are 4 × 180 = 720 insulated solid copper conductors in a slot. One litz wire contains, in principle, 180 solid subconductors in parallel, but to examine the amount of ac resistance factor inside a single sub-conductor with FEM, all the conductors have to be put into series to avoid circulating currents in the calculation. The average resistance factor of all the subconductors then gives the resistance factor for the whole winding caused by eddy currents inside subconductors. The same result is also valid for the ideally stranded litz wire with insulated strands. The end winding resistance also has to be included in the result to be comparable to actual winding.

The FEM result was also compared with the measurement results to evaluate how much of the resistance increase is caused inside subconductors and how much is due to the circulating currents between parallel subconductors the use of which the litz wire is trying to minimize. Since the transposition of the conductor is not ideal, there will be some circulating currents between parallel subconductors. A temperature of 20° C was used in the FEA as the temperature of the copper.

FEA of the form wound winding resistance factor was done in the same way as the litz wire FEA, with the exception that the circuit was modelled as a real winding consisting of both series-connected and parallel-connected conductors and a real number of slots per pole and phase. Every conductor, seen in Fig. 5, is described in the circuit as a solid conductor enabling internal eddy currents. Additionally, end winding resistance is included in the results because it affects the resistance factor. The amount of slot-bound copper is set to be equal with the copper in the air to be able to make a comparison with our measurement setup.

## V. RESULTS

### A. Litz wire comparison

Fig. 6 presents an example of the measured signals. The curve with less distortion is the current measurement signal,

and the other one is the voltage signal. The current has to be multiplied by 25, meaning that the current amplitude is about 10 A in all the frequency range. The voltage has to be divided by two to get the actual voltage values, and when frequency is increased, the voltage increases because the system impedance is increasing. The current stays about the same because the measured device has actually a lot smaller impedance than the inner impedance of the feeding system. FFT was used to obtain the measured resistance factor with fundamental frequency, but the factors calculated from the original signal only differ by a few thousandths.

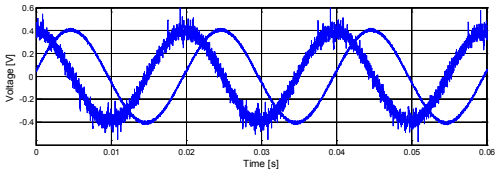


Fig. 6. Example of measured signals with 50 Hz.

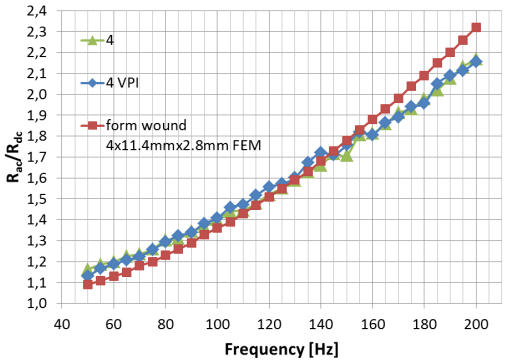


Fig. 7. Resistance factors of the FE-analyzed form-wound winding, the measured litz winding with 630 originally noninsulated subconductors with and without impregnation. See legends in Table I.

The measured resistance factor of the noninsulated litz wire and the FEM-simulated resistance factor of the form-wound winding are given in Fig. 7. Both of these windings have been used in an actual low voltage 3-MW PMG. No difference was observed between the different windings in the efficiency measurements of the machine. The results in Fig. 7 indicate that the initial measurements were correct. There is a small difference between the windings, but it would not be seen in the efficiency measurements because in this machine type the copper losses constitute only about 25 % of the total losses. Consequently, the difference in the results, based on Fig. 7, is only some hundreds of watts, which would be lost in the uncertainty of the efficiency measurement. Based on the information in Fig. 7, noninsulated litz wire with 630 subconductors could be used in this machine until 120 Hz if an ac resistance factor 1.5 is allowed for copper losses. The allowed increase in ac copper losses also depends naturally on how much losses the designed cooling system can handle.

Results for litz wire number 1 in Table I, i.e. litz wire with 1-mm insulated subconductors, are depicted in

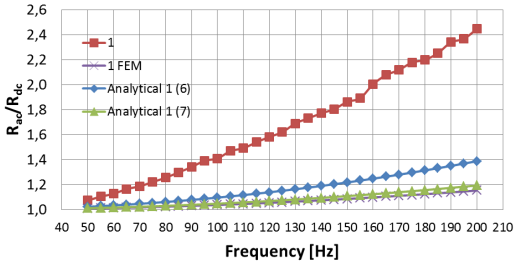


Fig. 8. Litz wire with 1 mm insulated subconductors. See legends in Table I.

Fig. 8. Curve "1" depicts the measurement results. "Analytical 1 (6)" depicts the results obtained according to Eq. (6) and "analytical 1 (7)" depicts the results obtained according to Eq. (7). Curve "1 FEM" depicts strand-level eddy currents in the case where all the subconductors are connected in series in the FEA. This should correspond to ideal litz wire, where there are no circulating currents between parallel conductors, only eddy currents inside solid subconductors (strand-level eddy currents).

The measured curve in Fig. 8 consists of dc-losses combined with losses inside a single sub-conductor (strand-level eddy currents) and circulating current losses. When the FEM result is subtracted from the measurement result, the remaining value is the total resistance factor caused by the circulating currents between the subconductors. The difference between the simulation and measurement results shows that the transposition is not ideal and there are circulating currents between subconductors. The analytical formula is based on the assumption that there is equal current sharing between the strands of the litz wire, meaning that there will be no circulating currents between the strands.

Equations (6) and (7) are used because they depict where the measurement result should be if the litz wire were designed and manufactured in a way that each bundle of subconductors would get an exactly equal amount of stray flux. Evidently, because of the large centre bundles and outer bundles, there are paths for circulating currents. That is why the measured litz wire ac resistance differs substantially from the results given by (6) and (7).

In addition, our improvement to (6) taking the end winding resistance into account in (7) seems to work, even though it is not an exact result. The error is small when comparing to the simulation result in Fig. 8.

The skin depth in copper in room temperature is 4.7 mm at 200 Hz and about 9.3 mm at 50 Hz. This indicates that there will be some eddy currents at 200 Hz, which can be seen in the results of Fig. 8.

The FEA analysis result of the current density at the top of the slot at 200 Hz is shown in Fig. 9. In the single wire, the ac resistance factor is always greatest at the top of the slot, due to the larger stray flux, which can also be observed in Fig. 9.

We also compared the litz wire with 1-mm subconductors with different insulations, and the results are depicted in Fig. 10. As expected there is a big difference between insulation levels at this frequency range.

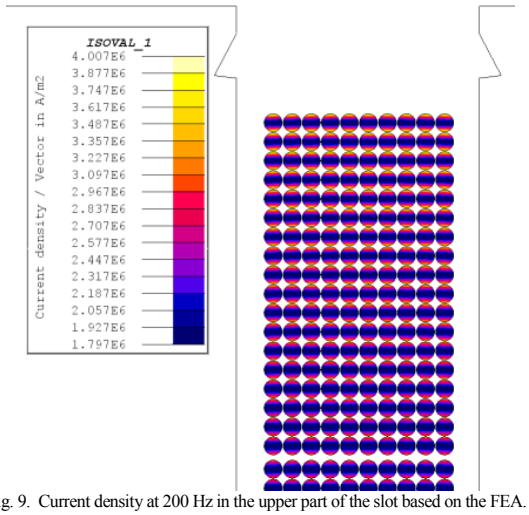


Fig. 9. Current density at 200 Hz in the upper part of the slot based on the FEA.

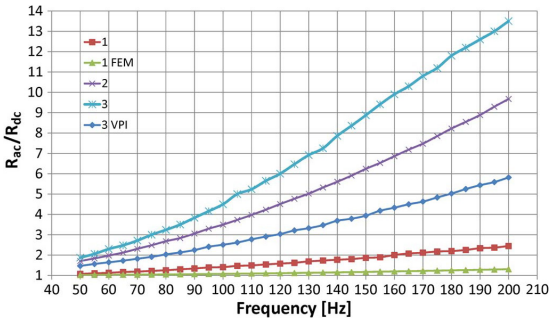


Fig. 10. Resistance factors from measurements and FEM. See legends in Table I.

### B. *Effect of impregnation on noninsulated litz wire*

Two different noninsulated litz wires were measured (no. 3 and no. 4 in Table I) before and after impregnation. The resin used was polyester CC1105. The impregnation was performed twice. In Fig. 7, there is no difference between the measurement results before and after impregnation in the litz wire with 0.5 mm subconductors. However, in Fig. 10, where 1 mm diameter subconductors have been used, there is a considerable difference in the curves. This might be for many reasons, e.g., how tightly the subconductors are packed, the bundle configuration, and the insulation tape of the litz wire. The wire was insulated with Nomex 410 tape in litz wire no. 3 and with mica packed with polyester film in litz wire no. 4. The resin cannot penetrate through the polyethylene teraphalate (PET) film. Instead, it flows between the layers of the film, preventing, for the most of the resin to flow to the wire. With Nomex tape, the resin can easily penetrate through the paper into the wire, which results in a better ac resistance than without impregnation.

The aforementioned can be considered inconclusive and more research is needed to determine the reasons why the ac resistance factor is different with or without impregnation.

## VI. Conclusion

Heavy litz wires with insulated or noninsulated strands are offered for megawatt-range low-voltage machine windings. The behaviour of the ac-resistance factor in such litz wires was studied in the paper. The litz wire with noninsulated strands is the most interesting because of the lack of additional insulation and therefore easy manufacturing and cheap price. It is difficult to calculate the ac resistance factor in the noninsulated litz wire strands; nevertheless, this paper gives insight into aspects to consider when developing more general analytical methods to estimate the ac resistance factor of litz wire with noninsulated strands.

An improvement is achieved in the accuracy of analytical equation by adding the end winding resistance to the analytical solution by Xu and Sullivan [5].

Although the results from the impregnation effect tests were inconclusive and further research is needed to determine the optimal insulation configuration method to achieve the best possible ac resistance factor, the measurements do however show that impregnation can have an effect on the ac resistance factor. Impregnation should therefore be considered when developing a more general analytical solution in the future.

In addition, it should be noted that tightness of packing can affect the ac resistance of litz wires with noninsulated strands.

Measurement of the resistance increase caused by the skin effect and proximity effects is very difficult in high-power low-voltage machines, due to the very small resistance compared with the large inductive reactance, which makes measurements very sensitive to errors, especially phase errors. In this study, as there were no available measurement devices with any measurement equipment manufacturers, a simple measurement device was developed to attain accurate phase shift measurement and overcome the disadvantageous signal-to-noise ratio.

The results presented in this paper show that litz wire with 630 originally noninsulated subconductors, used in a actual 3-MW PMG, is usable at frequencies even up to 120 Hz if a 50 % increase in copper losses can be tolerated.

## VII. References

[1] F. Caricchi, F. Maradei, G. De Donato and Capponi, F.G "Axial-Flux Permanent-Magnet Generator for Induction Heating Gensets," *IEEE Trans. Ind. Electron.*, vol. 57, no. 1, pp. 128 – 137, Jan. 2010.

[2] C.R. Sullivan, "Optimal choice for number of strands in a litz-wire transformer winding", *IEEE Trans. Power Electron.*, vol. 14, no. 2, pp. 283 – 291, Mar. 1999.

[3] C.R. Sullivan, "Computationally efficient winding loss calculation with multiple windings, arbitrary waveforms, and two-dimensional or three-dimensional field geometry", *IEEE Trans. Power Electron.*, vol. 16, no. 1, pp. 142 – 150, Jan . 2001.

[4] C.R. Sullivan, "Cost-constrained selection of strand diameter and number in a litz-wire transformer winding", *IEEE Trans. Power Electron.*, vol. 16, no. 2 , pp. 281 – 288, Mar. 2001.

[5] T. Xu and C.R. Sullivan, "Stranded wire with uninsulated strands as a low-cost alternative to litz wire", *IEEE 34th Annu. Power Electron. Specialist Conf.*, vol. 1, 15-19 Jun. 2003, pp. 289 – 295.

[6] T. Xu and C.R. Sullivan, "Optimization of stranded-wire windings and comparison with litz-wire on the basis of cost and loss" *IEEE 35th Annu. Power Electron. Specialist Conf.*, vol. 2, 20-25 Jun. 2004 pp. 854-860.

[7] N. Xi and C.R. Sullivan, "An Equivalent Complex Permeability Model for litz-Wire Windings", *IEEE Trans. Ind. Appl.*, vol. 45 , no. 2, pp. 854 - 860, Mar./Apr. 2009.

[8] N. Xi, C.R. Sullivan, "Simplified high-accuracy calculation of eddy-current loss in round-wire windings", *IEEE 35th Annu. Power Electron. Specialists Conf.*, vol. 2, 20-25 Jun. 2004, pp. 873 – 879.

[9] A.W. Lotfi and P.M. Gradzki, F.C. Lee, "Proximity effects in coils for high frequency power applications, " *IEEE Trans. Magn.*, vol. 28, no. 5, pp. 2169–2171, Sep. 1992.

[10] R.P. Wojda and M.K. Kazimierczuk," Analytical Optimization of Solid-Round Wire Windings" , *IEEE Trans. Ind. Electron.* Vol. 60, no 3, mar. 2013.

[11] J. Acero, R. Alonso, J.M. Burdio, L.A. Barragan and D. Puyal, "Frequency-dependent resistance in litz-wire planar windings for domestic induction heating appliances", *IEEE Trans. Power Electron*., vol. 21 , no. 4, pp.856 - 866 , Jul. 2006.

[12] G. Cerri, S.A. Kovyryalov and V.M. Primiani, "Modelling of a litz-wire planar winding ", *IET Measurement & Technology Science*, vol. 4, no. 4, pp. 214 - 219, Jul. 2010.

[13] W. Nick, M. Frank, G. Klaus, J. Frauenhofer and H.-W. Neumuller, "Operational Experience With the World's First 3600 rpm 4 MVA Generator at Siemens", *IEEE Trans. Appl. Supercond*., vol. 17, no. 2, Part: 2, pp. 2030 – 2033, Jun. 2007.

[14] D. Wua and E. Chen, "Stator Design for a 1000 kW HTSC Motor With Air-gap Winding" *IEEE Trans. Appl. Supercond.*, vol. 21 , no. 3 , Part 2, pp. 1093 – 1096, June 2011.

[15] J.A. Ferreira, "Analytical computation of AC resistance of round and rectangular litz-wire windings*", IEE Proc. Electric Power Appl.*, vol. 139 , no. 1, pp. 21 – 25, Jan. 1992.

[16] A.W. Lotfi and F.C. Lee, "A high frequency model for litz wire for switch-mode magnetics", *IEEE Conf. Ind. Appl. Society Annu. Meeting,* vol. 2, 2-8 Oct. 1993, pp. 1169 – 1175.

[17] F. Tourkhani and P. Viarouge, "Accurate analytical model of winding losses in round litz-wire windings", *IEEE Trans. Magn.*, vol. 37, no. 1, Part: 2, pp. 538 - 543, Jan. 2001.

[18] R.P. Wojda and M.K. Kazimierczuk, "Winding resistance of litz-wire and multi-strand inductors," *IET Power Electron.,* vol. 5, no. 2, pp. 257–268, Feb. 2012.

[19] M.K. Kazimierczuk, High-Frequency Magnetic Components. Chichester, U.K.: Wiley, 2009.

[20] M. Bartoli, N. Noferi, A. Reatti and M.K. Kazimierczuk, "Modeling litz-wire winding losses in high-frequency power inductors," in Proc. IEEE Power Electron. Spec. Conf., Baveno, Italy, 23–27 Jun. 1996, pp. 1690–1696.

[21] R. P. Wojda and M. K. Kazimierczuk, "Winding resistance of litz-wire and multi-strand inductors," *IET Power Electron.*, vol. 5, no. 2, pp. 257–268, Feb. 2012.

[22] P. L. Dowell, "Effects of eddy currents in transformer winding," *Proc. Inst. Elect. Eng.,* vol. 113, no. 8, pp. 1387–1394, Aug. 1966.

[23] R. Wrobel, A. Mlot, P.H. Mellor, "Contribution of End-Winding Proximity Losses to Temperature Variation in Electromagnetic Devices ", *IEEE Trans. Ind. Electron.*, vol. 59, no. 2, pp. 848 – 857, Feb. 2012.

[24] J. Gyselinck, P. Dular, N. Sadowski, P. Kuo-Peng and R.V. Sabariego, "Homogenization of Form-Wound Windings in Frequency and Time Domain Finite-Element Modeling of Electrical Machines", *IEEE Trans. Magn*., vol. 46, no. 8, pp. 2852-2855, Aug. 2010.

[25] G.S. Dimitrakakis and E.C. Tatakis, "High-Frequency Copper Losses in Magnetic Components With Layered Windings," *IEEE Trans. Magn*., vol. 45, no. 8, pp. 3187 – 3199, Aug. 2009.

[26] Von Roll, 2012 [Online] Available: http://www.vonroll.ch/media/files/downloads/brochures/Wire_US_20120516.pdf

[27] T. Chevalier, A. Kedous-Labouc, B. Cornut and C. Cester, "Estimation of magnetic loss in an induction motor fed with sinusoidal supply using a finite element software and a new approach to dynamic hysteresis," *IEEE Trans. Magn*., vol. 35, no. 5, pp. 3400 - 3402, Sep. 1999.


**H. Hämäläinen** received the M.Sc. degree in electrical engineering from Lappeenranta University of Technology (LUT), Lappeenranta, Finland, in 2009, where he is currently working toward the Ph.D. degree, studying permanent-magnet generators and their additional losses.

**J. Pyrhönen** (M'06) received the M.Sc. degree in electrical engineering, the Licentiate of Science (Technology) degree, and the D.Sc. (Technology) degree from Lappeenranta University of Technology (LUT), Lappeenranta, Finland, in 1982, 1989, and 1991, respectively.

In 1993, he became an Associate Professor in electric engineering with LUT, where since 1997, he has been a Professor in electrical machines.

**Janne Nerg** (M'99-SM'12) received the M.Sc. degree in electrical engineering, the Licentiate of Science (Technology) degree, and the D.Sc. (Technology) degree from Lappeenranta University of Technology (LUT), Lappeenranta, Finland, in 1996, 1998, and 2000, respectively.

He is currently an Associate Professor in the Department of Electrical Engineering at LUT. His research interests are in the field of electrical machines and drives, particularly electromagnetic and thermal modeling and design of electromagnetic devices.

**Joonas Talvitie** (M'12) received the B.Sc and M.Sc degrees in electrical engineering from Lappeenranta University of Technology, Finland, in 2010 and 2011, respectively, where he is currently working towards the Ph.D. degree in Laboratory of Applied Electronics.

His current research focuses on electrical sensor modeling and analog signal processing.

**Publication IV**



H. Hämäläinen J. Pyrhönen, J. Nerg, "AC Resistance Factor in One-Layer Form-Wound Winding Used in Rotating Electrical Machines," *IEEE Transaction on Magnetics*, vol. 49, no. 6, Jun. 2013.

# AC Resistance Factor in One-Layer Form-Wound Winding Used in Rotating Electrical Machines

Henry Hämäläinen, Juha Pyrhönen, and Janne Nerg

Lappeenranta University of Technology, Lappeenranta 53851, Finland

**Analytical calculation of circulating and eddy currents in windings has been under research for almost a century, yet the calculation accuracy has improved slowly. However, over the recent years, the development of finite-element methods (FEM) has boosted the research. A lot of effort has been taken to calculate the ac resistance losses in transformers in the past, whereas rotating electrical machines have received less attention. These models have not taken the end-winding effect into account. In this paper, 2-D FEM results are compared with analytical equations. Based on these results, a more accurate model compared with Dowell's model for single-layer form-wound windings used in electrical machines is developed empirically, and the end winding resistance is analytically taken into account in the results. A maximum error of 5% is achieved in the range of 0–200 Hz for a single-layer form-wound winding.**

***Index Terms*—Eddy current, proximity effect, skin effect, windings.**

## I. Introduction

OVER the latest few decades, the development of frequency converters has provided an opportunity to build machines with higher frequencies than the standard 50 or 60 Hz. It is important to perform a precise calculation of the ac losses in windings [1], [2]. Typically, form-wound windings are used in multimegawatt electrical machines. The strand heights usually vary between 2 and 3 mm, and the conductor height $h_c$ can be, especially, in large windmill generators, about 10 mm. This means that the conductor height is much larger than the skin depth when the machine is operating above 50 Hz.

Calculation of eddy currents in windings has been under research for at least a century. Various calculation methods and equations have been developed by Lyon [3], Richter [4], [5], Dowell [6], and Ferreira [7], to mention but a few. Lyon [3] and Richter [4], [5] concentrated on rotating electrical machines, whereas Dowell [6] and Ferreira [7] focused on transformers. Papers [8]–[26] have also contributed to development of the calculation of the ac resistance factor in electrical applications.

A drawback in these calculation methods is that they do not evaluate the effect of the end winding area on the ac resistance of the whole coil and only consider the turn number neglecting the number of parallel strands on top of each other. This means that they do not distinguish circulating currents (eddy currents that are circulating between the strands) and strand-level eddy currents (eddy currents that occur only inside of strands in their active lengths). In the case of parallel strands there is a significant possibility that circulating currents may occur if not minimized by design. Nevertheless, strand-level eddy currents are always present because they occur inside solid conductors, mainly, along the active length of the machine as depicted in Fig. 1.

Manuscript received November 06, 2012; revised December 21, 2012; accepted December 28, 2012. Date of publication January 16, 2013; date of current version May 30, 2013. Corresponding author: H. Hämäläinen (e-mail: henry.hamalainen@lut.fi).

Color versions of one or more of the figures in this paper are available online at http://ieeexplore.ieee.org.

Digital Object Identifier 10.1109/TMAG.2013.2240008

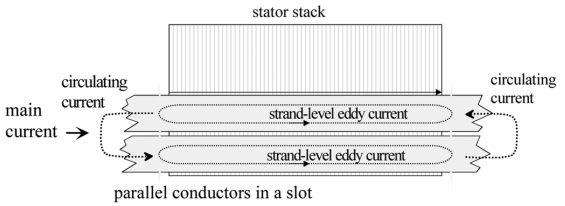


Fig. 1. Schematic illustrating the main current, the strand-level eddy current, and the circulating current in the case of two parallel strands in a slot.

Most of the stray flux crosses the slot near the slot opening, and in the case of solid or nontransposed stranded conductors, it forces most of the current to travel as close to the slot opening as possible. The proximity effect amplifies the phenomenon in such a way that the other side of the conductor, closer to the slot bottom, also seems to acquire a large current density, leaving the centre of the conductor with a lower current density. The proximity effect is always present in multilayered windings [24], [25].

There are many factors that can affect the amount of circulating currents, such as the end winding length and the number of parallel strands in a turn. Without knowledge of circulating currents, the error between an analytical solution and FEA results may be as large as 150%, which is unacceptable.

In electrical machines, the end winding length may be more than 50% of the total turn length, meaning that it obviously has a significant effect on the ac resistance factor. The end winding effect is acknowledged in [19]. The end winding also experiences some proximity and skin effects; however, almost all of the eddy currents originate in the slot area, and therefore, even though the target of the paper is to improve the calculation accuracy, the end winding proximity and skin effects are neglected.

The effect of an end winding cannot be calculated afterwards because the amount of circulating currents has to be known in the calculation of the skin and proximity effects in the slot areas, and the end winding impedance has a noticeable effect on the current density distribution. However, without making a significant error, the proximity and skin effects can be neglected in the end winding area and thus, only the circulating currents and

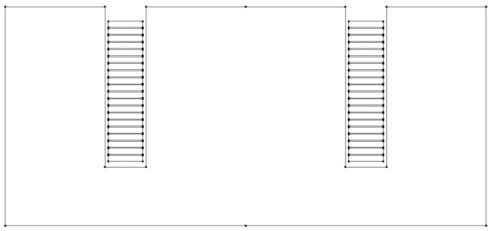

Fig. 2. 2-D FEM geometry describing a two-slot system.

the main current in the end winding are included in the calculation. The skin and proximity effects can be neglected because the end winding field is weak compared with the slot leakage field, mainly contributing to the current density distribution in the strands located in the slots.

To correctly calculate the total ac resistance factor, one has to know the amount of circulating currents between parallel strands and the extra losses created by them. In the simplified model, the end winding carries the circulating currents and the main current, whereas slot-bound conductors have three current components; the main current, the circulating current, and the strand-level eddy current. If there are parallel conductors on top of each other installed in a slot, there will be circulating currents, Fig. 1.

Xi [17] found that Dowell's [6] and Ferreira's [7] methods include significant errors exceeding 60% compared with FEA when applied in the design of transformers in the frequency range of 20 kHz–2000 MHz. The same applies to electrical machines, even though the frequencies are much lower.

In this paper, a model for calculating the ac resistance losses in a single-layer form-wound winding in electrical machines is introduced. In the model, the calculation accuracy is improved by calculating the circulating and strand-level eddy currents separately. The currents are calculated by using the Dowell equation and employing an empirical factor to take the proximity effect correctly into account to match the circulating and strand-level eddy currents. A maximum error of 5% is achieved compared with the 2-D FEM results in the 0–200 Hz frequency range when the thickness of a turn divided by the skin depth is $<2$. The skin depth is at 50 Hz 10.7 mm and at 200 Hz 5.4 mm with copper temperature of 100 °C.

## II. 2-D Finite Element Simulation

2-D finite element simulation is made with a simple geometry using a steady-state ac magnetic application. In Fig. 2, the geometry of the finite element analysis (FEA) is depicted and in Fig. 3 an example of a circuit model for five parallel strands and four turns is depicted. With this simple geometry, an approximately one-dimensional flux is achieved across the slot. The copper temperature is set to 100 °C. The slot dimensions are 14.09 mm $\times$ 54.52 mm in each case (Table I).

Solid conductor components (Fig. 3) are connected to the FEM model (Fig. 2) each of them depicting a strand, whereas lumped resistors (Fig. 3) depict the end winding resistances of strands. The resistance value is depending on the end winding length. FEM and circuit models are analyzed simultaneously. A Stray flux across the slot causes different voltages between the parallel strands in circuit model, creating circulating currents between the strands. The eddy currents are mostly generated in the slot-bound areas, and the effect of an end winding on the generation of eddy currents is minimal; thus, we have neglected the end winding inductance from the circuit model. The end winding effects are described by the bulky circuit parameters, which have a noticeable effect on the amount of circulating current flowing in the solid conductors in the slots. The end winding current can be divided into two current components, the main current and the circulating current. We define a circulating current factor

$$k_{\mathrm{circ}} = \frac{P_{\mathrm{ac\_end}}}{I^2 R_{\mathrm{dc\_end}}} - 1 \tag{1}$$

where $P_{\mathrm{ac\_end}}$ represents the ac losses in the end winding including the dc-losses and the extra losses caused by the circulating currents ($P_{\mathrm{ac\_end}} = I^2 R_{\mathrm{ac\_end}} = I^2(k_{\mathrm{circ}}+1)R_{\mathrm{dc\_end}}$). These are the losses of the lumped resistors in Fig. 3. $I$ is the rms current fed into the circuit model and $R_{\mathrm{dc\_end}}$ is the end winding dc-resistance. Its loss effects have to be subtracted by to extract the dc losses. From the total effect point of view it is not necessary to know the amount of circulating current losses in every strand just the total loss in all the strands.

In the slot-bound areas strand-level eddy current losses can be calculated by subtracting the circulating-current-caused losses and the dc losses from the total losses

$$k_{\mathrm{strand}} = k_{\mathrm{total}} - k_{\mathrm{circ}} - 1 \tag{2}$$

where $k_{\mathrm{total}}$ is the total ac resistance factor in the FEA. $k_{\mathrm{total}}$ can also be defined as $R_{\mathrm{ac}}/R_{\mathrm{dc}}$ in the slot-bound areas similarly as in the end winding regions.

Now, in the slot-bound areas there are three current components that can be compared with the analytical results. In the tests the current source In the tests a low-level sinusoidal current that does not saturate the slot leakage.

## III. Effect of the End Winding on the Total AC Resistance Factor

In Figs. 4–6, the effect of the end winding is clearly seen in different winding cases. The percentages represent the end winding length in proportion to the total winding length. From 0 to 50 Hz, the end winding length does not have a significant effect on the total ac resistance factor, but after 50 Hz, it has an increasing effect on the total ac resistance factor, which can be seen in all three cases. This is why the end winding cannot be neglected when calculating the ac resistance factor for electrical machines. When the end winding is included in the analysis, the amount of circulating currents has to be known, because circulating currents affect the end winding ac resistance factor as well as on the total ac resistance factor.

## IV. Modelling AC Resistance Factor

In this section, an analytical model is developed applying (3) given for instance by Dowell [6] to evaluate the phenomenon in a slot having $z_{\mathrm{Q}}$ conductors connected in series. The total ac

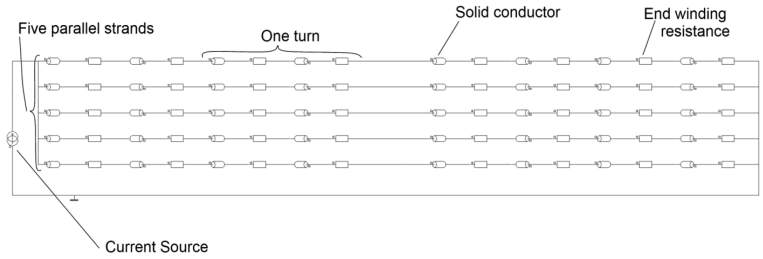


Fig. 3. Circuit model of the FEA.

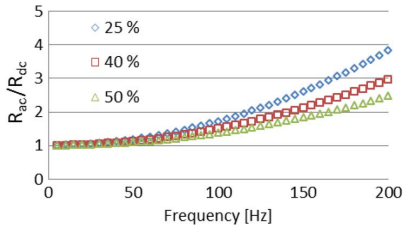


Fig. 4. Case 1: 2-D FEM results of the effect of an end winding resistance on the ac resistance factor. The percentages in the legend represent the length of the end winding in proportion to the total winding length.

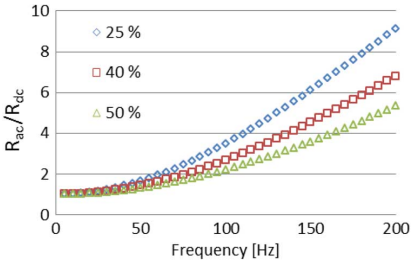


Fig. 5. Case 2: 2-D FEM results of the effect of an end winding resistance on the ac resistance factor. The percentages in the legend represent the length of the end winding in proportion to the total winding length.

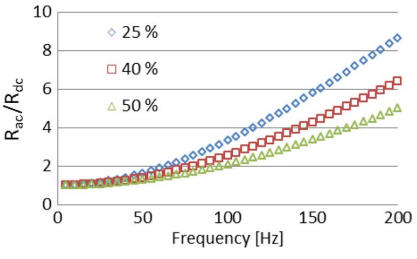


Fig. 6. Case 3: 2-D FEM results of the effect of the end winding resistance on the ac resistance factor. The percentages in the legend represent the length of the end winding in proportion to the total winding length.

resistance factor $k_\mathrm{r}$ in the slot areas, neglecting the effect of the end winding resistance, is now

$$k_\mathrm{r} = \frac{R_\mathrm{ac}}{R_\mathrm{dc}} = \xi \left[ \frac{\sinh 2\xi + \sin 2\xi}{\cosh 2\xi + \cos 2\xi} + \frac{2\left(z_\mathrm{Q}^2 - 1\right)}{3} \frac{\sinh \xi + \sin \xi}{\cosh \xi + \cos \xi} \right] \tag{3}$$

where

$$\xi = h_\mathrm{c} \sqrt{\frac{1}{2} \omega \mu_0 \sigma_\mathrm{C} \frac{b_\mathrm{C}}{b}} \tag{4}$$

and $h_\mathrm{c}$ is the solid conductor height (or the number of parallel strands on top of each other; $n_\mathrm{s} \times$ strand height), $\omega$ is the angular frequency of the exciting sinusoidal current, $\sigma_\mathrm{C}$ is the conductivity of the conductor material, $\mu_0$ is the permeability of vacuum, $z_\mathrm{Q}$ is the number of turns in a slot, $b_\mathrm{C}$ is the width of the conductor, and $b$ is the slot width.

A drawback of (3) is that it only considers the number of turns $z_\mathrm{Q}$ and neglects the number of strands and the end winding effects. The equation is therefore valid only for the slot area in an ideal case of no effects caused by the end winding. Eq. (3) assumes that the turn is made of solid copper, in which case the losses too large in any case. To calculate the strand-level eddy currents with (3), we have to assume that all the strands in a slot are connected in series, which results in $k_\mathrm{circ} = 0$. In such a case there cannot be any circulating currents as there are no parallel conductors, and we replace $z_\mathrm{Q}$ in (3) by the number of conductors in a slot $z_\mathrm{t} = n_\mathrm{s} z_\mathrm{Q}$. Equation (3) now gives an idea of strand-level eddy currents in the conductors in the slot areas, but that only. That is why a new way of calculating ac resistance factor is needed in the case of multi-turn and multistrand winding.

We apply the Dowell (3) to establish a semi-empirical way to calculate the ac resistance factor. Recognizing the fact that (3) is not fully correct when the current distributions are different because of the end winding impedance, we use it as a basis for calculating the circulating and strand-level eddy currents separately. With the FEA it is possible to extract the circulating currents for instance in the end winding areas. This provides an opportunity to calculate the total ac resistance factor from (2).

Assuming the main current the same, varying the amount of circulating currents affects the magnetic condition in the slot and thereby the proximity effect between the conductors. Consequently, this also affects the amount of strand-level eddy currents in different strands. The end winding length and the number of strands affect the amount of circulating currents. Because of the circulating currents, the proximity effect has to be corrected with a curve function $r_\mathrm{strand}$. In addition to that the number of turns in a slot $z_\mathrm{Q}$ is replaced in (3) by the number of conductors in a slot $z_\mathrm{t}$ and because $k_\mathrm{strand}$ only represent the losses due to strand-level eddy currents, it has to be subtracted by one to extract the dc losses. The curve fit is based on FEA

results. $r_{\mathrm{strand}}$ is a constant with respect to frequency, and when producing the curve fit, the $r_{\mathrm{strand}}$ is adjusted so that (5) matches the FEA results as closely as possible with different strand numbers. After producing the first degree polynomial fit, we do the same with different end winding lengths and get the combined result for it in (6)

$$k_{\mathrm{strand}} = \xi \left[ \frac{\sinh 2\xi + \sin 2\xi}{\cosh 2\xi + \cos 2\xi} + r_{\mathrm{strand}} \frac{2\left(z_Q^2 - 1\right)}{3} \frac{\sinh \xi + \sin \xi}{\cosh \xi + \cos \xi} \right] - 1 \quad (5)$$

$$r_{\mathrm{strand}} = n_{\mathrm{s}} \left( -\frac{l_{\mathrm{stack}}}{l_{\mathrm{turn}}} 0.1 + 0.4 \right) + \frac{l_{\mathrm{stack}}}{l_{\mathrm{turn}}} 1.065 \quad (6)$$

where $n_{\mathrm{s}}$ is the number of parallel strands in a turn, $l_{\mathrm{stack}}$ is the length of the copper conductor in a slot in a turn, and $l_{\mathrm{turn}}$ is the length of the turn.

For circulating currents we introduce a curve fit function in the same manner as for the strand-level eddy currents, but only difference to (3) is $r_{\mathrm{circ}}$. The original function only includes the number of turns. The function is used to correct the proximity effect, because the end winding resistance and the number of strands affect the circulating currents inside a turn

$$k_{\mathrm{circ}} = \xi \left[ \frac{\sinh 2\xi + \sin 2\xi}{\cosh 2\xi + \cos 2\xi} + r_{\mathrm{circ}} \frac{2\left(z_Q^2 - 1\right)}{3} \frac{\sinh \xi + \sin \xi}{\cosh \xi + \cos \xi} \right] - 1 \quad (7)$$

where

$$r_{\mathrm{circ}} = n_{\mathrm{s}} \frac{l_{\mathrm{stack}}}{l_{\mathrm{turn}}} 0.06 + \frac{l_{\mathrm{stack}}}{l_{\mathrm{turn}}} - 0.38. \quad (8)$$

In summary, $k_{\mathrm{circ}}$, $k_{\mathrm{strand}}$, and $k_{\mathrm{total}}$ are obtained by the following.

a) FEM-simulations with different winding layouts and end winding lengths.
b) Extraction of $k_{\mathrm{circ}}$ and $k_{\mathrm{strand}}$ from FEM results using (1) and (2).
c) Setting (6) as a constant with $l_{\mathrm{stack}}/l_{\mathrm{turn}} = 0.5$ in all the three cases, so that the result of (5) matches with $k_{\mathrm{strand}}$ from item b).
d) Using the three constants given in item c) are fitted with $n_{\mathrm{s}} = [2\ 4\ 5]$ using a first degree polynomial, then we have e.g. for 0.5 of $l_{\mathrm{stack}}/l_{\mathrm{turn}}$ (6) is $r_{\mathrm{strand}} = n_{\mathrm{s}} \times -0.01 + 0.55$.
e) Items c)–d) are now repeated twice for $l_{\mathrm{stack}}/l_{\mathrm{turn}} = 0.6$ and $0.75$.
f) now we have three different $r_{\mathrm{strand}}$ equations and the constants in the equations are fitted with $l_{\mathrm{stack}}/l_{\mathrm{turn}} = [0.5\ 0.6\ 0.75]$ using a first degree polynomial.
g) Setting (8) as a constant, so that the result of (7) matches with $k_{\mathrm{circ}}$ from item b) and also items d)–f) are repeated to obtain (8).
h) Now (5)–(8) can be used to easily calculate $k_{\mathrm{total}}$ from (2) for different configurations.

In the study, it was found that the proximity effect of a specific winding can be approximately corrected with a constant to calculate the circulating or strand-level eddy currents; however, to obtain an exact solution, this would require a value that changes as a function of frequency.

TABLE I
SIMULATED WINDINGS CONFIGURATIONS

| | Case 1 | Case 2 | Case 3 |
|---|---|---|---|
| Number of turns | 2 | 4 | 4 |
| Number of parallel strands in a turn | 8 | 4 | 5 |
| Strand size (height × width) mm | 2.65 × 11.8 | 2.65×11.8 | 2.05×11.8 |
| Slot size (height × width) mm | 54.52×14.09 | 54.52×14.09 | 54.52×14.09 |
| Copper temperature °C | 100 | 100 | 100 |

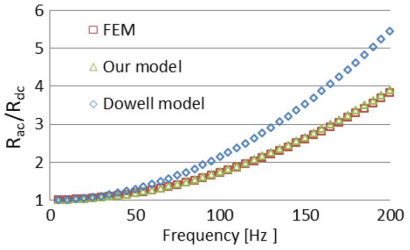


Fig. 7. Eight turns and two parallel strands; $l_{\mathrm{stack}}$ is 75% of the total length of the turn.

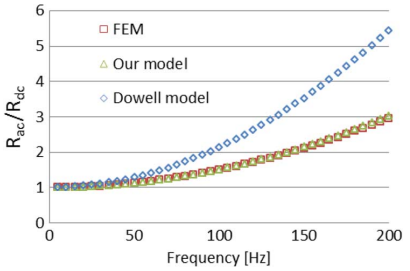


Fig. 8. Eight turns and two parallel strands; $l_{\mathrm{stack}}$ is 60% of the total length of the turn.

## V. RESULTS

In the following, we introduce three different winding examples (Table I) and demonstrate that the error of our model is less than 5% compared with the FEA results.

### A. Case 1

In this case, eight turns and two parallel strands are used. In Figs. 7–9, the error of our model is below 2.3%, whereas the Dowell model produces even a 120% error. The Dowell model has a fairly good accuracy (error $<$17%) up to 50 Hz, but after that, the error starts to increase rapidly.

### B. Case 2

In this case, four turns and four parallel strands are used. The strand height is the same as in case 1, only the number of turns

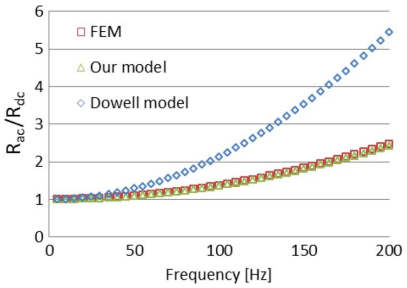


Fig. 9. Eight turns and two parallel strands; $l_{\mathrm{stack}}$ is 50% of the total length of the turn.

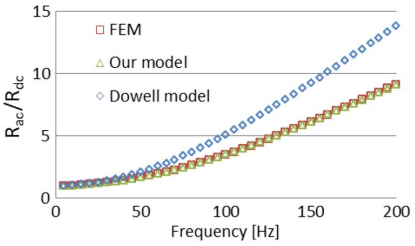


Fig. 10. Four turns and four parallel strands; $l_{\mathrm{stack}}$ is 75% of the total length of the turn.

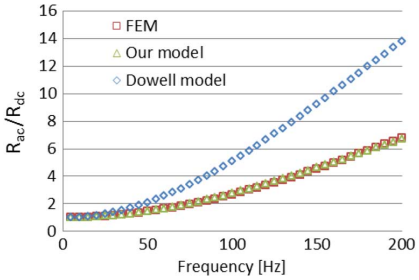


Fig. 11. Four turns and four parallel strands; $l_{\mathrm{stack}}$ is 60% of the total length of the turn.

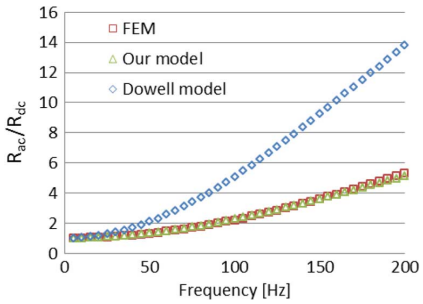


Fig. 12. Four turns and four parallel strands; $l_{\mathrm{stack}}$ is 50% of the total length of the turn.

and strands has been changed. In Figs. 10–12 the error of our model is below 4.2%, whereas the error of the Dowell model can be as large as 150%. Now, the Dowell model has a fairly good accuracy (error $<$17%) up to 25 Hz, but after that, the error starts to increase rapidly.

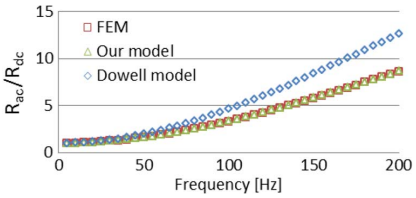


Fig. 13. Four turns and five parallel strands; $l_{\mathrm{stack}}$ is 75% of the total length of the turn.

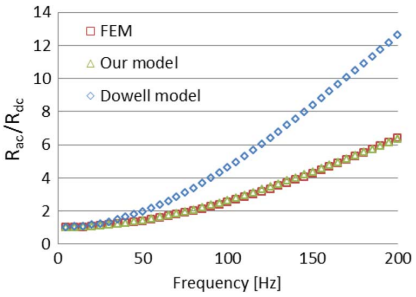


Fig. 14. Four turns and five parallel strands; $l_{\mathrm{stack}}$ is 60% of the total length of the turn.

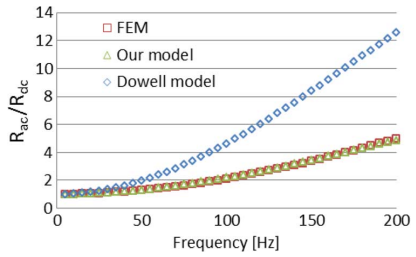


Fig. 15. Four turns and five parallel strands; $l_{\mathrm{stack}}$ is 50% of the total length of the turn.

### C. Case 3

In this case, four turns and five parallel strands are used. The strand height has been changed so that it is now 2.05 mm (2.65 mm in the other cases). Otherwise, the winding construction remains unchanged. In Figs. 13–15, the error our model is below 4.2% whereas the error of the Dowell model is even 150%. In this case, the Dowell model has a fairly good accuracy (error $<$17%) up to 25 Hz, but after that the error starts to increase rapidly.

### D. 180° Twist in the End Winding

It has now been shown how significant an impact the end winding has on the ac resistance factor. Next, we examine in case 1 the effect of twisting the end winding by 180° so that the strand on top of the slot will be placed at the bottom of the second slot (Fig. 16).

This way, all the strands will have an equal amount of slot leakage flux passing through them. Furthermore, this means that there will be no or negligible amount of circulating currents, only strand-level eddy currents. We will also examine whether our model still applies to this case. Only one end winding length

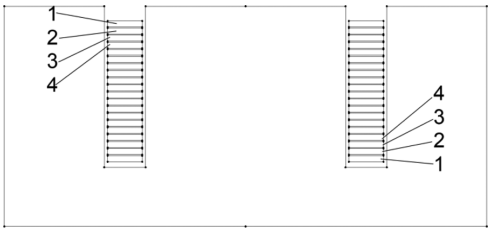


Fig. 16. FEM geometry and winding placement with a 180° end winding twisting.

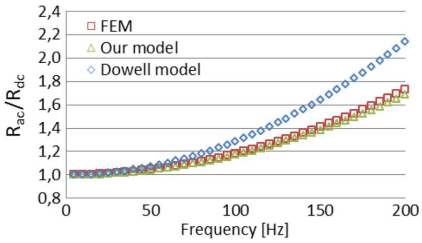


Fig. 17. End winding twisted by 180°. Eight turns and two parallel strands; $l_{\mathrm{stack}}$ is 60% of the total winding length. Our model is using (5) and (6).

is used to show the accuracy of the model, because the effect of the end winding has already been established.

Now, the model should be written as

$$k_{\mathrm{total}} = k_{\mathrm{strand}} + 1. \tag{9}$$

The Dowell model can be used to calculate the 180° twist by using the strand height $h_0$ instead of $h_{\mathrm{c}}$, and the number conductors in a slot $z_{\mathrm{t}}$ instead of $z_{\mathrm{Q}}$ ($z_{\mathrm{t}} = n_{\mathrm{s}} z_{\mathrm{Q}}$)

$$k_{\mathrm{r}} = \xi \left[ \frac{\sinh 2\xi + \sin 2\xi}{\cosh 2\xi + \cos 2\xi} + \frac{2\left(z_{\mathrm{t}}^2 - 1\right)}{3} \frac{\sinh \xi + \sin \xi}{\cosh \xi + \cos \xi} \right] \tag{10}$$

where

$$\xi = h_{\mathrm{c}} \sqrt{\frac{1}{2} \omega \mu_0 \sigma_{\mathrm{C}} \frac{b_{\mathrm{C}}}{b}}. \tag{11}$$

Yet again, (10) does not take into account the end winding, but it is valid for the slot active length of the machine.

In Fig. 17, our model uses (5) and (6), in this case the error is increasing with frequency but the maximum error at 200 Hz is 2.6%, which is very good. However, (6) that corrects the strand-level eddy current can be modified because we no longer have circulating currents, and the first term in (6), which is linked to the circulating currents, can be left out to get close to an exact solution for the strand-level eddy currents with the 180° twist

$$r_{\mathrm{strand-180}} = \frac{l_{\mathrm{stack}}}{l_{\mathrm{turn}}} 1.065. \tag{12}$$

After this modification, the error reduces to 1% at maximum in Figs. 18–20 where (12) has been used instead of (6). This 1%

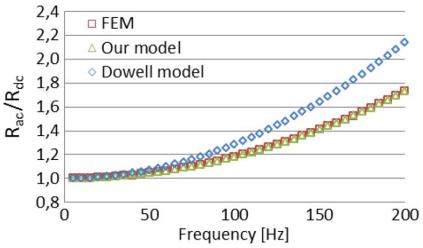


Fig. 18. End winding twisted by 180°. Eight turns and two parallel strands; $l_{\mathrm{stack}}$ is 60% of the total winding length. Our model is using (5) and (12).

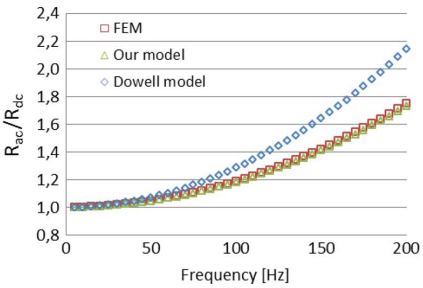


Fig. 19. End winding twisted by 180°. Four turns and four parallel strands; $l_{\mathrm{stack}}$ is 60% of the total winding length. Our model is using (5) and (12).

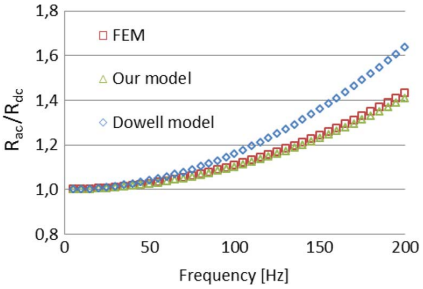


Fig. 20. End winding twisted by 180°. Four turns and five parallel strands; $l_{\mathrm{stack}}$ is 60% of the total winding length. Our model is using (5) and (12).

is due to the fact that there is still a small amount of circulating current in the FE model, yet the accuracy is very good.

Form-wound windings are usually used in large electrical machines. In the case of low voltage (690 V) 1500 r/min permanent magnet generators the strand height is in the range of 2–3 mm and the turn height around 10 mm. Our model applies when the height of the turn divided by the classical penetration depth is $<2$.

## VI. Conclusion

An approximate equation to evaluate the ac resistance factor in a single-layer form-wound winding was developed. The end winding resistance has been taken into account when calculating the ac resistance factor. A maximum error of 5% was achieved when the thickness of a turn divided by the skin depth was $<2$. In addition, a 180° twist in the end winding was analyzed and

a model was developed to calculate the ac resistance factor in that case.

## REFERENCES


[1] N. Shuangxia, S. L. Ho, W. N. Fu, and Z. Jianguo, "Eddy current reduction in high-speed machines and eddy current loss analysis with multislice time-stepping finite-element method," *IEEE Trans. Magn.*, vol. 48, no. 2, pp. 1007–1010, Feb. 2012.

[2] A. Bellara, H. Bali, R. Belfkira, Y. Amara, and G. Barakat, "Analytical prediction of open-circuit eddy-current loss in series double excitation synchronous machines," *IEEE Trans. Magn.*, vol. 47, no. 9, pp. 2261–2268, Sep. 2011.

[3] W. V. Lyon, "Heat losses in the conductors of alternating-current machines," *Trans. Amer. Inst. Elect. Eng.*, vol. XL, pp. 1361–1409, Jan. 1921.

[4] R. Richter, *Electrical Machines: Induction Machines (Elektrische Maschinen: Die Inductionsmaschinen)*, 2nd ed. Cambridge, MA, USA: Birkhäuser, 1954, vol. IV.

[5] R. Richter, *Electrical Machines: General Calculation Elements. DC Machines (Elektrische Maschinen: Allgemeine Berechnungselemente. Die Gleichstrommaschinen)*, 3rd ed. Cambridge, MA, USA: Birkhäuser, 1967, vol. I.

[6] P. L. Dowell, "Effects of eddy currents in transformer windings," in *Proc. Inst. Elect. Eng.*, Aug. 1966, vol. 113, no. 8, pp. 1387–1394.

[7] J. A. Ferreira, "Improved analytical modeling of conductive losses in magnetic components," *IEEE Trans. Power Electron.*, vol. 9, no. 1, pp. 127–131, Jan. 1994.

[8] R. E. Gilman, "Eddy current losses in armature conductors," *Trans. Amer. Inst. Elect. Eng.*, vol. XLIII, pp. 246–251, Jan. 1924.

[9] R. E. Gilman, "Eddy current losses in armature conductors," *Trans. Amer. Inst. Elect. Eng.*, vol. XXXIX, no. 1, pp. 997–1056, Jan. 1920.

[10] E. A. Hanney, "Heat losses due to load current in direct-current armature windings," *J. Inst. Elect. Eng.*, vol. 71, no. 427, pp. 263–283, Jul. 1932.

[11] A. B. Field, "Eddy currents in large slot-wound conductors," *Trans. Amer. Inst. Elect. Eng.*, vol. XXIV, pp. 761–788, Jan. 1905.

[12] M. P. Perry, "Multiple layer parallel connected air-core inductor design," *IEEE Trans. Power App. Syst.*, vol. PAS-98, no. 4, pp. 1387–1393, Jul. 1979.

[13] M. P. Perry, "Multiple layer series connected winding design for minimum losses," *IEEE Trans. Power App. Syst.*, vol. PAS-98, no. 1, pp. 116–123, Jan. 1979.

[14] K. Küpfmüller, *Introduction to Theoretical Electrical Engineering (Einführung in die theoretische Elektrotechnik)*, 6th ed. Berlin, Germany: Springer Verlag, 1959.

[15] C. R. Sullivan, "Computationally efficient winding loss calculation with multiple windings, arbitrary waveforms, and two-dimensional or three-dimensional field geometry," *IEEE Trans. Power Elect.*, vol. 16, no. 1, pp. 142–150, Jan. 2001.

[16] N. Xi and C. R. Sullivan, "Simplified high-accuracy calculation of eddy-current loss in round-wire windings," in *Proc. IEEE 35th Annu. Power Electron. Spec. Conf.*, 2004, vol. 2, pp. 873–879.

[17] N. Xi and C. R. Sullivan, "An improved calculation of proximity-effect loss in high-frequency windings of round conductors," in *Proc. IEEE 34th Annu. Power Electron. Spec. Conf. (PESC)*, 2003, vol. 2, pp. 853–860.

[18] R. Wojda and M. Kazimierczuk, "Analytical optimization of solid-round wire windings," *IEEE Trans. Ind. Elect.*, vol. 60, no. 3, pp. 1033–1041, Mar. 2013.

[19] R. Wrobel, A. Mlot, and P. H. Mellor, "Contribution of end-winding proximity losses to temperature variation in electromagnetic devices," *IEEE Trans. Ind. Elect.*, vol. 59, no. 2, pp. 848–857, Feb. 2013.

[20] W. G. Hurley, E. Gath, and J. G. Breslin, "Optimizing the AC resistance of multilayer transformer windings with arbitrary current waveforms," *IEEE Trans. Power Electron.*, vol. 15, no. 2, pp. 369–376, Mar. 2000.

[21] L. J. Wu, Z. Q. Zhu, D. Staton, M. Popescu, and D. Hawkins, "Analytical model of eddy current loss in windings of permanent-magnet machines accounting for load," *IEEE Trans. Magn.*, vol. 48, no. 7, pp. 2138–2151, Jul. 2012.

[22] I. Boldea and S. A. Nasar, *The Induction Machine Handbook*. Boca Raton, FL, USA: CRC, 2001.

[23] J. Pyrhönen, T. Jokinen, and V. Hrabovcová, *Design of Rotating Electrical Machines*, 1st ed. Hoboken, NJ, USA: Wiley, 2008.

[24] J. Gyselinck, P. Dular, N. Sadowski, P. Kuo-Peng, and R. V. Sabariego, "Homogenization of form-wound windings in frequency and time domain finite-element modeling of electrical machines," *IEEE Trans. Magn.*, vol. 46, no. 8, pp. 2852–2855, Aug. 2010.

[25] G. S. Dimitrakakis and E. C. Tatakis, "High-frequency copper losses in magnetic components with layered windings," *IEEE Trans. Magn.*, vol. 45, no. 8, pp. 3187–3199, Aug. 2009.

[26] M. J. Islam, J. Pippuri, J. Perho, and A. Arkkio, "Time-harmonic finite-element analysis of eddy currents in the form-wound stator winding of a cage induction motor," *IET Elect. Power Appl.*, vol. 1, no. 5, pp. 839–846, Sep. 2007.

**ACTA UNIVERSITATIS LAPPEENRANTAENSIS**

**481.** KORPIJÄRVI, JUHA. Aging based maintenance and reinvestment scheduling of electric distribution network. 2012. Diss.

**482.** KORHONEN, JUHAMATTI. Active inverter output filtering methods. 2012. Diss.

**483.** KLODOWSKI, ADAM. Flexible multibody approach in bone strain estimation during physical activity: quantifying osteogenic potential. 2012. Diss.

**484.** VUORENMAA, MARKKU. Osaamisen johtaminen pk-yrityksen kansainvälisen kasvun elinkaarella. 2012. Diss.

**485.** RAUTIAINEN, MARITA. Dynamic ownership in family business systems – a portfolio business approach. 2012. Diss.

**486.** LILIUS, REIJO. THE FINNISH IT INDUSTRIES IN TRANSITION Defining and measuring the Finnish software product and IT services industries by applying theoretical frameworks . 2012. Diss.

**487.** TUOMINEN, PASI. The purpose of consumer co-operation: implications for the management and governance of co-operatives. 2012. Diss.

**488.** SAARI, ESA. Suurnopeus-turbokoneroottoreiden termodynaaminen ja mekaaninen mallinnus sekä rakenneanalyysi. 2012. Diss.

**489.** PAANANEN, MIKKO. On innovative search: the use of internal and external sources of innovation among Finnish innovators. 2012. Diss.

**490.** BELOVA, POLINA. Quasiclassical approach to the vortex state in iron-based superconductors. 2012. Diss.

**491.** HIETANEN, IIRO. Design and characterization of large area position sensitive radiation detectors. 2012. Diss.

**492.** PÄSSILÄ, ANNE. A reflexive model of research-based theatre Processing innovation of the cross-road of theatre, reflection and practice-based innovation activities. 2012. Diss.

**493.** RIIPINEN, TOMI. Modeling and control of the power conversion unit in a solid oxide fuel cell environment. 2012. Diss.

**494.** RANTALAINEN, TUOMAS. Simulation of structural stress history based on dynamic analysis. 2012. Diss.

**495.** SALMIMIES, RIINA. Acidic dissolution of iron oxides and regeneration of a ceramic filter medium. 2012. Diss.

**496.** VAUTERIN, JOHANNA JULIA. The demand for global student talent: Capitalizing on the value of university-industry collaboration. 2012. Diss.

**497.** RILLA, MARKO. Design of salient pole PM synchronous machines for a vehicle traction application. 2012. Diss.

**498.** FEDOROVA, ELENA. Interdependence of emerging Eastern European stock markets. 2012. Diss.

**499.** SHAH, SRUJAL. Analysis and validation of space averaged drag model for numerical simulations of gas-solid flows in fluidized beds. 2012. Diss.

**500.** WANG, YONGBO. Novel methods for error modeling and parameter identification of redundant hybrid serial-parallel robot. 2012. Diss.

**501.** MAXIMOV, ALEXANDER. Theoretical analysis and numerical simulation of spectral radiative properties of combustion gases in oxy/air-fired combustion systems. 2012. Diss.

**502.** KUTVONEN, ANTERO. Strategic external deployment of intellectual assets. 2012. Diss.

**503.** VÄISÄNEN, VESA. Performance and scalability of isolated DC-DC converter topologies in low voltage, high current applications. 2012. Diss.

**504.** IKONEN, MIKA. Power cycling lifetime estimation of IGBT power modules based on chip temperature modeling. 2012. Diss.

**505.** LEIVO, TIMO. Pricing anomalies in the Finnish stock market. 2012. Diss.

**506.** NISKANEN, ANTTI. Landfill gas management as engineered landfills – Estimation and mitigation of environmental aspects. 2012. Diss.

**507.** QIU, FENG. Surface transformation hardening of carbon steel with high power fiber laser. 2012. Diss.

**508.** SMIRNOV, ALEXANDER. AMB system for high-speed motors using automatic commissioning. 2012. Diss.

**509.** ESKELINEN, HARRI, ed. Advanced approaches to analytical and systematic DFMA analysis. 2013.

**510.** RYYNÄNEN, HARRI. From network pictures to network insight in solution business – the role of internal communication. 2013. Diss.

**511.** JÄRVI, KATI. Ecosystem architecture design: endogenous and exogenous structural properties. 2013. Diss.

**512.** PIILI, HEIDI. Characterisation of laser beam and paper material interaction. 2013. Diss.

**513.** MONTO, SARI. Towards inter-organizational working capital management. 2013. Diss.

**514.** PIRINEN, MARKKU. The effects of welding heat input usability of high strength steels in welded structures. 2013. Diss.

**515.** SARKKINEN, MINNA. Strategic innovation management based on three dimensions diagnosing innovation development needs in a peripheral region. 2013. Diss.

**516.** MAGLYAS, ANDREY. Overcoming the complexity of software product management. 2013. Diss.

**517.** MOISIO, SAMI. A soft contact collision method for real-time simulation of triangularized geometries in multibody dynamics. 2013. Diss.

**518.** IMMONEN, PAULA. Energy efficiency of a diesel-electric mobile working machine. 2013. Diss.

**519.** ELORANTA, LEENA. Innovation in a non-formal adult education organisation – multi-case study in four education centres. 2013. Diss.

**520.** ZAKHARCHUK, IVAN. Manifestation of the pairing symmetry in the vortex core structure in iron-based superconductors. 2013. Diss.

**521.** KÄÄRIÄINEN, MARJA-LEENA. Atomic layer deposited titanium and zinc oxides; structure and doping effects on their photoactivity, photocatalytic activity and bioactivity. 2013. Diss.

**522.** KURONEN, JUHANI. Jatkuvan äänitehojakautuman algoritmi pitkien käytävien äänikenttien mallintamiseen. 2013. Diss.